THE IMPACT OF HIDDEN AGGREGATE STRUCTURE ON MOLECULAR CHAPERONE DISAGGREGATION REVEALED BY SINGLE PARTICLE FLUORESCENCE BURST ANALYSIS

A Dissertation

by

DANIEL WAYNE SHOUP

Submitted to the Office of Graduate and Professional Studies of
Texas A&M University
in partial fulfillment of the requirements for the degree of

DOCTOR OF PHILOSOPHY

Chair of Committee,	Hays Rye
Committee Members,	Sarah Bondos
	Ry Young
	Gregory Reinhart
Head of Department,	Gregory Reinhart

May 2016

Major Subject: Biochemistry

ABSTRACT

Molecular chaperones are tasked with folding and disassembling the misfolded and aggregated non-native proteins that arise during biosynthesis or upon environmental stress. However, the heterogeneous and dynamic nature of misfolded and aggregated non-native proteins makes it challenging to study the mechanism of protein disaggregation by molecular chaperones. A central unresolved question is whether it is the size or structure of non-native protein aggregates that limits how well cells clear potentially toxic aggregates. The work described herein demonstrates that protein aggregate size does not intrinsically limit how well protein aggregates are dismantled by molecular chaperones. Rather, the primary constraint appears to be the internal structure of aggregates. This conclusion is made possible, in part, by the application of a fluorescence-based single particle technique known as Burst Analysis Spectroscopy (BAS). Several novel extensions to the BAS method, that substantially extend both the power and general applicability of the method, are developed as part of this work and are also presented here. The potential of extensions that permit multi-color analysis and extend the analyzable size range are demonstrated in case studies of DNA packing in lambda phage, protein aggregation, and ENTH mediated vesiculation.

The CO_2-fixing enzyme ribulose-1, 5-bisphosphate-carboxylase

oxygenase (RuBisCO) from *R. rubrum* was employed as the model substrate protein in the study of protein disaggregation by molecular chaperones. Using BAS, non-native RuBisCO is shown to follow at least two general aggregation pathways, which can be distinguished by their unique population distributions and growth behavior. Visualized by EM, RuBisCO aggregates that grow slowly (slow growing) are amorphous in shape, while rapidly growing aggregates (fast growing) are fibroid-like. These two chemically identical but structurally and conformationally distinct aggregates respond very differently to active disaggregation by a model molecular chaperone network consisting of the *E. coli* Hsp70 and Hsp100 molecular chaperones. While fast growing aggregates can be disassembled by the Hsp70 system alone, slow growing aggregates require both the Hsp70 and Hsp100 systems. In all cases, BAS measurements demonstrate that the efficiency of RuBisCO aggregate disassembly is not impacted by aggregate size. Strikingly, slow growing aggregates display a dramatic shift in behavior with time, becoming increasingly refractory to disassembly with no detectable changes in size, and without losing the ability to bind Hsp70. Using inter-molecular fluorescence resonance energy transfer (FRET) measurements, it is shown that this shift in behavior is consistent with a compaction or tightening of the average aggregate structure. Additionally, the Hsp70 system is shown to alter this structure without inducing disassembly, consistent with models in which Hsp70s play a key role in preparing or loosening aggregates prior to engagement by Hsp100s.

DEDICATION

This dissertation is dedicated to my wife, Ginger, and my children, Phaelan and Esmond. In youth, my mind was consumed by darkness and I could not see who I was and what I was capable of. Ginger provided for me a guiding light that drove the darkness of my mind into the shadows of my form, which, allowed me to see the difference between my shadow and myself. Her love and assistance has given me the strength to carry on and to push past what I perceive are my limitations. I owe her for so much more than I can ever repay, and yet, she continues to be by my side.

Together we took on the journey of parenthood as Ginger bore our children, Phaelan and Esmond. Our children have changed us both for the better in numerous ways, but it has been the reawakening of something deep within us that we had forgotten as we became adults that we are most thankful for. Seeing the wonder in my children's eyes as they experience the world around them has given me a new perspective on the world that I would have never developed without them.

The gifts of my children, and the love I have for them, are things that I would not have experienced without Ginger. I will never be able to thank her enough, but she will always have my love, which I hope will always be enough.

ACKNOWLEDGEMENTS

All persons that I have interacted with have had in some way an impact on my life. Thus, everyone that has been a part of my life, whether positive or negative in influence, has contributed to who I am now and this work that I present herein. Having acknowledged the cumulative contribution of all that have had an impact on my life, I would like to extend special acknowledgments to the more prominent contributors to my life and this work.

To parents, grandparents, sister, cousins, and other extended family, I can never give enough thanks. Your influence in my life has been constant and your interactions with me were the founding experiences of my life that truly helped mold who I am. My mother and father not only taught me the ways of the world, they encouraged me to think creatively and never take things at face value. Seeing as I have become a biochemist as opposed to a paleontologist, I hope they do not feel they wasted the small fortune that they spent on dinosaur books.

To the friends that have come and gone though out my life, thank you for being there for me and giving me the chance to be apart of your life. The memories you gave me have both inspired me and shaken my beliefs. For those friends that have never let me go, thank you for keeping me in your life.

I would like to thank the Bio/Bio Department at TAMU as a whole. The secretaries and office staff in this department are superb. They keep this department organized and on task. The professors, secretaries, and BGA that make up the various advisory boards for the department put their best effort into the graduate program in this department. To the members of the BGA that I was close with, you have supported me in ways you never knew, thank you for keeping me positive and hopeful.

I would also like to thank my committee. They have helped me throughout my graduate carrier in more ways than just advising me on my project. Dr. Reinhart and Dr. Young not only advised me during classes, but also guided me as I rotated in their labs. Though Dr. Bondos was not an initial member of my committee, she has been a constant guiding presence during my graduate career. Thank you all for guiding me and keeping me on path as a scientist.

To my lab mates, both past and present, thank you for being a part of my career and life. Jeremy, Rajan, Lauren, Arielle, Louise, Drew, Allison, Kendra, and Laura have been with me as I have progressed through my scientific studies. We have kept each other sane and supported one another throughout our work. Thank you for helping me or giving me the chance to help you and further the way I understand the things I do.

I would like to give acknowledgments to Hays Rye, Chave Carr, and Jason Puchalla. When I started working for Hays, he helped me put together a good project, the way any caring professor would. Unfortunately, the best-laid plans often go awry, and the plans for my project were no different. As things fell through over and over, Hays never gave up on my project or me. I am thankful that he is just a stubborn and persistent as I am, I could never have made it to the end without his support. Thank you Hays.

To Chave, I am indebted for many different reasons. She not only took me under her wing and advised me, but she fought many battles for me that I did not always know about. She is truly a wonder. Thank you Chave.

To Jason, thank you becoming my second advisor and mentoring me. You passed knowledge and ideas to me freely and gave me so much of your precious time. I can never thank you enough for expanding my knowledge of spectroscopy, physics, and statistics. Thank you Jason.

Lastly, I would like to again acknowledge my wife. Her support has been paramount in my endeavors. I could not have done this without her.

TABLE OF CONTENTS

LIST OF FIGURES

CHAPTER I

INTRODUCTION AND LITERATURE REVIEW

Introduction

The seclusion of hydrophobic amino acids from solvent is a thermodynamically favorable process (Spolar et al, 1989) that normally helps drive protein folding and the oligomerization of native proteins (Vulevic et al, 1997). However, the tendency of solvent exposed hydrophobic amino acids to cluster helps drive non-native protein to oligomerize (Dill et al, 1997; Capaldi et al, 2002) into large aggregates (Simone et al, 2011; Morris et al, 2009, Chiti et al, 2002) with amorphous or fibrillar structures (Fandrich et al, 2007; Jackson et al, 2000; Groot et al, 2009). The aggregation of non-native protein can lead to the early onset of cellular senescence (Lindner et al, 2008; Erjavec et al, 2007; Liu et al, 2010) and cell death (Maisonneuve et al, 2008; Bucciantini et al, 2002). The consequence of non-native protein aggregation on cellular fitness was originally attributed to the loss of vital cellular proteins, such as those needed for metabolism. More recent studies have shown that aggregates of many non-native proteins possess toxic properties that are not connected to the normal cellular activity of these proteins (Bucciantini et al, 2002). Additionally, aggregates in early stages of growth tend to have a greater toxicity than mature aggregates (Zhu et al, 2000). Once formed, aggregates can be very stable, long-lived structures (Nichols et al, 2005). This means that non-native protein

aggregates can linger within a cell and poison cells long after conditions that foster protein denaturation have ceased (Erjavec et al, 2007).

In order to combat aggregate toxicity, cells have evolved a system of molecular chaperones capable of preventing aggregation (Garrido et al, 2010), disassembling aggregates (Haslberger et al, 2010; Zietiewicz et al, 2006), and aiding in the refolding of non-native protein (Farr et al, 2003). However, molecular chaperones can fail to clear non-native protein aggregates. Why molecular chaperones fail in some cases, and how molecular chaperone activity impacts various protein mis-folding and aggregation diseases, is not well understood. It is possible that features of non-native protein aggregates such as size and structure can make aggregates refractory to disaggregation. Unfortunately, non-native protein aggregates are heterogeneous by nature and a single solution of aggregating protein can contain a wide range of structures, sizes, shapes, and subunit conformations. This complexity has made it difficult to study the relationship between aggregate features and the disaggregation activity of molecular chaperones.

Brief Overview

The core work presented in this dissertation explores the relationship between the size, structure, and subunit conformation of non-native protein aggregates and the disaggregation activity of molecular chaperones. Most

experiments are carried out with a range of fluorescence-based techniques from FRET to a novel single particle technique, called Burst Analysis Spectroscopy (BAS). However, adequately studying the impact of aggregate qualities on disaggregation required the creation of extensions to BAS. The development, testing, and demonstration of the broader application of these extensions to BAS make up the rest of the work presented in this dissertation.

Scope of the Literature Review

In order to better set the context and justification for this project, the rest of this chapter contains a review of what is known about non-native protein aggregation, molecular chaperones, and the study of complex macromolecular systems, as they pertain to this project. The first section of this literature review summarizes the seminal investigations into protein misfolding and aggregation. The following few sections review the contemporary models for the aggregation of non-native protein and how these structures impact cellular fitness. The section that follows bridges the discussion of non-native protein aggregation to an introduction of molecular chaperones, by discussing how cells protect themselves from the negative effects of protein misfolding and aggregation. The next section broadly reviews the discovery and initial characterization of molecular chaperones. The discussion of molecular chaperones narrows in subsequent sections to centralize around the Hsp70 family of molecular chaperones and their co-chaperones. These sections detail the numerous roles

of the members of the Hsp70 family of proteins, the mechanism of their activity, their role in disaggregation, and how they co-operate with other molecular chaperone systems. The section that follows details the extent of what is known about Hsp70 assisted disaggregation. The next sections outline why a deeper understanding of disaggregation is limited with current methodologies and they introduce BAS, how it works, its limitations, and how it can be applied to reach a deeper understanding of aggregation and disaggregation. The final sections of this literature review begin to transition the discussion into the core work of this dissertation by introducing the specific chaperone system, and its non-native protein aggregate substrate, used in this study and why they were found ideal for this work.

Literature Review

Discovery of the Nature of Protein Folding and Aggregation

In the early 1800's, microscopists noticed that stressed, damaged, or diseased cells contained granule deposits of what was originally thought by Rudolf Virchow to be carbohydrates, due to their ability to be stained by iodine (Virchow, 1854). These granule structures were thus named amyloids after the Latin root word for starch. However, it was later revealed in 1859, that these granules were composed of protein and not carbohydrates (Friedreich et al, 1859). Why protein granules formed in damaged or stressed cells did not become apparent until 1910. That year, Harriet Chick and C. J. Martin found

that proteins had a “native” state, in which they possessed enzymatic activity, that could be converted to a “non-native” state that lacked enzymatic activity, through a process termed denaturation. The process of denaturation was found to be induced by changing the temperature, pH, and salt concentration of a protein containing solution. They also found that non-native protein was prone to precipitation (Harriette et al, 1910). The observation that the denaturation and precipitation of non-native protein occurred without modification of the molecular formula of proteins led to the hypothesis that denaturation altered the arrangement, or conformation, of a protein's components. By extension, this meant that the native state of a protein had to be a specific conformation of a protein's components, which had been previously determined to be covalently bonded amino acids, or polypeptides, by Hermann Emil Fischer and Ernest Fourneau (Fischer et al, 1901).

Over the next four decades, scientists attempted to unravel how protein conformations were stabilized and what constituted the structure of proteins, which some at the time assumed could be a branching structure. During this time, two prominent models arose for how the components of a protein's structure interacted and stabilized the conformation of a protein. These models centered around hydrophobic interactions, proposed by Dorothy Wrinch and Irving Langmuir in the late 1930s, and hydrogen bonding between amino acids, proposed by William Astbury in 1933 (Langmuir et al, 1939; Astbury, 1933).

While both models claimed that each was the primary means of stabilizing protein conformations, the accepted model for how amino acids interact and stabilize the conformation of proteins was later determined to be a combination of both models. In this combined model, the polypeptide backbone of proteins forms hydrogen bonds with itself in order to form the "secondary structures" known as beta-sheets, first proposed by William Astbury, and alpha-helices, proposed by Linus Pauling (Astbury, 1933; Pauling et al, 1951). Secondary structures can be held together through hydrogen bonding between amino acid side chains (Chen et al, 1993), however, secondary structures are primarily driven together and stabilized by the interaction of hydrophobic and hydrophilic amino acids with water (Pace et al, 2011) (Figure 1-1 A). This concept is simplified in a model proposed by Walter Kauzmann in the 1950s. Kauzmann proposed that the interaction of amino acid side chains with water caused proteins to adopt a conformation that adequately buried hydrophobic amino acids within the protein and exposed hydrophilic amino acids to water (Kauzmann, 1956). While the models worked out by Kauzmann and his predecessors are still used today to understand protein conformation, the structure of proteins was not truly identified until Frederick Sanger sequenced the protein insulin and determined that it was composed of linear chains of amino acids (Sanger, 1949). The hypothesis that proteins could be composed of branching chains was not fully discredited until the 1950s, when George Palade discovered the ribosome, which produces proteins as linear chains of

amino acids (Palade, 1955; Schweet et al, 1966). Because linear polypeptides must bend around themselves, or fold, the process by which a protein transits from a linear polypeptide into its native conformation is referred to as “protein folding”. The native conformation of folded proteins was determined by Christian Anfinsen to be determined by the amino acid sequence of polypeptides (Anfinsen et al, 1961). Interestingly, the native fold of a protein represents only a small fraction of the astronomical number of possible non-native conformations that a protein is capable of assuming. This observation was the source of Levinthal’s paradox, which states that the length of time required for a polypeptide, which contains 100 amino acids, to sample every possible conformation is greater than the age of the universe. Levinthal’s solution to this paradox was that the folding of proteins is sped up by the local interactions between amino acids, which could then guide further intra-protein interactions (Levinthal, 1969) (Figure 1-1 C).

Native and Non-Native Protein Oligomerization

Fredrick Sanger's work showed that insulin is a dimer of two polypeptide chains linked together by a disulfide bond (Sanger, 1949). However, the disulfide bond between insulin subunits is not the only contact between the two-polypeptide chains. Side chain interactions can be observed in Dorthy Hodgkin's crystal structure of insulin (Adams et al, 1969) (Figure 1-1 B). This work, and the work of numerous others, shows that the same intra-molecular

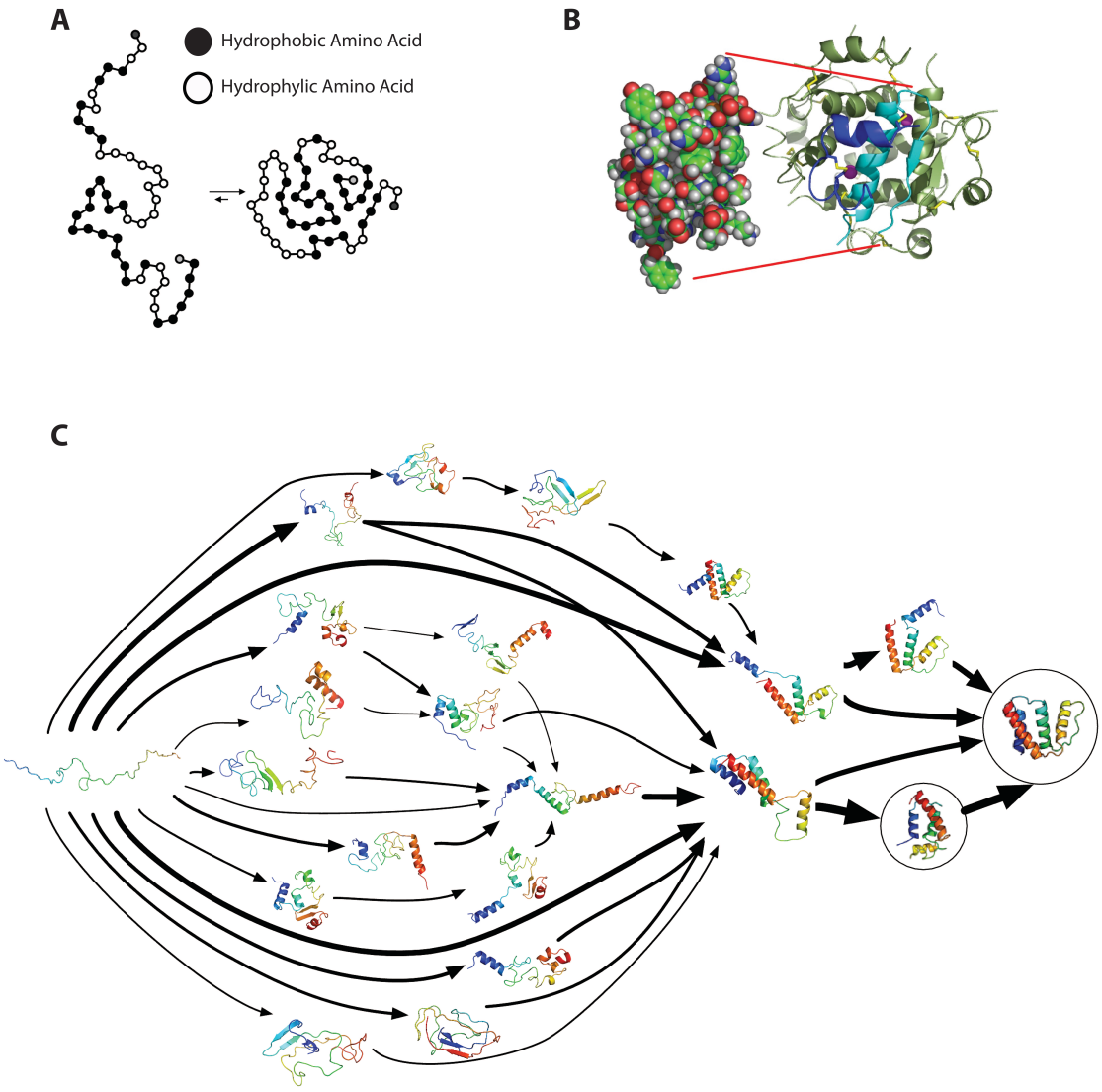

<u>Figure 1-1</u> Protein Folding is a Multi-Step Process That is Driven by Local Intra-Protein Interactions and Interactions with Water. (A) Polypeptides fold in a way that minimizes the exposure of hydrophobic amino acids to water while maximizing the exposure of hydrophilic amino acids to water. (B) In the folded state of the insulin heteroligomer, numerous inter- and intramolecular interactions can be seen stabilizing the folded state of insulin. (C) The various intramolecular interactions that stabilize folded protein form during the various steps of protein folding. The development of local intra-protein interactions during folding helps to guide proteins into the native state.

Images presented in this figure were obtained and edited for republication with full rights from:
(A) https://commons.wikimedia.org/wiki/File:Protein_folding_schematic.png
(B) https://commons.wikimedia.org/wiki/File:InsulinMonomer.jpg
(C) https://commons.wikimedia.org/wiki/File:ACBP_MSM_from_Folding@home.tiff

interactions found in folded protein (i.e. hydrophobic interactions, salt bridges, and hydrogen bonding) can be found inter-molecularly between two or more proteins (Jones et al, 1996). These interactions not only stabilize the association of multiple folded polypeptides, but can also help drive proteins to oligomerize, as is the case with interactions between hydrophobic amino acid side chains. The same interactions that help native proteins to oligomerize can cause non-native proteins to form oligomers as well (Jahn et al, 2008).

The oligomerization of native proteins is typically reversible and the number of subunits in native protein oligomers is normally a discrete value (Cornish-Bowden et al, 1971). Conversely, it is common for non-native proteins to oligomerize into large aggregates with a non-discrete number of subunits. The dissociation constant for aggregate subunits is typically very low, as subunit dissociation tends to expose the hydrophobic amino acids of polypeptides to water, which is thermodynamically unfavorable (Fink, 1998; Roberts, 2006). The structure, size, and shape of non-native protein aggregates are highly variable even when a population of aggregating protein contains only a single polypeptide (Weiss et al, 2007; Puchalla et al, 2008). This is in part due to the large number of possible non-native conformations a protein can assume. Despite the large number of possible peptide conformations and aggregate structures, non-native protein aggregates can have uniform structures that can be formed similarly between different polypeptides. The work of Christopher

Dobson has shown that most non-native proteins, given the right conditions, are able to aggregate into long fibers where each subunit is connected by a uniform beta-sheet structure that runs along the fiber's axis (Knowles et al, 2014) (Figure 1-2 D). Known as amyloid fibrils and amyloids, the deposition of these aggregates in cells and tissue is associated with numerous human diseases, such as Alzheimer's disease (Alzheimer, 1907). The regular structure of amyloids can be identified by various stains, such as Thioflavin-T and Congo Red (Vassar et al, 1959; Bennhold, 1922) (Figure1-3 B). The ease of amyloid identification has allowed researchers to study the various ways amyloids can impact cellular fitness. However, most aggregates are not amyloids and often have irregular and inconsistent structures that are difficult to identify and characterize (Lewandowska et al, 2007; Vetri et al, 2007; Krebs et al, 2008). For this reason, most non-amyloid aggregates are referred to as 'amorphous' aggregates. While amyloid fibrils and amorphous aggregates are structurally dissimilar, amorphous aggregates can in some cases seed the formation and fiber elongation of amyloids (Bucciantini et al, 2002) (Figure 1-2 A-C). Interestingly, both amyloids and amorphous aggregates have a negative impact on cellular fitness.

The Impact of Protein Mis-Folding and Aggregation on Cellular Fitness and Disease Progression

The aggregation of non-native proteins stabilizes the non-native

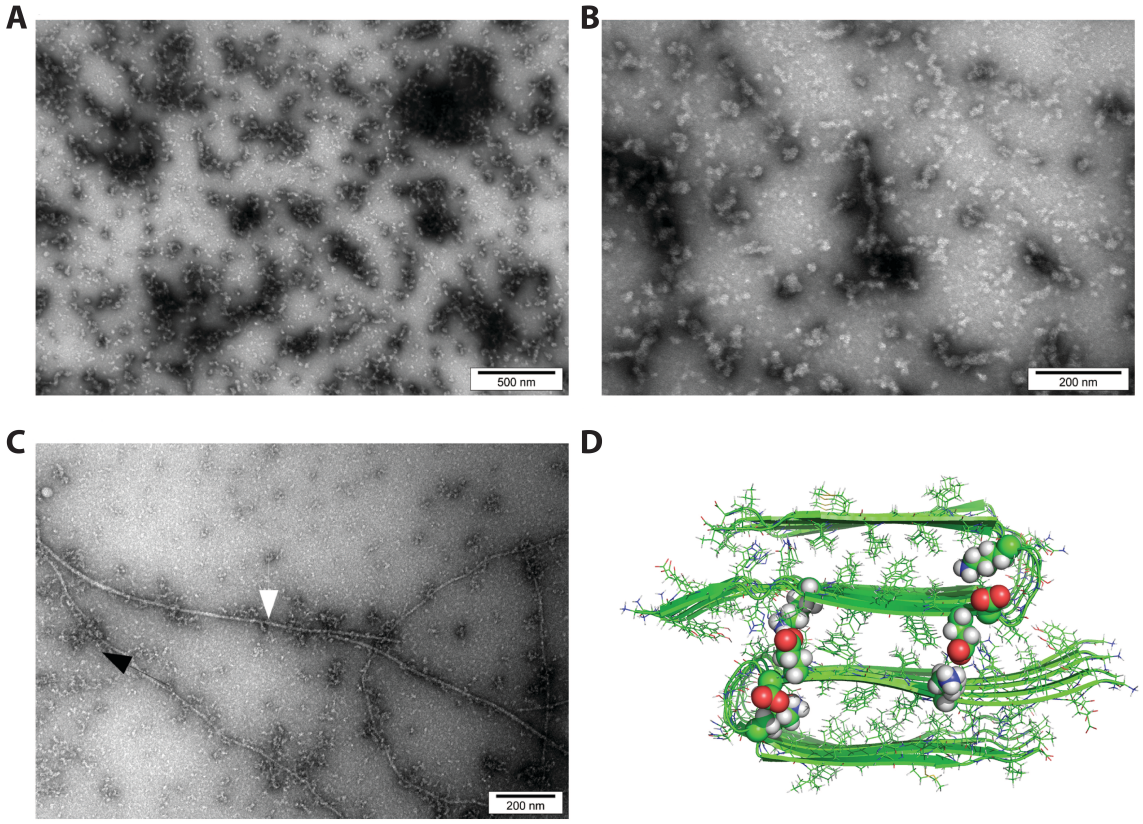

Figure 1-2 Amyloid Fibers Are Connected by Organized Beta-Sheet Folds That Can Be Nucleated from Amorphous Pre-Fibrillar Aggregates. (A,B) Non-native myostatin precursor proteins can form amorphous aggregates, observed here via electron microscopy, with pre-fibrillar character. With time these structures can seed the formation of amyloid fibrils. (C) Shown via electron microscopy are insulin amyloid fibrils, which were used as positive controls to monitor the fibrillation the myostatin precursor protein. (D) Amyloid fibrils oligomerize in such a way that organized beta-sheet structures link each subunit together.

---

conformation of proteins and prevents them from reaching the native state. Thus, protein aggregation represents a loss of the activity that would have been provided by the native proteins. If proteins aggregate before ever reaching a native conformation then cells lose the resources used to make the protein without gaining any benefit. This loss of material can strain cellular activities, but when vital cellular proteins are lost to aggregation, cells may be unable to maintain homeostasis and could die. Additionally, non-native protein aggregates are toxic and can interfere with vital cellular processes and disrupt homeostasis (Stefani et al, 2003).

Non-native protein aggregates can interfere with cellular processes by interacting with other cellular proteins, membranes, and by physically obstructing cellular machinery involved in activities such as transport and signaling. However, physical obstruction of cellular activities can occur both inside and outside a cell. In Alzheimer's disease, extracellular amyloid fibrils, composed of the Aβ protein, can cluster into large plaques that can obstruct synaptic signaling (Sheng et al, 2012), neuronal rearrangement, and the flow of fluid around the brain (Weller, 1998) and cerebral arteries (Roher et al, 2012). Intraneuronal fibers of the amyloid-beta (Aβ) protein block the transport of mitochondria (Zhao et al, 2010), the recycling endosome (Cataldo et al, 2000), and brain-derived neurotrophic factor (BDNF), which encourages neuronal synapse growth and differentiation (Umeda et al, 2015). While obstruction of extra and intracellular

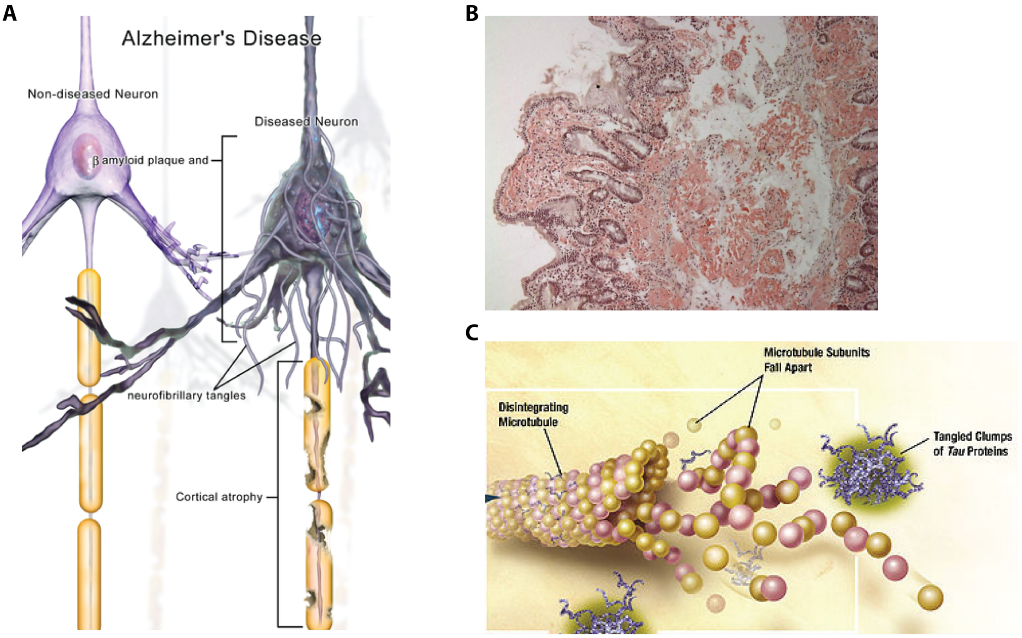

Figure 1-3 In Alzheimer's Disease, the Formation of Aβ Amyloid Fibrils is Linked to Neuron Dysfunction and Death. (A) The interaction of Aβ amyloid fibrils with neurons leads to a cascade of cellular dysfunction that can inevitably lead to neuron death. (B) The presence of amyloid fibrils and fibril plaques (also referred to as fibril tangles) can be can be detected with various amyloid-binding dyes. Shown is a segment of human brain stained with Congo Red, which is a common stain used for identifying amyloids. (C) One-way that Aβ amyloid fibrils contribute to cellular dysfunction is through interaction with tau. When Aβ amyloids interact with tau, the tau protein forms granules that are inactive. Without active tau proteins, microtubules become destabilized and as a result cellular transport and structure become abnormal.

---

processes by amyloid fibrils has a catastrophic impact on cell and tissue health, monomeric non-native Aβ proteins, and Aβ proteins in the early stages of aggregation, also significantly contribute to the progression of Alzheimer's disease (Figure 1-3 A). Intraneuronal Aβ proteins, as small aggregates and monomers, interact with other cellular proteins, such as the microtubule stabilizing protein tau. When non-native Aβ protein binds to tau, it causes tau to oligomerize into large granule-like structures (Stancu et al, 2014). This depletes the tau within neurons and leads to the destabilization of micro-tubules (Gendron et al, 2009), which are critical for supporting cellular structure and intracellular transport (Figure 1-3 C). Additionally, when non-native Aβ protein interacts with membrane, membranes can become permeable to ions and small molecules. Aβ proteins do this by growing along the membrane surface, which introduces lesions or tears into membranes, or by forming small ion-selective pores (Prangkio et al, 2012; Sciacca et al, 2012; Kawahara, 2010). Non-native and aggregated Aβ proteins cause the most damage when they develop on mitochondria (Camilleri et al, 2013) and on the plasma membrane (Lin et al, 2001). While the nature of interactions with other cellular proteins varies between amyloids composed of different polypeptides, the physical obstruction of cellular processes and the disruption of membranes, via formation of pores and lesions, are common pathologies in amyloid related diseases, including Parkinson's disease (Hilal et al, 2002) and type 2 Diabetes (Anguiano et al, 2002).

While a colossal amount of research has been dedicated to the study of amyloids, the formation and cellular impact of amorphous non-native protein aggregates has been ill studied by comparison. However, it is known that the presence of amorphous aggregates within cells is associated with a decrease in cellular fitness, an early onset of cellular senescence, and cell death. Thus the fate of cells harboring both amorphous and amyloid aggregates is similar (Bucciantini et al, 2002; Erjavec et al, 2007; Lindner et al, 2008; Liu et al, 2010).

Interestingly, both amorphous and amyloid aggregates can develop early in the lifespan of single or multi-celled organisms (Baker-Nigh et al, 2015). However, these structures can persist in young organisms without producing a disease phenotype. Indeed, non-native Aβ proteins can form amyloid fibrils in the brains of children and teenagers, but not cause Alzheimer's disease until later in life (Baker-Nigh et al, 2015). Cells are able to prevent disease progression in young cells through the activity of protein quality control systems (Morely et al 2002). Thus, disease phenotypes may develop because protein quality control machines are down-regulated with age (Kikis et al, 2012), highly toxic aggregates form that are resistant to the activity of quality control machinery (Morely et al, 2002), or aggregates build-up and overwhelm quality control machines (Erjavec et al, 2007; Lindner et al, 2008).

Despite the activity of quality control machinery, aggregates are observed

to slowly grow throughout the life of a cell (Ollikainen et al, 2010). The continuous growth of aggregates occurs even if cells are not periodically exposed to cellular conditions that promote aggregation (Maisonneuve et al, 2008). Instead, these aggregates primarily grow from the failure of newly synthesized protein to fold properly, which in some cells can be up to 30% of all proteins (Schubert et al, 2000), and from exposure to reactive oxygen species, which can damage proteins and cause them to unfold and aggregate (Maisonneuve et al, 2008; Imlay, 2013; Muller et al, 2007). The accumulation of damaged protein and non-native protein aggregates occurs despite cells being equipped with a diverse system of protein quality control machines. This not only puts an ever-increasing strain on quality control machinery, it also demonstrates that non-native protein, and the aggregates they form, can resist the activity of a cell's quality control machinery (Maisonneuve et al, 2008; Ollikainen et al, 2010).

Cells Possess a Variety of Protein Quality Control Systems That Are Meant to Protect Them from Protein Mis-Folding and Aggregation

The primary protein quality control systems of cells are composed of proteins known as molecular chaperones. These proteins are able to prevent non-native protein aggregation, control the aggregation process, store aggregated protein, disassemble non-native protein aggregates, and assist in protein folding (Hartl et al, 2011). Despite their role in controlling aggregation

and storing non-native and aggregated protein, the goal of the molecular chaperone system is to help proteins reach their native state (Hartl et al, 2011). Their role in aggregation and storage is meant to prevent non-native proteins from forming aggregates that cannot be disassembled and preventing them from interacting with other cellular components until they can be disassembled and folded properly (Bakthisaran et al, 2015; Hartl et al, 2011). In this way, molecular chaperones act similarly to their namesake in human society (i.e., they guard proteins and prevent bad things from happening) (Lakey et al, 1978).

When non-native proteins cannot be folded, or their aggregates cannot be disassembled, cells will employ a system of proteases to degrade and recycle them. However, determining when proteases should intercede is a complicated process. In eukaryotes, non-native proteins are ubiquitinated in order to make them targets of proteolytic degradation (Prakash et al, 2004). Cells can also shift protein out of the molecular chaperone systems and into the proteasomal network with adaptor proteins like CHIP (McDonough et al, 2003). Some bacteria employ similar systems that utilize ubiquitin-like proteins (Pearce et al, 2008), however, most bacteria encode protease signal sequences into their proteins that are exposed when misfolded (Sauer et al, 2004).

In the case that proteins fail to be refolded or degraded, they are often forced into storage to minimize their impact on the internal cellular environment.

Eukaryotes transport misfolded and aggregated protein on dynein motors, which run along microtubules, to a central point of storage for misfolded protein, known as the aggresome (Johnston et al, 1998). Bacteria lack such an elaborate system, but still manage to store non-native protein in inclusion bodies (Garcia-Fruitos et al, 2011). The inability of cells to internally eliminate aggresomes and inclusion bodies can trigger cells to employ a triage system to either expel aggregates into the extracellular space (Lee et al, 2005), asymmetrically segregate aggregates during cell division (Lindner et al, 2008), or destroy aggregates via autophagy (Zaarur et al, 2014). However, releasing toxic proteins into the interstitial space between cells can cause further damage (Alvarez-Erviti et al, 2011) and some non-native protein aggregates can resist lysosomal degradation during autophagy (Tanik et al, 2013). Non-native protein aggregates, that are resistant to lysosomal degradation, can become stuck in lysosomes and inevitably cause lysosomal dysfunction, which can trigger apoptosis (Martinez-Vicente et al, 2010). In the case of asymmetrical segregation, one daughter cell takes most of the non-native and aggregated protein while the second daughter cell is produced without this protein baggage (Lindner et al, 2008; Lloyd-Price et al, 2012). This extreme solution, found throughout all organisms, produces one rejuvenated cell and a cell with a shortened life span (Liu et al, 2010). In multicellular eukaryotes, this tactic is commonly used to cleanse gametes of non-native and aggregated protein prior to reproduction (Strandkvist et al, 2014; Unal et al, 2011).

Why non-native proteins, and the aggregates they form, become resistant to protein quality control machinery is not well understood. However, it is primarily a failure of the molecular chaperone systems that allows these structures to persist. In order to set the context for a discussion of chaperone activity and why it can be hampered, the following section will broadly cover the discovery of molecular chaperones and their initial characterization.

The Serendipitous Discovery and Characterization of Molecular Chaperones

In the early 1960s, an Italian fly geneticist, named Ferruccio Ritossa, observed that when *D. melanogaster* cells were incubated at temperatures higher than physiological temperature, their DNA would appear to produce "puffs". This puffing of DNA was due to a large increase in transcriptional activity (Ritossa, 1962). The transcriptional response to heat was referred to as the "heat shock response" and the proteins produced in response to incubation at elevated temperatures were named "heat shock proteins". While it was not recognized at the time, this discovery was the first documented cellular response to protein stress that promoted protein denaturation and aggregation. Thus, the discovery of heat shock proteins was also the discovery of a group of molecular chaperones that are expressed in response to heat (Ang et al, 1991; Becker et al, 1994). However, despite the initial discovery of molecular chaperones in flies, it was the study of the relationship between phage and their hosts that

would ultimately lead scientists to uncover the activity and function of a few key molecular chaperones.

In the late 1960s, the geneticists Ira Herskowitz and Costa Georgopoulos started a collaboration to find mutations in the genome of *E. coli* that disrupted the replication cycle of bacteriophage lambda (Georgopoulos, 2006). The genes that they identified as important for lambda replication were dubbed "*gro*", as they were required for the growth of phage (Georgopoulos, 1971). Some of the first mutants they identified would later be mapped to the gene for GroEL, which was determined to be important in the folding of viral capsid proteins. Later screens by Georgopoulos would lead to the isolation of mutants in the gene for DnaK, which was found to be required for removing phage proteins from the DnaB helicase that recruit DnaB to lambda DNA (Georgopoulos, 1977; Ang et al, 1991; Liberek et al, 1998). Later, it would be discovered that both DnaK and GroEL are molecular chaperones that are essential for cell survival (Bukau et al, 1998; Craig et al, 2006).

The mutant screen that was used to find both GroEL and DnaK was a simple screen for colony size. In this screen, the *E. coli* strain C600, which produces the supE amber suppressor, was mutagenized with nitrosoguanadine

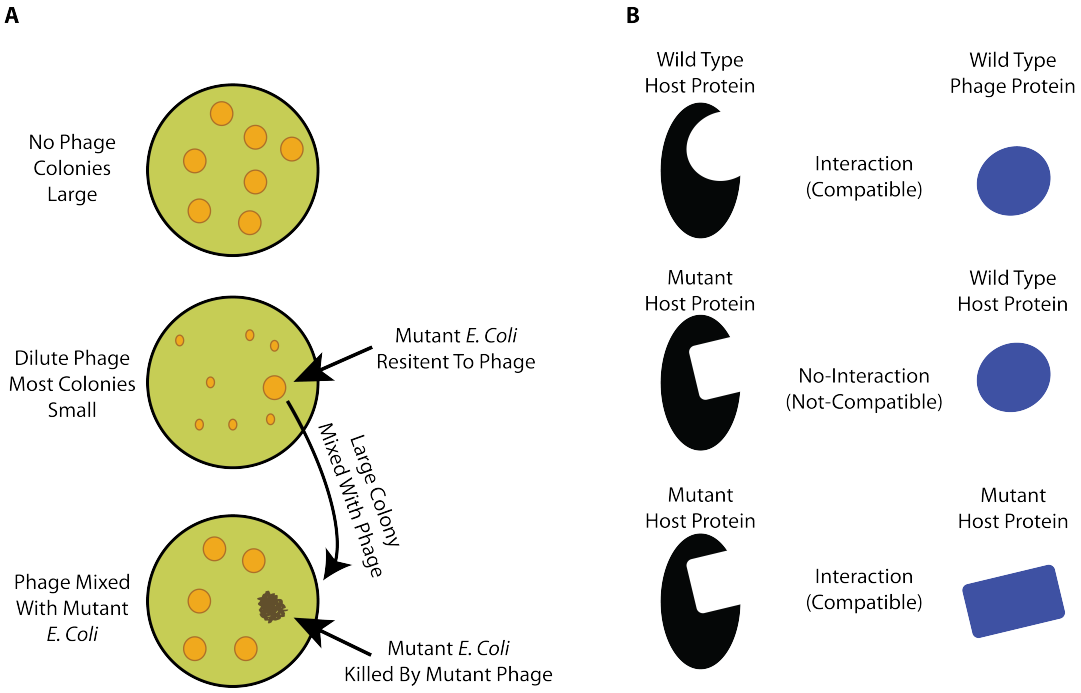

Figure 1-4 Host Proteins That Are Important for Phage Development Can Be Found with a Simple Screen for Colony Size. (A) *E. coli* growing on a plate with a dilute amount of phage spread across the surface will continue to grow in size until they encounter a phage. This will kill the *E. coli* and keep the growing colony small. *E. coli* that can continue growing possess a mutation that prevents them from being infected with phage. These colonies can be remixed with phage and plated in order to screen for phage that can infect the mutant *E. coli*, that were isolated in the screen for colony size. (B) Mutant *E. coli* that resist phage infection are likely to possess a protein with a novel interface that wild-type phage protein cannot efficiently interact with. In the second screen, random mutations in phage can allow their proteins to interact with mutant *E. coli* proteins. This allows the phage to survive and form plaques.

and then plated onto media with a specific concentration of two non-lysogenic lambda phages that targeted different *E. coli* surface receptors (Georgopoulos, 1971). The concentration of phage was tuned so that as *E. coli* colonies grew, they would encounter phage and die. This greatly slowed the growth of *E. coli* colonies. Conversely, *E. coli* that possessed mutations in genes that code for proteins essential for phage replication, called *gro*, prevented the replication of the phage they were simultaneously plated with. Only the *gro* mutant *E. coli* produced colonies of visible size on the plates.

In order to find phage genes whose protein products interacted with the protein products of different *gro* genes, plaque-forming revertants were obtained by plating wild-type phage on lawns of *gro* mutant *E. coli* (Georgopoulos, 1971; Georgopoulos, 1978). Some lambda phage revertants contained mutations in the capsid gene *E* and thus associated *gro* mutants were renamed *groE* (Georgopoulos, 1973; Georgopoulos, 1972). Interestingly, the protein products of capsid gene *E* were suppressing a problem with lambda protein B, which means *groE* should be *groB* (Kochan et al, 1983). Later it was found that GroE proteins are also required for T4 head assembly (Revel et al, 1980; Takano et al, 1972).

The first purification of a *groE* gene product came with the development of lambda transducing phage that carried a *groE* gene (Hendrix, 1979; Hohn et al,

1979). The *groE* gene, carried by lambda, was over expressed so that large amounts of the GroE protein could be produced for purified. The product of this *groE* gene was found to be ~60 kDa in size and was found to oligomerize into a structure containing two seven-subunit rings. However, this protein was found to not be the only gene product of a *groE* gene (Tilly et al, 1981; Tilly et al, 1992). When different *E. coli* strains bearing *groE* mutations were infected with the previously described λgroE, only about half of the *E. coli* mutants formed plaques. In other words, the *groE* gene carried by lambda phage could only complement half of the *E. coli* groE mutants, which meant there had to be at least two *groE* genes. The second *groE* gene product was found to be ~15 kDa and the phenotypes for lambda phage development were the same for mutations in both *groE* genes (Tilly et al, 1981). The large *groE* gene product of the *groE* locus was named GroEL and the small gene product was named GroES.

Electron micrographs of *groE* mutant *E. coli*, infected with wild type lambda phage, showed aberrant phage head assembly (Georgopoulos et al, 1973). It was thus thought that the GroE proteins were required for proper assembly of the macromolecular structure of the phage head. However, it was not until the work of George Lorimer that phage researchers realized that GroEL and GroES were needed for the proper folding of phage capsid components (Goloubinoff et al, 1989). In Lorimer's work, he found that GroEL and GroES

form a chaperone machine that was capable of assisting protein folding. His work was first done with the carbon-fixing protein RuBisCO, which was found to be incapable of reaching its native state without GroEL and GroES in *E. coli* and *in vitro*.

The DnaK chaperone system was discovered in much the same way that the GroEL system was. *E. coli* strains bearing *gro* mutations were mixed with lambda phage and spread on solid media. One set of *gro* mutations was compensated for by mutations in the lambda gene *P*, which at the time had already been determined to be important for the replication of lambda DNA (Georgopoulos et al, 1977). The *gro* mutants that were complemented by mutations in lambda gene *P* were named *groP* (Georgopoulus et al 1971). All *groP* mutants isolated by Georgopoulos were mutations in the *dnaB* gene, except one. This mutant, originally named $groP_{AB756}$, was found to completely block lambda DNA replication and was unable to form colonies at 42°C (Georgopoulos et al, 1977).

Around the same time Georgopoulos was characterizing $groP_{AB756}$, two other groups were independently characterizing similar mutants. The first, the Feiss lab in Iowa (Sunshine et al, 1977), used a screen similar to Georgopoulos' to find a *groP* mutation dubbed $groP_{C259}$. The difference between the two methods was that Georgopoulos screened for colony size on plates covered with

phage, while the Feiss lab screened for colonies that did not turn into phage plaques.

The second group, the Uchida lab in Japan, screened for *E. coli* strains tolerant to phage infection by growing *E. coli* strains, that contained a lambda prophage, at 42°C (Saito et al, 1977). Survival of the *E. coli* strain was based on the strain's ability to suppress prophage replication. The *E. coli* mutations that were isolated were named *grp*, which stood for *groP*-like mutations. They isolated two important mutations. The *grpC* gene was located near the $groP_{C756}$ and $groP_{C259}$ genes and had a similar phenotype. The $grpE_{280}$ gene mapped to a different region of the bacterial genome than previously discovered *groP* mutations.

The ensuing collaboration between these groups determined, through a series of simple sedimentation and nucleotide incorporation assays, that mutations in these genes were affecting their gene products ability to not only replicate bacteriophage DNA but also replicate host DNA. Thus, $groP_{C756}$ and $groP_{C259}$ were renamed *dnaK* and *dnaJ*, respectively, as their protein products were found to be important for DNA replication (Yochem et al, 1978). While the protein product of *grpE* was also found important for DNA replication, it was never renamed.

These proteins were found to help lambda DNA replication by disassembling the lambda-P-O-DnaB replication complex. The lambda O protein binds to the lambda DNA origin and the lambda P protein binds to DnaB and recruits this protein to the lambda DNA origin. However, the interaction between these proteins is strong and requires DnaK, DnaJ, and GrpE to disassemble the complex (Ang et al, 1991; Wickner, 1979). Later it was found that DnaK is the workhorse in this disassembly process and that DnaJ recruits protein to DnaK while GrpE helps DnaK release substrate by exchanging nucleotide bound to DnaK (Bukau et al, 1998).

With time, it was discovered that homologues of DnaK, DnaJ, and GrpE could be found ubiquitously. This greater family of structurally and functionally conserved proteins came to be known as the Hsp70 chaperone system, which consists of an Hsp70, DnaK, an Hsp40, DnaJ, and a nucleotide exchange factor, GrpE. The conservation of this molecular chaperone system throughout life came to become a reflection of the importance of these proteins to all cells (Morano, 2007). Indeed, these proteins have not only been found to be important in regulating various native protein systems, but also in preventing protein aggregation, assisting in protein folding, and in disassembling non-native protein aggregates (Mayer et al, 2005). Because of its importance in non-native protein aggregation, this protein will be the focus of our deeper discussion of chaperone activity.

The Hsp70 Molecular Chaperone Family

Molecular chaperones are commonly referred to as “heat shock proteins” and are generally denoted by the abbreviation Hsp, followed by the average molecular weight of the chaperone in kilo-Daltons. The members of the Hsp70 family of chaperones act as ATP driven molecular clamps. They are assisted in the binding and release of peptide substrates by two main co-chaperones: the peptide recruitment co-factor, Hsp40, and a nucleotide exchange factor (Mayer et al, 2005). The binding of either co-factor stimulates conformational changes in Hsp70 that can alter peptide binding affinity (Mayer et al, 2005) and the rate of ATP hydrolysis (McCarty et al, 1995). In the ATP bound state, the Hsp70 peptide-binding domain is open and substrate can either bind directly to it or be recruited by Hsp40 (Kampinga et al, 2010), which stimulates the ATPase activity of Hsp70 (McCarty et al, 1995). After ATP hydrolysis, the lid of the peptide-binding domain closes on the recruited peptide and Hsp40 dissociates from Hsp70 (Schlecht et al, 2011). The peptide remains tightly bound to Hsp70 until ADP is removed by a nucleotide exchange factor (Brehmer et al, 2004). This allows Hsp70 to bind ATP and open its substrate-binding domain, releasing peptide from Hsp70.

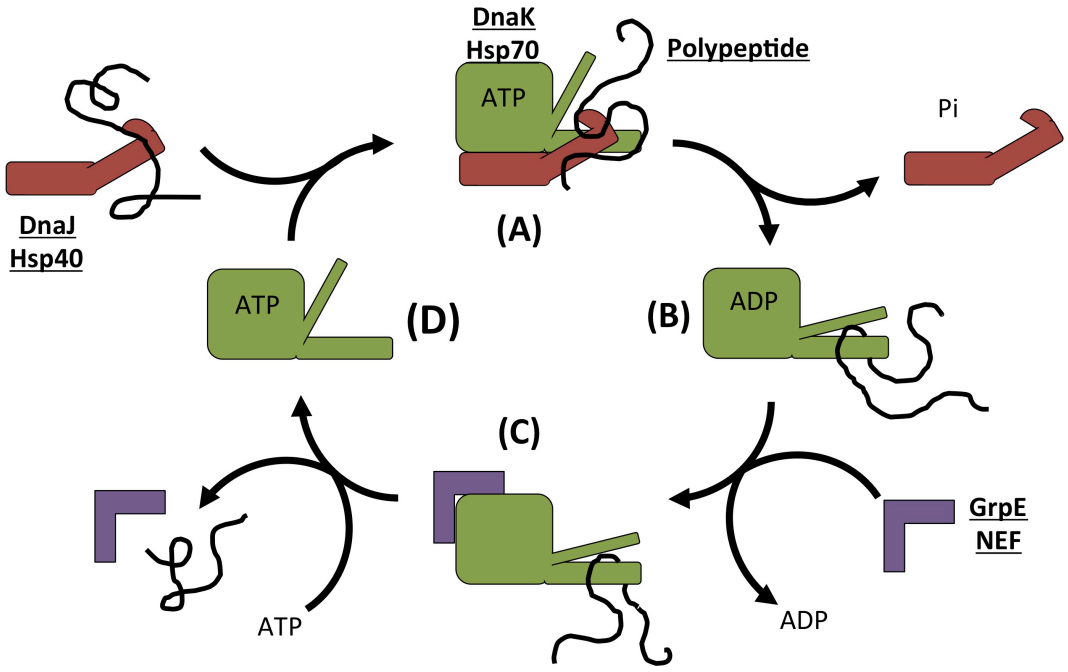

Figure 1-5 The Hsp70 Reaction Cycle. (A) First, Hsp40 binds to a polypeptide and then Hsp40 binds to Hsp70, which is bound to ATP. (B) Second, the binding of Hsp40 to Hsp70 stimulates the ATPase activity of Hsp70. Upon ATP hydrolysis, the polypeptide-binding domain of Hsp70 closes on the recruited polypeptide and Hsp40 disengages from Hsp70. (C) Third, the polypeptide stays bound to Hsp70 until a nucleotide exchange factor binds to Hsp70 and catalyzes the release of ADP. (D) Finally, ATP can bind to Hsp70, altering its conformation so that the polypeptide-binding domain of Hsp70 opens. This releases the nucleotide exchange factor and the polypeptide.

The Amino Acid Sequence Hsp70 Binds to is Normally Buried in Native Protein

Hsp70s are generally thought to recognize and bind to peptide sequences that contain a core of 4-5 hydrophobic amino acids, flanked by 3-4 positively charged amino acids (Rudiger et al, 1997). This amino acid sequence is extremely common in proteins and on average can be found in proteins every 30 to 40 amino acids (Rudiger et al, 1997). Furthermore, Hsp70s can be recruited to amino acid sequences, for which they have a low affinity for, by the Hsp40 co-chaperone (Rudiger et al, 2001). The peptide sequence that Hsp40s bind has diversified throughout evolution, however, Hsp40s normally bind to regions rich in hydrophobic amino acids. For the *E. coli* DnaJ protein, the target binding sequence appears to be composed of stretches of eight hydrophobic amino acids with aromatic and large aliphatic side chains. Although the binding sequence of DnaJ is generally hydrophobic, DnaJ can also tightly bind patches of amino acids that contain arginine (Rudiger et al, 2001). The combination of frequent Hsp70 binding domains and site recruitment by Hsp40s allows Hsp70s to be highly promiscuous and bind a wide range of proteins. Normally, Hsp70 binding sites are typically buried on the interior of native proteins and are thus not normally accessible by Hsp70s (Rudiger et al, 1997). Native protein substrates that do interact with Hsp70s either recruit Hsp70s with special co-evolved Hsp40s, or have evolved to maintain exposure of Hsp70 binding sites while in the native state (Rodreguez et al, 2008). Some Hsp70s also possess

specialized domains, such as the EEVD and TPR domains, that are used to interact with other adaptor proteins and chaperones such as HOP and Hsp90 (Brinker et al, 2002).

Possible Mechanisms for the Activity of Hsp70 Chaperones

The binding of a protein by the Hsp70 substrate-binding clamp is associated with unfolding or destabilization of native protein (Rodreguez et al, 2008), which in some cases is linked to the disruption of native protein complexes (Bocking et al, 2011). In some cases, Hsp70s can also disassemble aggregates of non-native proteins (Haslberger et al, 2010; Zietkiewicz et al; 2006). However, Hsp70s can assist in protein folding and prevent protein aggregation (Farr et al, 2003). How Hsp70s perform this wide range of activities through a simple cycle of substrate protein binding and release is not well understood. It has been postulated that Hsp70s use the same basic mechanism in all cases (Goloubinoff et al, 2007) and the specific effect of a given Hsp70 interaction on a particular protein depends upon the conformational dynamics and amino acid sequence of the target protein substrate.

The mechanisms proposed for the action of Hsp70s can be broadly categorized as either passive, where Hsp70 binding acts only to alter the equilibrium between different protein conformations (e.g. a Brownian Ratchet), or active, where conformational changes in Hsp70 generate mechanical forces

that drive directed-conformational rearrangements in a substrate protein. More recently, a variation on the classical Brownian Ratchet model has been proposed, in which the local dynamic restriction of an Hsp70 bound protein sequence results in a directed pulling force that alters substrate protein conformation (Goloubinoff et al, 2007; Nillegoda et al, 2015). This so-called "entropic pulling" force is thought to be capable of disrupting intra-protein interactions, thus leading to local unfolding or loss of inter-protein interactions, which then disrupt oligomer complexes. While the "entropic pulling" model offers the simplest explanation for the mechanism of Hsp70's activity, the possibility that the conformation of substrate protein is affected by structural changes in the Hsp70, such as the closing of the lid to the peptide binding domain, cannot be discredited due to a lack of experimental evidence.

When assisting in folding, Hsp70 is thought to not be directly involved in facilitating protein folding. Rather, Hsp70s are thought to either prevent substrate proteins from misfolding in the first place, or unfold misfolded proteins (Natalello et al, 2013; Scholl et al 2014), giving the substrate protein another chance at spontaneous folding. In support of this idea, Hsp70s have a limited ability to alter the structure of proteins on the folding path to the native state (Farr et al, 2003). While it is not the goal of this work to determine the actual mechanism that Hsp70s use, it is important to consider that the Hsp70s' simple system of binding and release has profoundly different effects on different

substrates.

Hsp70 is a Crucial Part of a Larger Disaggregation Chaperone Network

On their own, Hsp70s are thought to have a limited capacity for disaggregation. Nonetheless, Hsp70s are a crucial part of the cellular disaggregation network that works in concert with, and orchestrates the activity of, other molecular chaperones. Examples of other molecular chaperone systems that participate with the Hsp70s in protein disaggregation include the small Hsps (Ratajczak et al, 2009), Hsp100s (Haslberger et al, 2007), and Hsp110s (Nillegoda et al, 2015). The small Hsps (sHsps) are typically 10 to 30 kDa monomers that contain the highly conserved alpha-crystalline domains (Haslbeck et al, 2005). The sHsps are found ubiquitously in life and can co-assemble with aggregating non-native proteins. Aggregates that contain sHsps have a far greater chance of being fully disassembled by Hsp70s than those without (Ratajczak et al, 2009). However, it is not known if sHsps directly interact with Hsp70 or simply modify the structure of protein aggregates.

Hsp70s in most species of eubacteria, plants, and fungi form a bi-chaperone system with the Hsp100 chaperones, which are generally thought to be recruited to aggregates by Hsp70s (Mogk et al, 2015). Hsp100s are efficient disaggregases and members of the AAA+ ATPase family of proteins, which makes them relatives to chambered proteases like Clp (Haslberger et al, 2010).

Hsp100s form six subunit rings that act as ATP driven molecular threading motors and extrude substrate proteins through a central pore in the Hsp100 hexamer (Tessarz et al, 2008). In the absence of Hsp70s, the Hsp100s are generally not active in disaggregation. Hsp70s are thought to both target Hsp100s to the surface of protein aggregates and to regulate the Hsp100 ATPase activity by direct interaction with the Hsp100 M-domain (Haslberger et al, 2007; Mogk et al, 2015). The resulting Hsp70-Hsp100 bi-chaperone system possesses potent disaggregation activity. Surprisingly, Hsp100s are not found in higher metazoans. The absence of Hsp100 chaperones in higher metazoans is thought to be due to a genomic deletion event that occurred early in metazoan evolution (Erives et al, 2015). Interestingly, despite the lack of Hsp100s in higher metazoans, the disaggregation activity of Hsp70s appears to have been conserved, and the Hsp70 from humans can recruit and activate the Hsp100 from budding yeast (Shorter, 2011). However, the interactions between Hsp100s and Hsp70s can be specific, as the bacterial Hsp70s cannot activate eukaryotic Hsp100s (Glover et al, 1998).

In the absence of Hsp100, higher metazoans use Hsp110s to help Hsp70s clear non-native protein aggregates (Rampelt et al, 2012). Hsp110 is a eukaryotic-specific chaperone that is structurally homologous to Hsp70s, but has extra domains that allow Hsp110s to act as nucleotide exchange factors for Hsp70s (Schuermann et al, 2008). In higher metazoans, specialized Hsp40s

also seem to be able to form Hsp40-Hsp40 complexes and co-recruit multiple Hsp70s and Hsp110s to a specific location. It is thought that the recruitment of multiple Hsp70s and Hsp110s generates a larger centralized entropic pulling force that aids disaggregation (Nillegoda et al, 2015). Together, the Hsp70-Hsp110 system has been shown to clear aggregates in the absence of an Hsp100 chaperone (Rampelt et al, 2012).

The Current View of Hsp70 Mediated Disaggregation and the Limits of What is Known About the Hsp70s Disaggregation Activity

Since their discovery, Hsp70 proteins and their co-chaperones have been identified in a wide range of cellular processes. Their role in disaggregation was initially overshadowed by the Hsp100 family of chaperones. This was largely due to the significant increase in disaggregation and subsequent refolding observed in the presence of Hsp100s (Glover et al, 1998; Parsell et al, 1994, Sanchez et al 1992). This led many to classify Hsp100s as the primary cellular disaggregase chaperones (Weibezahn et al, 2004; Mogk et al, 2004), despite the failure to identify an Hsp100 homologue in higher metazoans, including humans. During this time, researchers continued to unravel the mysteries of the intricate machinery of the Hsp100 chaperones while hoping that an Hsp100 homologue would eventually be found in humans and that Hsp100 research in other organisms would directly translate to a better understanding of disaggregation in humans (Weibezahn et al, 2004; Mogk et al, 2004; Schirmer et

al, 1997; Shorter, 2007; Bianco et al, 2008). However, detailed genomic studies would lead to the discovery that the metazoan line that gave rise to higher metazoans not only lacked an Hsp100 homologue, but various other enzymes and metabolic proteins that were found throughout lower metazoans (Westbrook et al, 2008; Shorter, 2011; Erives et al 2015). It was hypothesized that a massive genomic deletion event occurred early in the evolution of higher metazoans and that this event deleted the Hsp100 gene from the metazoan genome. Within the past few years, James Shorter and Bernd Bukau independently discovered that metazoans could clear non-native protein aggregates with nothing more than the Hsp70 chaperone system and the Hsp110 chaperone (Shorter, 2011; Rampelt et al, 2012). Interestingly, the activity of the metazoan Hsp70/Hsp110 systems was found to be not as efficient as the well-studied bacterial Hsp70/Hsp100 chaperone systems.

In 2015, the labs of Bernd Bukau and Richard Morimoto collaboratively found that efficient disaggregation and folding in metazoans is dependent on the presence of two different Hsp40 homologues. Their work found that two different Hsp40 homologues could form larger oligomer complexes that they believed could simultaneously recruit multiple Hsp70s and Hsp110s to a single region of an aggregate (Nillegoda et al, 2015). In the same work, Bukau and Morimoto postulated that the two Hsp40 homologues recruited Hsp70s to two different types of aggregates and that the hetero-oligomer may have a novel

specificity for certain aggregates. They tested this hypothesis by using gel-filtration columns to quantify aggregate populations, before and after exposure to molecular chaperones. From their observations, they concluded that one Hsp40, classified as type B, recruits Hsp70 to large aggregates and the other Hsp40, classified as type A, recruits Hsp70 to small aggregates. They also concluded that a mixture of the two Hsp40s would allow Hsp70 to be recruited to intermediate sized aggregates. However, their conclusions were predicated on the assumption that large aggregates that could be disassembled would be completely disassembled to monomer when the type B Hsp40s were used to recruit Hsp70s. This assumption removed from their conclusions the possibility that large aggregates were disassembled into intermediate and small sized aggregates with type B Hsp40s, which would have negated the possibility that Hsp40s can bind to aggregates based upon their size.

At this turning point in the field, the role of Hsp70s in disaggregation is being revisited. The activity of the Hsp70 systems is considered passive, unlike the active threading activity of the Hsp100s. If true, this would mean that Hsp70 mediated disaggregation is very dependent upon the strength of inter-molecular interactions between aggregate subunits and possibly intra-molecular interactions within each aggregate subunit. However, solutions of aggregating non-native proteins are often heterogeneous and possess a broad range of sizes, shapes, and structures. This can make a detailed study of the

relationship between aggregate qualities and their disaggregation potential difficult. This is in part due to the limitations and constraints of contemporary methodologies.

Constraints to Current Methodologies Used to Study Protein Aggregates

The dynamic features of heterogeneous macromolecule solutions are often lost in ensemble measurements where measurements yield only an average of all populations in solution. Additionally, protein disaggregation is commonly studied by monitoring the recovery of protein activity. Unfortunately, this method monitors folding as opposed to directly studying disaggregation. Alternatively, the use of separation methods (e.g. gel-filtration) can severely perturb the system under study and can alter delicate molecular structures (Philo et al, 2006).

In gel-filtration chromatography, objects are flowed over a resin composed of porous beads. Objects that are small enough to fit into the pores will do so, while larger objects will not. Objects that enter pores in the resin will flow more slowly, while larger objects transit more quickly through the resin. This simple method is commonly used to study the size of protein oligomers and was used by Bukau and Morimoto to test if Hsp40s select aggregates by their size. However, this method cannot study size changes in real time, the analysis can take on average 30 minutes to run, non-equilibrium conditions can drive

changes in state distributions, proteins adsorb to size-exclusion resin in non-uniform ways, and shear stress can develop as a result of solution flow through the column. While the first two problems can often be disregarded when working exclusively with endpoints in an assay, protein adsorption and shear stress are ever-present problems in gel-filtration chromatography.

Proteins can be driven to adsorb, or adhere, to surfaces by their shape and exposure of both their hydrophobic and hydrophilic amino acids, which can vary with conformation (Andrade et al, 1986). The amount of native protein that adsorbs to a column can be consistent and thus predicted in later experiments (Kongsberg et al, 1977). However, even minor changes in the conformation of native proteins can have large impacts on adsorption potential (Wang et al, 2011). Another compounding factor is that adsorption of protein, even when reversible, can alter the conformation of proteins (Wang et al, 2011; Moskovitz et al, 2014; Felsovalyi et al, 2012). This makes the study of non-native protein aggregate, that have been exposed to molecular chaperones, difficult. Not only can chaperones stay bound to aggregates, and change their absorption potential, but also chaperones can alter the structure of aggregates and the conformation of their subunits. In addition to adsorption, shear forces, or forces produced when a particle is flowed past a surface, can alter the conformation of proteins (Stasio et al, 2010). Interestingly, shear forces found in blood vessels can also affect protein conformation. Additionally, the resins used in column

chromatography can compound this issue as large particles can experience shear degradation when caught in the narrow spaces of a resin (Trathnigg, 2000).

Alternatively, fluorescence based single-particle methods are minimally perturbing techniques that can resolve the dynamic species distributions of heterogeneous macromolecule populations in free solution (Bieschke; 2000). The most common single-particle techniques utilize the fluorescence intensity fluctuations of highly concentrated fluorescent objects to differentiate fluorescent sub-populations by either their diffusion rate or brightness (Chen et al, 2003; Muller et al, 2000). At low concentrations, large objects, which diffuse slowly, can dominate diffusion-based measurements, even when they represent a small fraction of the total population. Under these conditions, the intensity fluctuations of fluorescent particles are not well described by a Poisson distribution, a necessity for a traditional brightness analysis (Chen et al, 1999). Additionally, protein aggregation can be too rapid at the object concentrations required for fluorescence fluctuation based assays. For this reason, traditional fluctuation methods are not well suited for the study of highly complex and heterogeneous systems, such as those found when non-native proteins aggregate.

Burst Analysis Spectroscopy is a Suitable Method for Studying Non-Native Protein Aggregates

A complementary approach to current methodologies, termed Burst Analysis Spectroscopy (BAS), was developed to quantify the brightness and concentration of fluorescently labeled species with broad size distributions, in free solution and at low concentrations (Puchalla et al, 2008). BAS utilizes advective sample flow in combination with confocal microscopy to examine the intensity distribution of dilute (10-100 pM) fluorescent objects as they transit the detection zone of the microscope at a rate substantially faster than diffusion. Under these conditions, objects do not linger or diffuse within the excitation volume during a measurement, as they would with a fluctuation-based analysis. Instead, objects transit unidirectionally through the excitation volume and produce their peak fluorescence as they cross the central plane of the excitation volume. Where a fluorescent object crosses the central plane of the excitation volume also impacts the amplitude of the observed fluorescence peak (Figure 1-6 A). This makes it difficult to distinguish between a bright object crossing the edge of an excitation volume and a dim object crossing directly through the center. This problem can be addressed numerically with a simple analysis strategy that employs information about the experimental point spread function of the microscope to correct the observed burst distribution for crossing trajectory (Puchalla et al, 2008) (Figure 1-6 B). In order to do this, objects are logarithmically binned by their intensity.

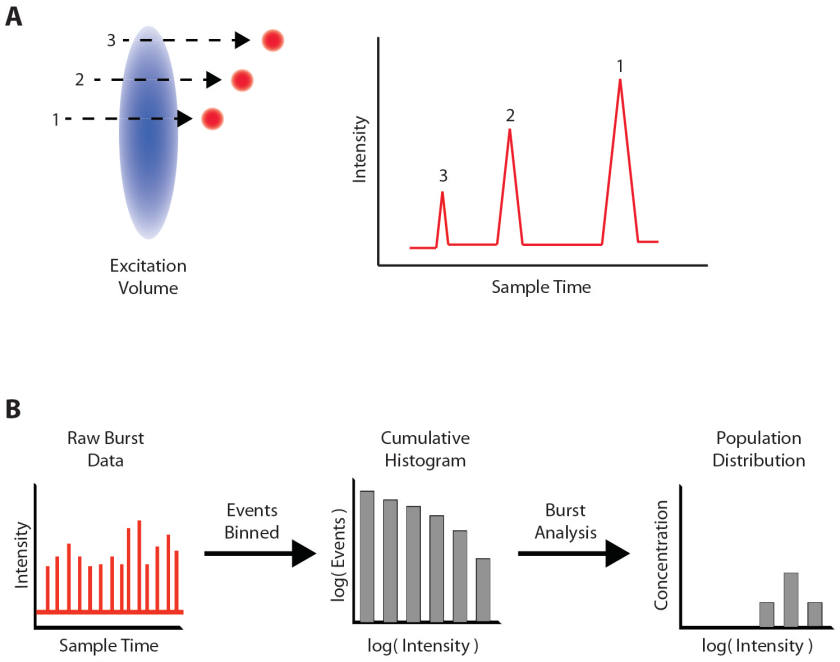

Figure 1-6 Burst Analysis Spectroscopy (BAS) Measures the Size Distribution of Fluorescent Species in Free Solution. (A) BAS requires objects in a dilute solution transition unidirectionally through the excitation volume of a confocal microscope at a rate faster than particle diffusion (*left*). The burst intensity of single fluorescent particles (*right*) is a function of both the intrinsic particle brightness and the crossing trajectory of the particle through the excitation volume. (B) Logarithmic binning of bursts in both intensity and frequency results in a raw burst distribution tat is equivalent to the cumulative distribution of all observed crossing events (*center*). Bursts in the highest intensity of this cumulative distribution contain information about the brightest objects as they transverse the center of the detection region. This information, in combination with knowledge of the microscope characteristic function, can be used to reconstruct the particle intensity distribution (*right*)

The analysis works by first characterizing the brightest observed burst in the highest intensity bins with the explicit assumption that these bursts are derived from the brightest object crossing through the center of the excitation volume. The contribution of this object to lower intensity bins is calculated and subtracted from all lower intensity bins. The contribution of object to all lower intensity bins, as a result of crossing trajectories through regions of lower excitation power, is best fit by a power law. The brightest events are thus fit to a power law equation, their contribution to lower intensity bins is then calculated, and then the contribution is to each bin is subtracted. After the first correction, the contribution of the second brightest bin to all lower intensity bins is calculated. These values are then subtracted from all lower intensity bins and the process is then repeated until all bins have been corrected (Figure 1-7 A-C). The end result is a corrected burst histogram that estimates the number distribution for each fluorescent species in a complex mixture.

Preliminary measurements demonstrated that BAS is a potentially powerful way to study heterogeneous and dynamic macro-molecular systems such as those found when non-native proteins aggregate (Puchalla et al, 2008). However, as originally implemented, BAS has a restricted dynamic range (~100-fold in burst intensity), imposing significant limits on the types of measurements and systems that can be examined. Chapter III of this work demonstrates a method that can be used to extend the dynamic range of BAS by at least

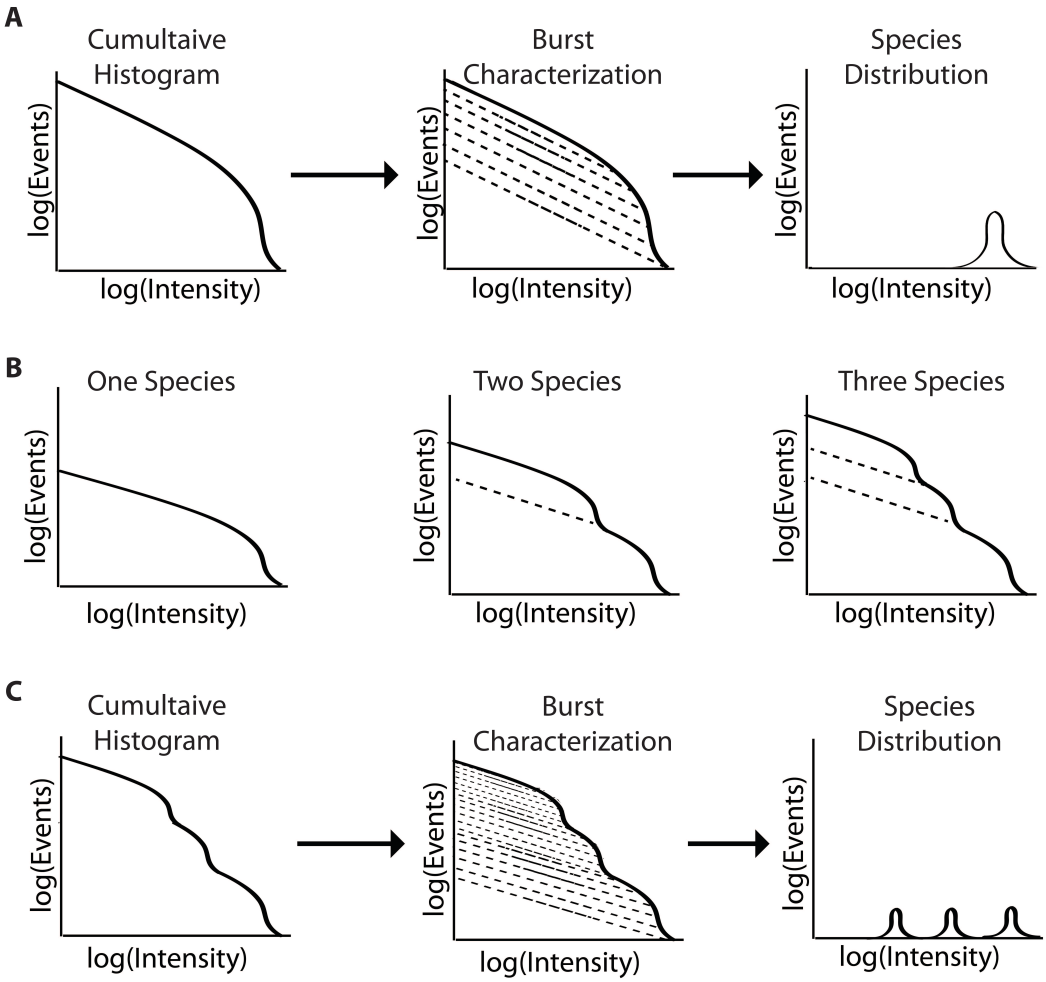

Figure 1-7 Correcting the Cumulative Burst Histogram. A double log plot of burst events that have binned by their intensity is shown in (A) (Left). The plot is a cumulative histogram for a single fluorescent species. (Middle) The underlying species distribution can be calculated by first characterizing the contribution of higher intensity bins to lower intensity bins. (Right) The single underlying species is shown after the cumulative histogram is corrected. (B) Each fluorescent species adds to the cumulative plot in a predictable way. The combined cumulative burst histogram for three fluorescent species is just a sum of the individual burst plots for each fluorescent species. (C) In order to extract separate species distributions for each sub-species, the same correction is done.

another order of magnitude. The usefulness of this approach will be illustrated through its application to a case study of epsin-mediated membrane fission in Chapter IV (Shoup et al, 2015). It will also be shown in Chapter III that BAS can be extended to simultaneously study multiple fluorescent probes permitting a highly sensitive multi-channel analysis. The power of this multi-probe extension of BAS will be demonstrated through two, well-defined case studies in Chapter III. These enhancements to the basic BAS approach, in combination with traditional BAS, are applied to a detailed study of protein disaggregation by molecular chaperones in Chapter V.

Identification of a Good Model Substrate Protein for Studying Disaggregation

In order to fully understand the impact of structure on aggregate disassembly by molecular chaperones, the exact structure of different protein aggregates would have to be determined in detail. However, the heterogeneous and dynamic nature of non-native protein aggregates are immense hurdles for such studies (Tanaka et al, 2015). An alternate approach would require comparing chemically identical, but structurally distinct, aggregates. To date, most disaggregation studies have examined chaperone-dependent disaggregation with very different substrate proteins (Natalello et al, 2013), which makes the correlation between structural elements of aggregates and disaggregation difficult or impossible. In one case, disaggregation of a single

protein, which was forced into different aggregated states, was examined (Lewandowska et al, 2007). In this case the structurally distinct aggregates were generated by denaturing the target protein and growing aggregates under different buffer conditions, which altered chaperone activity and biased the observations (Kummer et al, 2013). In this work, temperature is used to control the aggregation of the RuBisCO protein from *R. rubrum* and to generate aggregates that differ in structure and growth kinetics in the same buffer. RuBisCO makes an ideal substrate because it aggregates easily and has been engineered with many non-pertubative cysteine mutants that can be labeled with exogenous fluorescent probes (Rye et al, 1997; Rye et al, 1997; Lin et al, 2008; Lin et al, 2004). The qualities of RuBisCO aggregates, as generated by this method, are explored in more detail in Chapter V.

Studying RuBisCO Disaggregation with the DnaK-ClpB Bi-Chaperone System

In this work, the Hsp70-Hsp100 bi-chaperone system from *E. coli*, known as DnaK-ClpB, is employed as a model disaggregation network to examine the impact of RuBisCO aggregate size and structure on disaggregation. To date, RuBisCO has been well studied as a folding substrate of the GroEL/ES proteins (Lin et al, 2004), the Hsp60/Hsp10 foldase chaperone system from *E. coli,* but has only been studied in a few papers as a substrate for the DnaK-ClpB chaperone system. Prior to this work, it was known that expressing soluble

RuBisCO in *E. coli* required ClpB, which implies that RuBisCO is a substrate of both ClpB and DnaK (Thomas et al, 2000). In chapter V, the impact of RuBisCO aggregate structure on DnaK and ClpB disaggregation activity will be explored.

CHAPTER II

DEVELOPMENT AND APPLICATIONS OF EXTENDED RANGE AND MULTI-DIMENSIONAL BURST ANLYSIS SPECTROSCOPY

Summary

Complex molecular assemblies are ubiquitous in biological organisms and are central to a wide range of critical phenomena. However, the heterogeneous and dynamic nature of these structures often makes them challenging to study. The single-particle fluorescence spectroscopy technique known as Burst Analysis Spectroscopy (BAS) was developed to facilitate real-time measurement of macromolecular size distributions in a minimally perturbing, free-solution environment (Puchalla et al, 2008). Here, we develop two enhancements of the BAS method that substantially extend the capabilities of this method. We first show that particle size distributions, within three orders of magnitude, can be reliably quantified by combining two or more overlapping burst distribution measurements (cBAS). We then develop and validate a multi-channel extension of BAS (MC-BAS), in which correlated fluorescent bursts from multiple spectrally distinct probes are used to simultaneously examine relative size and binding stoichiometry distributions. As examples of the utility of cBAS and MC-BAS, we apply these techniques to (1) quantify lambda phage particle subpopulations that display aberrant DNA loading and (2) test models for fibroid protein aggregate growth.

Introduction

Biological systems are dependent on the assembly and disassembly of macromolecular complexes. However, the dynamic and heterogeneous nature of these structures can make them challenging to study with ensemble methods (Hernandez et al, 2011; Tanaka et al, 2015). Fluorescence-based techniques are sensitive enough to detect the light from a single fluorescently labeled particle and are thus powerful tools for studying the dynamic behavior of complex macromolecular systems (Chen et al, 2003; Muller et al, 2000). Unfortunately, sub-populations in highly heterogeneous macromolecule systems can be challenging to quantify with traditional fluorescence-based single particle methods. To address this problem, a fluorescence technique known as Burst Analysis Spectroscopy (BAS) was developed (Puchalla et al 2008). BAS can estimate the population distribution of complex particle assemblies and track dynamic changes in these distributions, under minimally perturbative, free solution conditions.

During a BAS measurement, a solution containing fluorescent objects is advectively flowed through the detection volume of a confocal microscope at a bulk rate faster than macromolecule diffusion. This configuration results in objects moving unidirectionally through the excitation volume (Puchalla et al, 2008). At sufficiently low concentrations (<100 pM), the resulting burst amplitudes are a combination of (1) the intrinsic brightness of the object, which

is related to particle size, and (2) the point at which the object crosses the microscope detection volume (Figure 1-6 A). The convolution of these two parameters (size and crossing trajectory), presents a conundrum: how can a bright object crossing the edge of the excitation volume be distinguished from a dim object crossing directly through the center of the excitation volume without knowing the size of objects in solution *a priori*?

This problem is solved by first logarithmically binning the experimentally observed burst intensities and their occurrence frequency. Burst frequency is then plotted against burst intensity to produce a raw burst distribution plot (Figure 2-1 B) that is equivalent to the cumulative distribution of all excitation volume crossing events for all fluorescent species. This plot is referred to as the cumulative histogram. The shape of this plot is dictated by the characteristic function of the measurement system (Puchalla et al, 2008), which is a fixed property of the optical system and detection strategy employed. With a confocal microscope, a simple power law describes the cumulative crossing distribution (in log-log space) of a pure, single species of fluorescent objects (Puchalla et al, 2008). Importantly, the same characteristic function also describes the burst distribution of each additional fluorescent species in a heterogeneous population, except each power law equation varies by a coefficient that accounts for differences in relative concentration. Thus, a mixture of fluorescent species will, generate a cumulative burst distribution plot that is the sum of the individual

power law equations for each fluorescent species it contains (Puchalla et al, 2008).

In order to reconstruct the underlying species distribution from the cumulative burst distribution, the concentration of at least one species in the sample must be established. In principle, the largest bursts observed during a BAS measurement should only come from the brightest object passing near the center of the excitation volume, where excitation and detection are maximal. With sufficiently robust sampling, the brightest bin of the cumulative burst distribution provides direct concentration information about this brightest species (Puchalla et al, 2008). In combination with the established characteristic function of the microscope, the contribution of the brightest species to all lower intensity bins of the raw burst distribution can then be calculated. Once the contribution of the brightest object are accounted for, any bursts that remain in the next brightest intensity bin must come from distinct species of particles. This process can be repeated until the intensity distribution for the total population has been calculated (Figure 1-6 B). Provided the size of each species is directly proportional to its fluorescence intensity, the recovered brightness distribution can then be easily converted to a size distribution.

While simple, flexible and robust, the original implementation of BAS is subject to a significant set of limitations. First, classical BAS cannot reliably

measure particle distributions if the size range the object intensities span a range greater than approximately 100-fold (Puchalla et al, 2008). A particularly serious problem arises when a very dim object is present in the same solution as very bright objects. Error propagation and fitting variability during the analysis of the brightest objects can have a large downstream effect on the analysis of dim objects. Thus, mixtures of macromolecular complexes that span a wider size range, like protein aggregates, can contain important small populations that are inaccessible to a BAS analysis. Second as a single-particle technique, BAS requires that the concentration of objects remain below a threshold (~100 pM) where individual bursts can be reliably assigned to single objects. In many cases, the disassembly of a starting particle population, which may initially satisfy this concentration constraint, can result in concentrations of products that that are far too high for a quantitative analysis by BAS. A symmetric problem exists for binding and assembly reactions. Third, because BAS was initially validated only as a single-channel technique, questions involving simultaneous assembly of multiple different components cannot be easily addressed. While collection of BAS data in multiple spectral channels is implicit in the original description of the method (Puchalla et al, 2008), precisely how such multi-dimensional BAS data are to be quantitatively analyzed, and what types of information can be extracted, has not been explored.

Here we overcome these limitations by developing procedures that permit

a substantial expansion in the addressable size range for BAS. We then develop methods for the collection and analysis of multi-channel BAS data sets. These extensions to the core BAS methodology are first validated with a set of well-established fluorescent standards and are then explored in two biologically relevant case studies.

Methods

Protein Expression and Purification

Wild-type RuBisCO was expressed and purified as previously described (Lin et al, 2008; Lin et al, 2006).

YFP Lambda Phage and Ghost Phage Purification

In order to produce pure YFP lambda phage, a YFP fusion of the lambda capsid protein, gpD, was incorporated into assembling phage during the lysis of the LE392(λ_{LZ1}) *E. coli* strain and subsequently purified after lysis as previously described (Zheng et al, 2011). The YFP lambda phage used in this work was a generous gift from Chanda Bhat of the Zheng lab. The culture was then warmed to 42°C to induce the lambda lytic cycle. YFP lambda phage were then transformed into ghost phage, by forcing them to eject their DNA, and purified as was described previously (Konopa et al, 1975).

Protein Labeling

Wild-type RuBisCO was fluorescently labeled with Alexa488 or Alexa647, both of which are thiol-reactive dyes that were obtained from Invitrogen, at Cys58 as previously described (Rye et al, 1999; Lin et al, 2008; Lin et al, 2006). The efficiency of labeling, for both RuBisCO-58Alexa488 and RuBisCO-58Alexa647, was determined to be ~100% as previously described (Madan et al, 2008; Rye, 2001). The conjugation specificity was determined as described previously (Lin et al, 2006; Lin et al, 2004; Rye, 2001).

DNA Labeling

Dimeric intercalating cyanine dyes were used to transform double stranded DNA (dsDNA) into novel two-color fluorescent standards that could be used to test the resolution of MC-BAS and label the genomic DNA of lambda phage. TOTO-3 and YOYO-1 were bound to DNA by following modified methods from previously published protocols (Rye et al, 1992b; Rye et al, 1992a; Rye et al, 1993a; Rye et al, 1993b; Clarke et al, 1993; Bowen et al, 2003). The total concentration of dye was also kept below 100 nM and the ratio of base pairs to dye never exceeded 5 to 1 in order to prevent cross-bridging (Rye et al, 1992b). DNA labeling was conducted by mixing a given cyanine dimer with a target DNA sample in TE or TAE buffer and incubating for 30 min. The labeled DNA used for standards was produced by cleaving the pProex-DnaK plasmid with NarI, which cuts a single time. The resulting linearized

plasmid was gel purified prior to use. TOTO-3 and YOYO-1 were incubated with linear dsDNA at a base pair to dye ratio of either 10 to 1 or 20 to 1. The final concentration of each labeled DNA population was typically 30 pM when analyzed separately or mixed together. Lambda phage DNA was labeled by incubation with TOTO-3 so that the labeling ratio of genomic DNA was 10 to 1 base pairs to dye. DNA labeling reactions were carried out for 1 hr for lambda phage DNA.

Fluorescent Bead Set-Up

Fluorescent nanospheres of defined sizes were employed as BAS calibration standards to demonstrate the effectiveness of cBAS and MC-BAS. Yellow-Green nanospheres were used in all cases and each had an excitation and emission of 505 and 515, respectively. FluoSphere nanospheres, sold by Invitrogen with 20 nm, 40 nm, and 100 nm diameters, were obtained as 2-5% solid suspensions. Fluoro-Max nanospheres, sold by Duke Scientific with 40 nm and 75 nm diameters, were obtained as 1% solid suspensions. All nanosphere samples were diluted to 100 pM in pure water when analyzed individually. Fluoro-Max 40 nm and 75 nm beads were diluted to 66 pM each when mixed together. FluoSphere 20 nm, 40 nm, and 100 nm beads were diluted to 50 pM each when mixed together.

Microscope Set-Up and Data Collection

The single particle detection platform was configured essentially as described previously (Puchalla et al, 2008), with the following modifications. The system is built on a research quality, vibrationally isolated 4'x8' optical table, and is constructed around a Nikon Eclipse Ti-U inverted microscope base using a 60x/1.4NA CFI Plan Fluor oil immersion objective. The microscope base is outfitted with a precision, 2-axis stepper motor sample stage (Optiscan II; Prior) and a custom-designed confocal bench with three independent detection channels. Each detection channel is configured with an optimized band-pass filter set for wavelength selection and a low-noise, single photon counting APD unit (SPCM-AQRH-15; Excelitas). Photon pulses are collected and time stamped with either a multichannel hardware correlator (correlator.com) or high speed TTL counting board (NI9402; National Instruments). The samples excitation is provided by either one or a combination of three lasers: two diode lasers (488 nm and 642 nm; Omicron) and one diode-pumped solid laser (561 nm; Lasos). The free-space beams of each laser are each coupled to a 3-channel fiber combiner (PSK-000843; Gould Technologies) and the combined output is directed into the sample objective with a custom, triple-window dichroic filter (Chroma). Each laser is addressable from the integrated control and data acquisition software, custom developed using LabView (National Instruments). The coverslip cassette was clamped to a high precision, computer controlled, 2-axis translation stage connected to a customized microscope system, and data

were collected as previously described (Puchalla et al, 2008; Krantz et al, 2013). Coverslip assemblies were rotated at 500 μm/s. Photon arrival time data was binned using 500 ms bins. Burst data was collected for anywhere from 3 to 40 min. Coverslips were cleaned in Helmanex and then thoroughly rinsed with water before being blocked in 1-2 mg/mL BSA for 30 min. Blocked coverslips were gently rinsed in water before being dried under a stream of dry nitrogen gas. Sample volumes ranged from 10 to 15 μL and samples were kept from evaporating on the coverslip by covering the sample with a sensitive humidity-regulating chamber.

Heat Maps

In this work, heat map plots were used to compare numerous data sets, typically histograms, in a way that is easy to visualize. All single-color BAS data was placed in rows where each square represents a bin from a histogram. For two-color BAS data, a grid is first constructed with an equal number of rows and columns. In this grid, the squares that run along the diagonals represent bins from separate histograms. The center diagonal runs from the bottom left square to the upper right square of the grid and each of the other diagonals in the grid run parallel to the center diagonal. In two-color BAS, each histogram represents a different fluorescence ratio, which correlates to a different binding ratio between two objects labeled with different fluorescent probes. Each histogram runs along the grids parallel diagonals because the bins are on logarithmic

scaling and appear linear. If the bins were linearly scaled, the diagonals would possess different slopes and would appear to all intersect at the bottom left of the grid.

Results

Data Can Be Concatenated to Increase the Analyzable Size Range of BAS

When a solution contains very bright and very dim objects, dim objects can be difficult to analyze. However, diluting a sample can make dim objects easier to analyze at the cost of being able to properly analyze bright objects. A simple solution to this problem is to concatenate the burst data from concentrated and diluted samples together before burst analysis. However, a region of optimal overlap between the data sets, as well as the precise dilution factor, must first be determined. In order to do this, the cumulative histograms for both the concentrated and diluted samples are generated with the same number of bins and the same minimum and maximum intensity range (Figure 2-1 A). The histograms from samples taken at different dilution are then divided by one another to generate a histogram ratio (Figure 2-2 B). Next, the average and standard deviation for the ratio of the first five bins of the histogram are calculated. The average and standard deviation are then repeatedly calculated using a sliding window, five bins wide, over the entire ratio histogram. The bin with the lowest standard deviation is the point of concatenation, while the average at this point yields the precise dilution factor (Figure 2-1 B). The bins

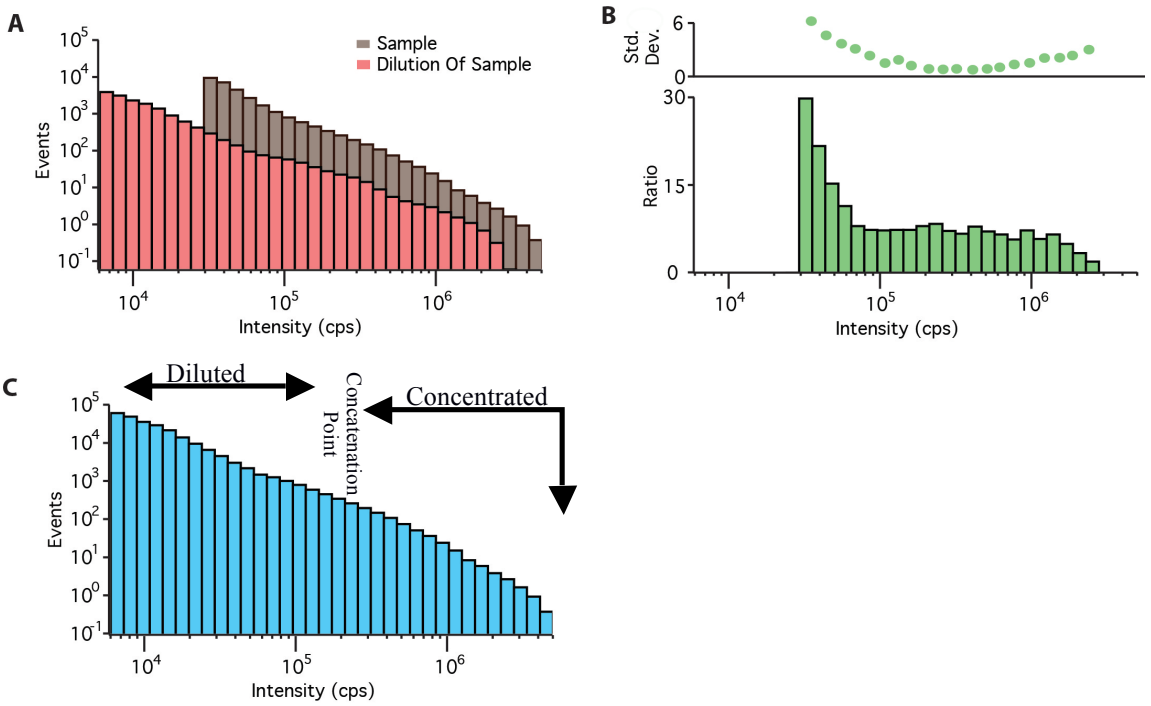

<u>Figure 2-1</u> BAS Data Can Be Concatenated in Order to Improve the Size Range of Fluorescent Species That Can Be Simultaneously Burst Analyzed. (A) Cumulative histograms of a mixture of particles spanning more than two orders-of-magnitude in size, where the smallest objects are present at a much higher concentration than the largest objects. Typical BAS measurement conditions permit good sampling of the largest objects (*gray*) but result in poor or inaccessible measurements of the smallest objects. Dilution permits high-quality sampling of the smallest objects, but results in severe under-sampling of the largest objects. Reconstruction of the overall particle distribution is possible when the two BAS data sets are linked through their overlap region. (B) The optimal sampling overlap is established by first examining the cumulative histogram ratio for the two individual samples (*bottom*). Next the point at which the standard deviation, contained in the overlap region, was minimized was determined (*top*). (C) By exploiting information contained in the overlap region, along with knowledge of the sample dilution factor, the total cumulative histogram can be reconstructed to generate a concatenated BAS (cBAS) data set.

from the histogram for the diluted sample are then multiplied by the dilution factor. Below the concatenation point, the bins in the concentrated sample are replaced with the bins from the diluted sample that were corrected by the dilution factor. This concatenated cumulative histogram can then be burst analyzed (Figure 2-1 C). In total, we refer to this method as concatenated BAS or cBAS.

cBAS Resolves 20, 40, and 100 nm Fluorescent Bead Standards

In order to validate cBAS and examine its potential benefits, 20 nm, 40 nm, and 100 nm fluorescent beads were analyzed with and without cBAS. The particular distributions for 20, 40, and 100 nm beads, examined individually, are all well resolved by a traditional BAS analysis (Figure 2-2 A). When all three beads are mixed at equal concentrations, the 40 nm and 100 nm beads are visible, thought the left side of the 40 nm distribution is distorted and difficult to specify. The distribution for the 20 nm beads cannot be determined at all, as the signal for the smallest beads is indistinguishable from noise (Figure 2-2 B). Conversely, cBAS allows all three-bead populations to be readily resolved and their population distributions correctly specified (Figure 2-2 C).

A Method for Analyzing Multi-Color Experiments by BAS That Preserves Binding Information

If a particle composed of two different fluorescent probes passes through the excitation volume of a BAS microscope that is configured with two, co-

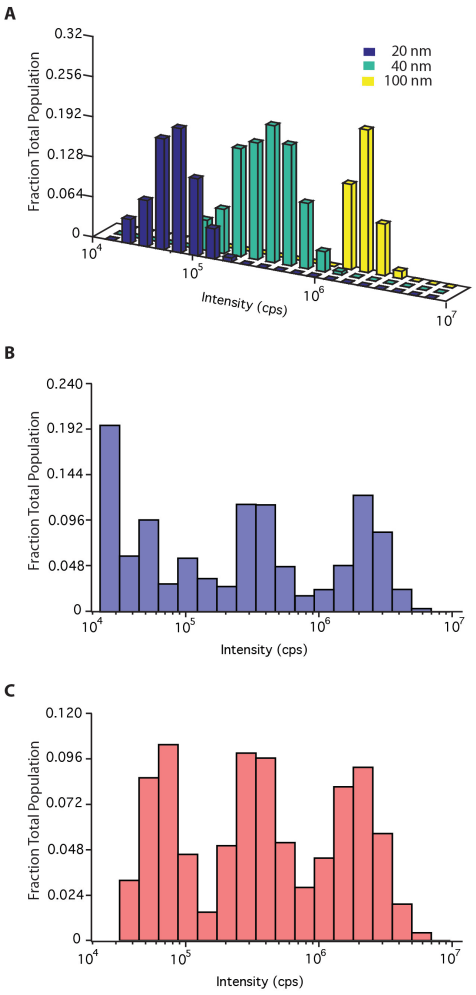

Figure 2-2 cBAS Accurately Recovers the Population Distribution of a Mixture of 20, 40, and 100 nm Fluorescent Nanospheres. (A) Conventional BAS analysis of three separate samples containing single populations of fluorescent nanospheres. (B) Calculated population distribution of a 1:1:1 mixture of 20, 40, and 100 nm nanospheres from conventional BAS. (C) Examination of the same nanosphere mixture using systematic dilution and cBAS permits much more accurate reconstruction of the total poulation distribution.

Figure 2-3 The Conceptual Basis of Multi-Channel BAS (MC-BAS). (A) Raw burst plot for a theoretical sample composed of two interacting particles labeled with two, spectrally distinct fluorescent probes. The fluorescence signal from each probe is measured with two co-aligned excitation lasers and two separate detection channels (*blue*, channel 1; *red*, channel 2). (B) When particles assembled from different monomers cross the excitation region (*left*), they produce correlated fluorescence bursts in both channels (*center*). As with conventional BAS, the absolute burst amplitude varies in each channel as a function of both size and crossing trajectory. However, the ratio of fluorescence between two probes does not vary with crossing trajectory (*right*). The MC-BAS analysis begins by identifying and categorizing particles by their fluorescence ratio. The burst intensity distribution from each input channel, for a given intensity ratio, is then examined by BAS and plotted in a two-dimensional heat map (C, *left*). Lines of fixed intensity ratio are along the positive diagonal and divide the resulting MC-BAS heat maps. The lines run parallel to each other due to the logarithmic scaling. As an example, two theoretical populations of doubly labeled objects are illustrated, where the relative probe stoichiometry differs by 2-fold. One particle population consists of smaller, more tightly distributed co-assemblies (I). The second population is larger, more widely distributed, and centered at a different relative monomer stoichiometry (ii). The BAS intensity distributions in each detection channel are also shown as one-dimensional histograms (*center* and *right*). Note that the shape and width of each histogram captures information about the population distribution, while the position of the two histograms relative to one another is a function of the monomer stoichiometry for each particle.

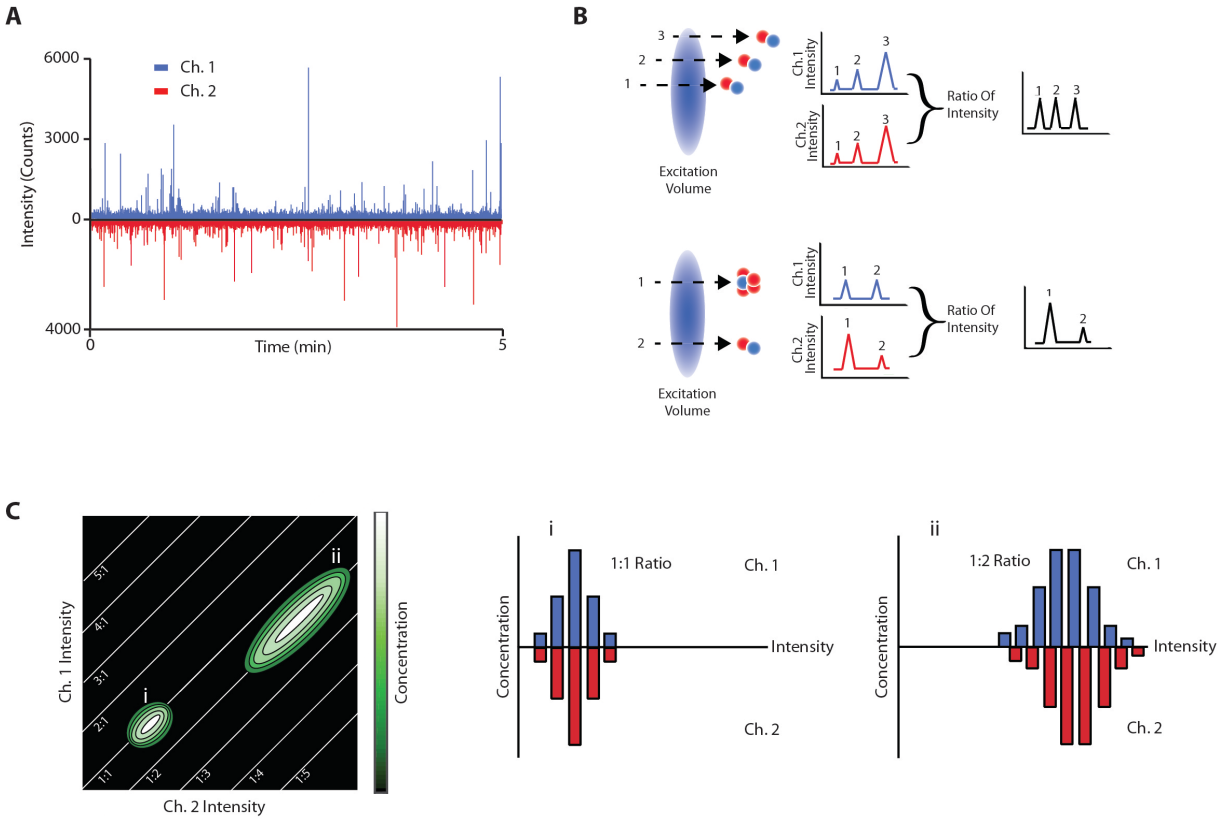
A
6000
3000
0
4000
Intensity (Counts)
Ch. 1
Ch. 2
0
Time (min)
5
B
3
2
1
Excitation Volume
Ch.1 Intensity
Ch.2 Intensity
Ratio Of Intensity
1
2
C
Ch. 1 Intensity
Ch. 2 Intensity
Concentration
5:1
4:1
3:1
2:1
1:1
1:2
1:3
1:4
1:5
i
ii
1:1 Ratio
1:2 Ratio
Ch. 1
Ch. 2
Intensity
Concentration

aligned excitation lasers, the fluorescence intensity from each probe can be separately recorded in two, separate detection channels (Figure 2-3 A). In a standard burst analysis, the fluorescent events in each channel are binned independently of each other. However, substantial additional information is also contained in the sub-populations of events that produce either coincident or non-coincident fluorescence bursts in each detection channel. One simple approach to using BAS to analyze the sub-population of co-incident events involves first separating these events by their burst intensity ratio. This approach is useful because the ratio of the probe's intensities is independent of excitation volume crossing trajectory (Figure 2-3 B). Cumulative histograms can then be generated for each burst intensity ratio and burst analyzed separately. Subsequently, the individual burst analyzed plots can be combined and plotted as a two-dimensional contour heat map (Figure 2-3 C). In these plots, the X and Y-axes show logarithmically distributed bins of fluorescence. The diagonals of the plot represent the different fluorescence ratios and the color represents the concentration. The individual one-dimensional burst analyzed plots for each intensity ratio can then be placed along respective diagonals in the heat map. Note that regions of constant intensity ratios run along the parallel diagonals of these plots, rather than along lines of varying slope, due to the log-log axes employed. We refer to this type of multi-channel BAS as MC-BAS.

Validating MC-BAS with Leakage from Single Color Beads

In order to validate MC-BAS as an approach, we first examined fluorescent nano-spheres that can be excited with a single excitation laser, but that show a sufficiently broad emission to allow simultaneous observation in two detection channels. The goal was to examine the robustness of MC-BAS using a sample that displayed a known and fixed signal coincidence between the two detection channels. For this test, 40 and 75 nm beads were examined both separately and as mixed samples. As expected, both the 40 and 75 nm beads possess a tight range of intensity ratios and most co-incident events can be found along a narrow range of diagonals (Figure 2-4). Interestingly, MC-BAS is able to detect a subtle shift in the diagonal region of the 40 nm, versus the 70 nm beads, which suggests slight differences in the fluorescent properties of these two bead samples. Importantly, when the 40 nm and 70 nm beads are mixed together, MC-BAS robustly detects both bead sub-populations, correctly recovering the approximate shape of the individual particle distributions, as well as the subtle shift in diagonal position (Figure 2-4).

Two Color DNA-Based Standards Can Be Used to Validate MC-BAS and Examine the Resolution of MC-BAS

In order to more fully explore the detection and resolution limits of MC-BAS, we examined mixed samples of particles that contained two different fluorescent probes in a range of total intensities and relative ratios. These

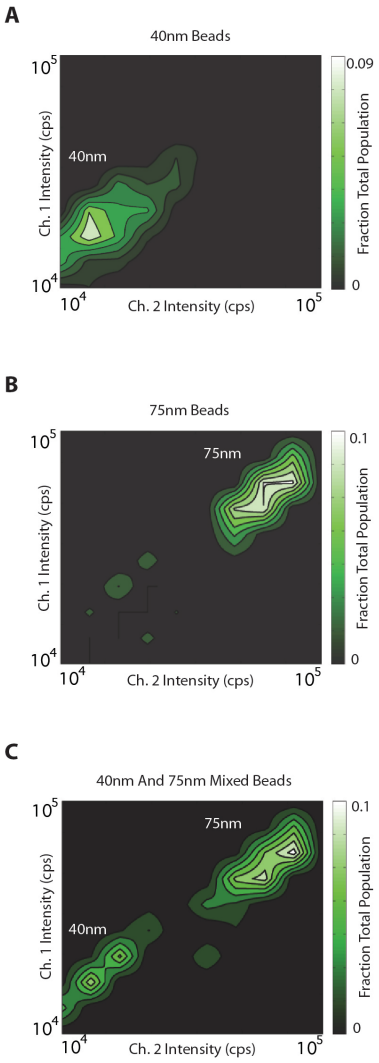

Figure 2-4 Different Populations of 40 and 75 nm Fluorescent Nanospheres Are Easily Distinguished with MC-BAS in Mixed Samples. (A) MC-BAS heat map of a solution containing 40 nm fluorescent nanospheres. The nanospheres are embedded with a fluorescent dye that has excitation and emission properties spanning both channels of a BAS microscope. (B) MC-BAS heat map of a solution containing slightly larger, 75 nm nanospheres of the same composition. (C) MC-BAS heat map of a 1:1 mixture of 40 and 75 nm nanospheres. Differences in the mean particle size, as well as the size distribution, for each bead subpopulation are readily distinguished in the mixed sample. Additionally, the 40 nm and 75 nm nanospheres fall along measurably distinct diagonals of the MC-BAS heat map, suggesting that the two particles differ slightly in their excitation and emission characteristics.

standards were constructed from double stranded B-form DNA and the DNA-binding, asymmetric cyanine intercalators named TOTO-3 and YOYO-1 (Figure 2-5 A). Different standards can be easily created by simply incubating DNA with different concentrations of TOTO-3 and YOYO-1. Additionally, these intercalating dyes are highly fluorescent when bound to DNA, but virtually non-fluorescent when in free solution. A linearized, 6.5 kb plasmid derived from pBR322 was employed as a DNA source. Pairs of different two-color DNA standards were mixed and then analyzed by MC-BAS. In all cases, the concentration of TOTO-3 was kept the same while the concentration of YOYO-1 was varied. MC-BAS readily distinguished doubly labeled DNA from singly labeled DNA. Additionally, the resulting BAS distributions were remarkably tight, consistent with the relatively sequence-independent, high affinity binding of these cyanine dyes to dsDNA (Figure 2-5). By varying the relative ratios of the TOTO and YOYO dyes, we systematically examined the ability of MC-BAS to resolve different populations of doubly labeled DNA. Even when the relative dye stoichiometry was as low as 2:1, MC-BAS readily resolved a mixture of two differently labeled DNAs (Figure 2-5).

The Character and Amount of Lambda Phage DNA Can Be Determined with MC-BAS

Viruses are persistent infectious agents that have evolved to infect all forms of life. While viruses can pose a serious health risk for humans, they can also protect humans by killing infectious bacteria. Thus, researching the means

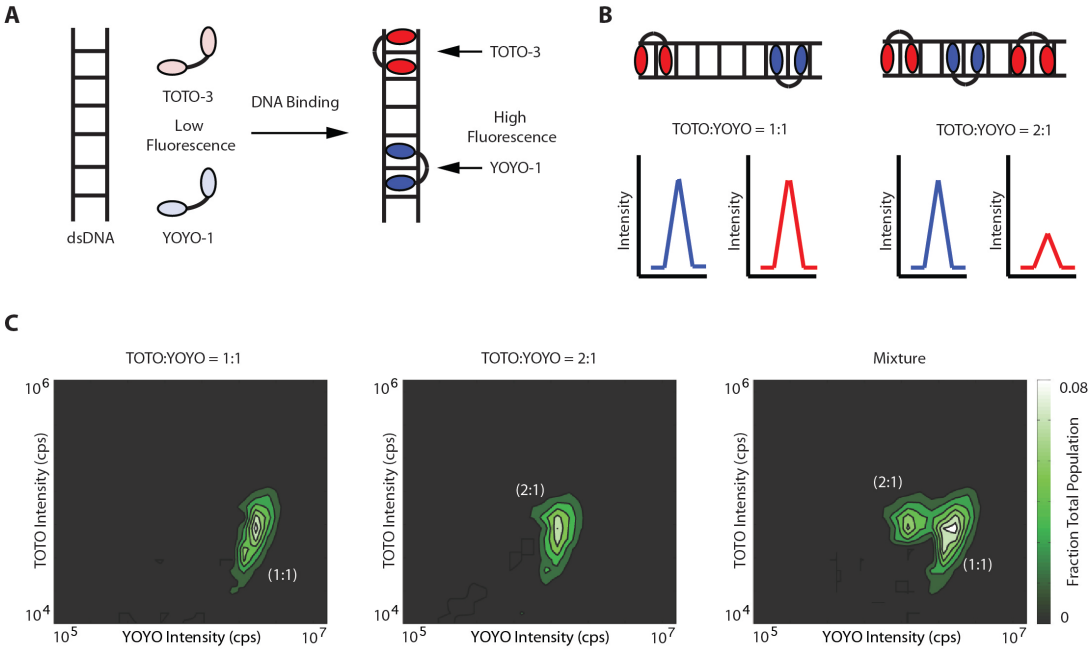

Figure 2-5 MC-BAS Can Resolve Individual Subpopulations of dsDNA Labeled at Different Levels with Bis-Intercalating Dyes. (A) linear dsDNA can be easily labeled with bis-intercalating dyes like TOTO-3 and YOYO-1. These dimeric, asymmetric cyanine dyes are spectrally distinct, bind to dsDNA non-covalently, but tightly, and are virtually non-fluorescent in free solution but highly fluorescent when intercalated into DNA. (B) By varying the amount of dye added, DNA molecules that carry different average numbers of dyes, over a range of relative dye ratios, can be easily prepared. Importantly, these differently labeled dsDNA molecules should produce distinct fluorescence burst ratios. (C) MC-BAS can distinguish relative intensity differences less than 2-fold in a mixed population of differentially labeled DNA molecules. An MC-BAS heat map of a 6.5 kbp fragment of linear dsDNA, labeled at a TOTO:YOYO stoichiometry of 1:1 and a total helical saturation of 10:1 bp/dye, is shown (*left*). The heat map of the same DNA fragment labeled at TOTO:YOYO stoichiometry of 2:1 and a total helical saturation of 20:1 bp/dye, is also shown (*center*). When these two populations of labeled DNA are mixed and analyzed by MC-BAS, the two populations are readily resolved in free solution (*right*).

by which bacterial viruses, also known as bacteriophages, infect and kill bacteria could yield a deeper understanding of how to use viruses to cure bacterial related disease in humans. One facet of phage biology still under scrutiny is the means through which phage load and pack their DNA into the viral particle. This process is in no means perfect and DNA can be packed imperfectly or fail to be loaded into phage altogether, which are also referred to as ghosts. Quantifying the amount of phage that are incapable of infection, and what percentage of those are ghost phage, is essential for studies aimed at understanding the process of phage particle assembly. Indeed, the study of infectious viral particle assembly in most systems requires robust access to this type measurement. However, quantitation of infectious viral titers can be slow and inefficient. Here, we examine the utility of MC-BAS to directly determine the extent of intact bacteriophage particle assembly with a single measurement that takes only a few minutes and needs just a few microliters of sample. Lambda bacteriophage carrying a genetically encoded YFP-labeled capsid protein, gpD, were first produced and purified before being mixed with TOTO-3, which binds to phage DNA (Figure 2-6 A). However, because ghost phage lack genomic DNA, they will not bind the TOTO dye and should produce fluorescent bursts in one channel of the MC-BAS microscope. In principle, the fraction of YFP bursts that display coincident bursts in the TOTO-3 channel can then be used to determine the fraction of intact phage particles (Figure 2-6 B). At the same time, the particle size distribution and level of homogeneity can be determined. Analysis

of a doubly labeled phage sample with MC-BAS revealed a highly homogeneous assembly distribution of the YFP-labeled capsid protein, but a surprisingly wide dispersion in the extent of TOTO-3 bound per particle (Figure 2-6). About 4% of the lambda phage appears to have genomic DNA that, for some reason, can bind much more TOTO-3 (Figure 2-7 D).

Combining cBAS and MC-BAS

MC-BAS and cBAS can be combined to increase the analyzable size range in two color experiments. This combined method, called MC-cBAS, is capable of tracking the interaction of very dim objects, such as individually labeled monomers, in the presence of very bright objects, such as oligomers. The application of MC-cBAS could further the understanding of complex and dynamic macromolecular structures, such as protein aggregates. The heterogeneity in these systems can make them difficult to study, which is unfortunate because of their importance to cellular fitness, disease, and aging. Here, aggregating non-native RuBisCO, labeled with Alexa488 or Alexa647, is used to show that MC-cBAS can distinguish whether aggregate growth occurs by exclusive monomer addition or whether preformed aggregates can coalesce. How aggregation proceeds can be simply examined by tracking the intensity ratio of co-incident events. The co-aggregation of equally sized large objects should result in an intensity ratio close to one, which is typically the central diagonal of a MC-cBAS contour plot. However, the addition of monomers to

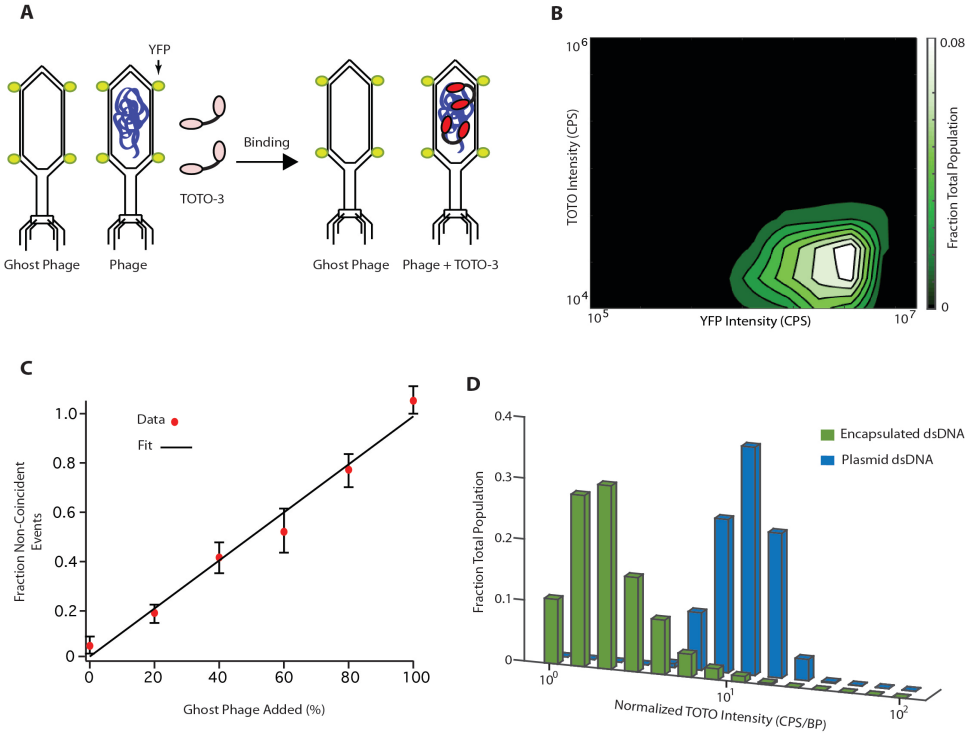

Figure 2-6 MC-BAS Can Be Used to Examine the Loading of Genomic Lambda DNA into Intact Phage Particles. (A) Schematic of experimental design. The proteinaceous shell of the lambda phage head is genetically labeled by fusing the phage coat protein gpD to YFP. The genomic DNA of purified, intact phage particles is stained *in situ* with the dimeric asymmetric cyanine dye TOTO-3. (B) Examination of a double-labeled phage sample using MC-BAS permits sensitive identification of phage particles that contain intact genomic DNA. (C) Phage particles that prematurely eject their genomic DNA are identifiable as burst events that show a strong YFP signal with no correlated TOTO-3 signal. To examine the ability of MC-BAS to measure fractional population difference, a sample of intact lambda phage was systematically diluted with different amounts of 'ghost' phage particles, which have been chemically treated to induce phage DNA ejection without disruption of the assembled phage head. The fraction of total YFP-positive events that show no correlated TOTO-3 signal is plotted versus the known fraction of ghost phage added. (D) Detailed examination of the TOTO-3 intensity distribution of the intact phage particles demonstrates as a substantially different dye binding distribution for packaged phage DNA compared to naked DNA.

aggregates of medium or larger size results in an intensity ratio far from one, which would be found at a diagonal closer to the edges of a MC-cBAS heat map plot.

As can be seen in Figure 2-7, the formation of medium size aggregates containing both monomers is easily detected by MC-BAS as early as 30 sec after the initiation of aggregation. The entire population of doubly-labeled aggregates appear near the central diagonal of the contour plot, as expected for the equa-probable addition of each monomer to an aggregate. At the same time, there does appear to be some separation of a second sub-population of aggregates at a slightly different monomer stoichiometry. With time, however, the total population appears to collapse toward a larger, but equally labeled population of aggregates (Figure 2-7 A). In order to examine aggregate growth under conditions where both non-native monomers and aggregates exist, RuBisCO-647 was aggregated separately for 15 sec before being mixed at equimolar ratios with monomer RuBisCO-488. Time points were taken at 15 sec and 60 sec after mixing, which is 30 sec and 75 sec total aggregation time respectively (Figure 2-7 B). As might be expected, at early times, the co-labeled aggregates display an MC-BAS distribution far off the 1:1 diagonal (Figure 2-7 B). Specifically, the co-labeled aggregates are highly enriched in monomers labeled with Alexa488, the probe carried by the RuBisCO sample that was initially pre-aggregated. However, if the subsequent addition of monomers, as

well as the coalescence of aggregates, was equa-probable, we would expect that as the aggregates grew in size, they should mature toward the central diagonal of the MC-BAS plot. Surprisingly, however, this is not what was observed. Instead, while the co-labeled aggregates continued to grow in size, their relative monomer stoichiometry stayed well off the central diagonal and strikingly close to their starting ratio (Figure 2-7 B). This unexpected behavior suggests that some level of conformational selection or growth patterning is imposed on the aggregates at the earliest stages of aggregation. In this case, the preformed aggregates (labeled with Alexa647), while competent to recruit a sub-population of the Alexa488 labeled monomers, were far more pre-disposed to interact with themselves, and excluded the sub-population of new, temporally delayed and smaller aggregates, labeled only with Alexa488, that also formed when this population of non-native monomer was added.

In order to examine aggregate growth under conditions where non-native monomers have been depleted, RuBisCO-488 and RuBisCO-647 were aggregated separately for 15 sec before being mixed at equimolar. Time points were taken at 15 sec and 60 sec after mixing, which is 30 sec and 75 sec total aggregation time respectively (Figure 2-7 C). Again, co-labeled aggregates are robustly detected by MC-BAS, with a slightly bifurcated population very close to the central diagonal. This observation not only demonstrates that RuBisCO aggregates can grow by accretion of already formed aggregate states, but that

Figure 2-7- **The Combination of MC-BAS and cBAS Detects Subtle Differences in Protein Aggregate Growth.** The CO_2-fixing enzyme RuBisCO from *R. rubrum* is a well-established model for studying protein aggregation and molecular chaperone-dependent folding. The enzyme can be efficiently labeled at single, surface-exposed Cys residues with reactive, exogenous fluorescent probes like Alexa488 (*blue*) or Alexa647 (*green*). (A) MC-BAS heat maps of RuBisCO aggregate growth observed when aggregation is initiated from a 1:1 mixture of non-native RuBisCO monomers. The formation of co-labeled aggregates at early (left) and late (right) time points is shown. (B) Population-resolved aggregate growth observed when small, preformed aggregates (labeled with Alexa488), at a final monomer-mixing ratio of 1:1. (C) Population-resolved aggregate growth observed when deferentially labeled RuBisCO samples are first pre-aggregated separately prior to mixing at final monomer ratio of 1:1. In each case, formation of co-labeled aggregates, which shift across almost three orders of magnitude in size, can be observed as a function of time.

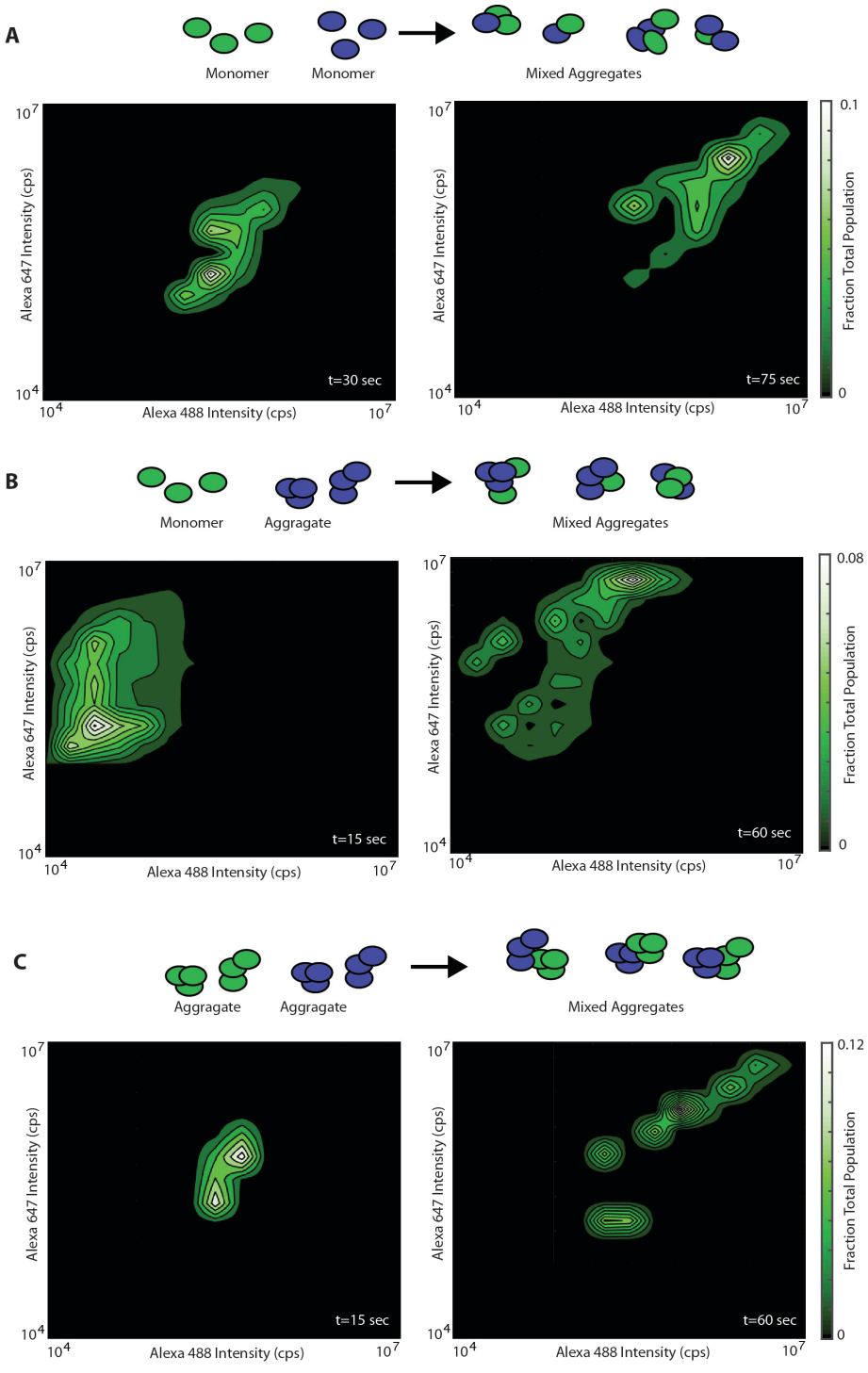
A
Monomer
Monomer
Mixed Aggregates
Alexa 647 Intensity (cps)
Alexa 488 Intensity (cps)
t=30 sec
t=75 sec
Fraction Total Population
0.1
0
B
Monomer
Aggregate
Mixed Aggregates
t=15 sec
t=60 sec
0.08
C
Aggragate
Aggragate
Mixed Aggregates
t=15 sec
t=60 sec
0.12

this assembly process appears to also follow an equa-probability progression, so that all assemblies have a roughly equivalent chance of sticking to all others. With time, as was seen when the co-aggregation was initiated from non-native monomers, the co-labeled aggregates continue to grow in size, while maintaining about the same relative starting ratio of labeled monomers (e.g. they grow along the same diagonal of the MC-BAS contour plot where they began).

Discussion

As shown, both cBAS and MC-BAS enhance the utility of an already versatile method. The cBAS method is ideal for studying populations that have very broad brightness and concentration ranges. MC-BAS allows BAS to be used to study the interaction between different molecules, which greatly expands the versatility of BAS. However, BAS is designed for working at low concentrations where association phenomena can be difficult or impossible to study, depending on the strength of the binding event. The examples presented here form stable complexes that have low observed dissociation constants, which allow these complexes to be studied at the low concentrations required for MC-BAS. Another constraint is that MC-BAS works best when the sample displays little, or very slow, change in population distribution with time. This is because MC-BAS requires the acquisition of many more total burst events than standard BAS. Samples that change too quickly can be difficult to analyze because an insufficient number of events will be collected within a given time

window.

The development of MC-BAS opens up a new avenue of study for a wide range of biological phenomena. For example, MC-BAS could be used to further probe DNA packing in the capsid of lambda, or other, bacteriophage particles. One question that could be addressed is what is the relationship between the genomic sequence of DNA, the packing of DNA in phage heads, and the ability of phage to infect a new host. This could be tested by making mutations to the phage genome and then packing the DNA into capsids. If certain mutations affect the ability of DNA to be packed properly, they may bind more TOTO-3 than normally packed lambda DNA. The percentage of phage with DNA packing anomalies could then be compared to the percentage of phage that were able to infect new hosts. Experiments of this nature could discern whether lambda phages have certain mutations that are not permissible because they impact DNA packing and injection during infection, as opposed to the character of protein translated from mutant genes. A discovery of this nature would have far reaching effects into various aspects of virology, including the prediction of yearly flu mutations, which MC-BAS could be adapted to study. With the knowledge that certain mutations are not permissible, due to their impact on nucleotide packing, mutation prediction algorithms could be adapted to make the prediction of flu strains and the development of flu vaccines more efficient.

In regards to non-native protein aggregates, MC-BAS could provide a stunning level of insight into the process of aggregation and disaggregation by molecular chaperones. Not only could MC-BAS be used to track the interaction of molecular chaperones with aggregates during disaggregation, but also MC-BAS could be used to track the way disassembly occurs. MC-BAS could also be used to study the interaction of vesiculation machinery with liposomes, DNA repair machinery with DNA, or even polysaccharide synthases with polysaccharide chains. All of these examples could be better studied with MC-BAS, but, MC-BAS can be further improved. In this work, MC-BAS is demonstrated with only two fluorophores, which both required separate lasers and detectors. More lasers and detectors could be added to a system so that three for even four fluorophores could be simultaneously used to study protein interactions. These developments would most certainly make the future usage of MC-BAS even brighter.

CHAPTER III

SINGLE PARTICLE FLUORESCENCE BURST ANALYSIS OF EPSIN INDUCED MEMBRANE FISSION*

Summary

Vital cellular processes, from cell growth to synaptic transmission, rely on membrane-bounded carriers and vesicles to transport molecular cargo to and from specific intracellular compartments throughout the cell. Compartment-specific proteins are required for the final step, membrane fission, which releases the transport carrier from the intracellular compartment. The role of fission proteins, especially at intracellular locations and in non-neuronal cells, while informed by the dynamin-1 paradigm, remains to be resolved. In this study, we introduce a highly sensitive approach for the identification and analysis of membrane fission machinery, called Burst Analysis Spectroscopy (BAS). BAS is a single particle, free-solution approach, well suited for quantitative measurements of membrane dynamics. Here, we use BAS to analyze membrane fission induced by the potent, fission-active ENTH domain of epsin. Using this method, we obtained temperature-dependent, time-resolved measurements of liposome size and concentration changes, even at sub-micromolar concentration of the epsin ENTH domain. We also uncovered, at 37°C, fission activity for the full-length epsin protein, supporting the argument that the membrane-fission activity observed with the ENTH domain represents a

*Reprinted, with modification, with permission from "Single particle fluorescence burst analysis of Epsin induced membrane fission" by Shoup, D., Brooks, A., Kustigian, L., Puchalla, J., Carr, C., Rye, H. (2015) PlosONE, 10(3): e0119563, Copyright (2015) by PlosONE

native function of the full-length epsin protein.

Introduction

The parting and merging of lipid bilayers, as occurs in vesicle budding (membrane fission) and in the delivery of vesicle contents to a target compartment (membrane fusion), are irreversible events. In order to impart specificity to the timing and integrity of each of these membrane remodeling events in the cell, proteins specialized to catalyze fission and fusion have evolved, as have regulatory factors, thus preventing indiscriminant events that would lead to intracellular disorganization (Carr et al, 2010; Campelo et al, 2012; Daumke et al, 2014). While much progress has been made in the characterization of membrane fusion proteins (Chernomordik et al, 2008; Wickner et al, 2008), an understanding of the mechanism of membrane fission remains limited (Daumke et al, 2014; Hurley et al, 2010). In part, this is due to the technical constraints of current methodologies. Bulk biochemical methods (such as sedimentation (Boucrot et al, 2012; Neumann et al, 2013)), tend to be inefficient, slow and provide only an estimate of the average observable activity of a complex system. While imaging methods can, in principle, circumvent this problem, to date these studies have either required intact cells, where detailed biochemical analysis of a system is not possible (Loerke et al, 2009; Merrifield et al 2005; Massol et al, 2006; Taylor et al, 2011), are constrained by small event numbers (Pucadyil et al, 2008), suffer from limited knowledge of population

distributions and sampling bias, or are affected by surface perturbations of tethered objects (Boucrot et al, 2012; Roux et al, 2006). Here we develop an alternative approach to the study of membrane fission, in which we apply a single particle fluorescence technique called Burst Analysis Spectroscopy (BAS; (Puchalla et al, 2008)). BAS permits analysis of the dynamics of complex particle distributions in free solution, including populations of liposomes undergoing fission. As a test of the utility of this approach for studying membrane fission, we have applied BAS to the study of changes in size and concentration of liposomes over time, when mixed with the simple, fission-potent, epsin N-terminal homology (ENTH) domain (Boucrot et al, 2012).

Epsin is a 94 kDa protein, identified in screens for binding partners of *α*-adaptin and Eps15, both clathrin coat associated proteins involved in clathrin-mediated endocytosis in neurons (Wang et al, 1995; Chen et al, 1998). Epsin is generally believed to function in cargo selection and bud site nucleation, through direct interactions with Eps15, the clathrin adaptor protein, AP-2, endocytic cargo and with clathrin, itself (reviewed in ref.(Legendre-Guillemin et al, 2004)). At the amino terminus of epsin is the highly conserved, ~140 amino acid ENTH domain shared with other endocytic proteins, including AP180/CALM (Simpson et al, 1999). This domain contains an N-terminal amphiphathic helix (the H_0 helix), which is known to insert into the outer-leaflet of membranes in a PtdIns(4,5)P_2-dependent fashion (Ford et al, 2002). Membrane insertion of the

H_0 helix is thought to facilitate membrane curvature and tubulation, prior to fission.

Recently, it was suggested that insertion of the ENTH H_0 helix into a lipid bilayer could directly facilitate fission (Boucrot et al, 2012). This work reported potent fission activity when liposomes were mixed with the isolated ENTH domain, though full-length epsin did not appear to possess fission activity. Recently, the conclusions derived from those results have been called into question: the observed ENTH-domain activity was suggested to be an artifact of a non-native protein domain at high concentration interacting non-specifically with liposomes to generate small vesicles and/or micelles (Neumann et al, 2013).

Here we have reexamined liposome membrane fission mediated by the ENTH-domain and full-length epsin protein with BAS. We find that the rate of membrane fission by the ENTH domain is sensitive to both temperature and protein concentration, and that fission activity can be observed at a sub-micromolar protein concentration, comparable to studies of dynamin-2 (Neumann et al, 2013). By exploiting the inherent sensitivity of BAS, we also observed measurable membrane fission activity for full-length epsin, albeit attenuated when compared to the ENTH domain. These observations not only support the argument that membrane fission is a function of full-length epsin, but

also demonstrate that BAS offers a flexible and highly sensitive approach to the study of membrane dynamics.

Methods

Protein Expression and Purification

The coding sequence of the epsin ENTH domain (residues 1–164) from *Rattus norvegicus* was obtained from Addgene and was sub-cloned into the pPROEX HTb vector (Shorter et al, 2008) for expression in *E. coli* BL21. In brief, clarified lysates were run on a Ni-NTA column equilibrated with column buffer (20 mM Tris pH 8.0, 500 mM NaCl, 20 mM imidazole, 5 mM β-mercaptoethanol) and eluted with a step gradient of the same buffer, plus 500 mM imidazole. ENTH-domain containing fractions were pooled and dialyzed against column buffer with 0.4 μM His6-TEV protease. His6-TEV and the His6 tag were separated from the untagged protein using the nickel affinity column. Untagged ENTH domain from the flow-through was further purified by ion exchange chromatography on a Source S column equilibrated in Source S Buffer A (20 mM Tris pH 7.4, 2 mM DTT) and eluted with a linear gradient of Source S Buffer B (20 mM Tris pH 7.4, 2 M NaCl, 2 mM DTT). Purified ENTH was stored at -80°C, in 20 mM Tris pH 7.4, 150 mM KCl, 2 mM DTT. The coding sequence of full-length rat epsin was obtained from Addgene (pCDNA3.1-Epsin1; plasmid 22225) and was sub-cloned into the pEX-N-His6-GST vector (Origene) for expression in *E. coli* BL21[DE3]. Purification of full length epsin followed the

same affinity chromatography and proteolytic cleavage protocol used for the ENTH domain, followed by further purification by ion exchange with a high-resolution Mono Q column equilibrated and washed with Buffer A (20 mM Tris pH 7.4, 2 mM DTT) and eluted on a linear gradient with Buffer B (20 mM Tris pH 7.4, 2 mM DTT, 2 M NaCl).

Liposomes Preparation

Liposomes were prepared as previously described, with minor modifications (Boucrot et al, 2012). Briefly, brain lipid Folch extracts from Avanti (cat. 131101P) and Sigma (cat. B-1502) were mixed 1:1, with 5% PtdIns(4,5)P2 (Avanti, cat. 840046C) and 0.03% acyl-chain, Ω-carbon labeled TopFluor-PtdEth (Avanti, cat. 810282C). Lipids were dried under a stream of dry argon, vacuum desiccated to remove residual solvents, re-suspended, with freezing and thawing, to 1 mg/ml in liposome buffer (20 mM HEPES pH 7.4, 150 mM NaCl) and then extruded through polycarbonate filters with the indicated diameters with 11 passes in a mini extruder (Avanti), followed by 10 passes through a high-pressure manifold extruder (Northern Lipids), and used within 6 hr. Liposomes used at later times no longer respond to addition of ENTH domain or epsin, presumably due to loss of liposome binding upon PtdIns(4,5)P2 hydrolysis.

Liposome Fission Assay by BAS

Liposomes diluted to 0.01 mg/mL in liposome buffer were mixed with

ENTH domain, or full-length epsin, at the concentrations indicated. Efficient fission of large (~ 200 nm) liposomes into small (20–30 nm) liposomes should result in a large (100 to 200-fold) increase in object concentration, read out as fluorescent bursts with amplitudes proportional to individual object sizes. From a starting sample of 50–100 pM large liposomes, this increase in object number will violate the single-particle concentration limit (< 500 pM) required for BAS. Additionally, due to limited knowledge of the instrument point spread function, an individual BAS measurement can only quantitatively probe an approximately 100-fold range in object intensity for a single, uniformly labeled species (Puchalla et al, 2008). The fission of large liposomes into much smaller ones leads to a highly inverted population dominated by smaller particles. In this case, the resolving power of BAS deteriorates for the low intensity events, due to the high species concentrations that no longer permit single particle detection. Therefore, to accurately examine liposome populations produced during fission, we employed cBAS to permit BAS histograms to be constructed over a three order of magnitude range of object sizes.

Heat Map Normalization

To convert the number of burst events in each bin to fractional intensity, we normalized the object intensities with the below equation. In cases where a data is split into two plots or subsets, the normalization remained unchanged and can still be considered a continuous plot. In the following equation:

$$[I_i C_i] / [\Sigma (I_n C_n)]$$

where Ii is the intensity of each bin, Ci is the concentration of objects in each bin, and Σ starts at 1 and stops at the total number of bins. The denominator represents the total fluorescence of all bins (the sum of intensity in a row) for a given sample.

Results

BAS is Sensitive to Changes in Liposome Size and Concentration

In order to quantify the size of vesiculation products, it is necessary to establish the relationship between liposome size and intensity. In order to do this, liposomes were extruded to 200 nm, 100 nm, and 50 nm. Inspection by BAS revealed the expected dependence of burst size on liposome size (Figure 3-1 A). The difference in the brightness between each liposome population should be proportional to the difference in surface area between them. For example, the surface area of the 200 nm liposomes should be ~ 4-fold higher than the 100 nm liposomes and ~ 16-fold higher than the 50 nm liposomes. Upon burst analysis, the mean intensities for each liposome population were found to be appropriately proportional (Figure 3-1 B). A Monte Carlo simulation was used to bracket the size variation of liposomes to be between 35-50% CV (coefficient of variation). This is somewhat higher than the manufacturer specification of ± 25% CV. This variation is likely due to a higher incidence of multi-lamellar objects.

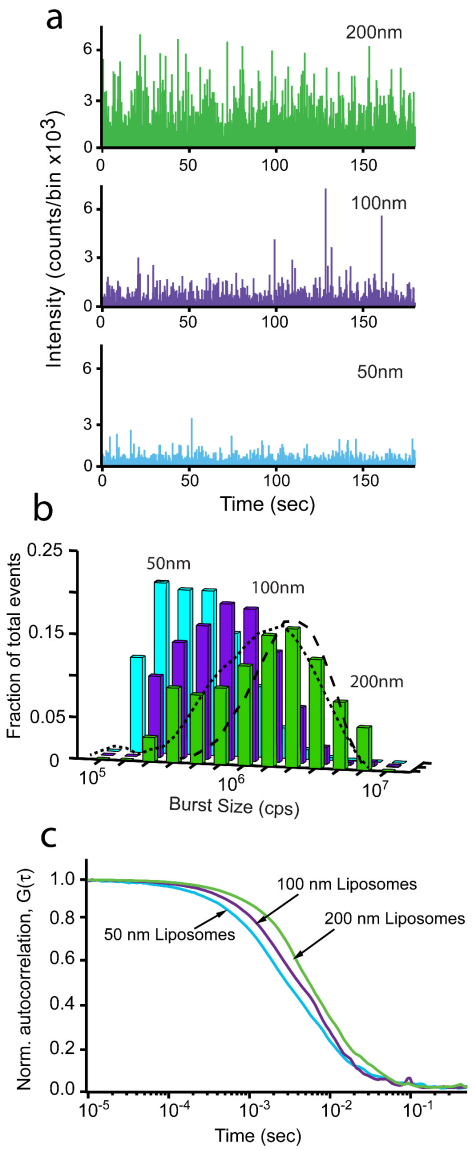

Figure 3-1 BAS Assay Distinguishes Liposomes of Different Sizes. The size distribution of 200 nm, 100 nm and 50 nm fluorescent liposomes was examined by FCS and BAS. (a) Fluorescent burst data of TopFluor-labeled Folch liposomes extruded to 200 nm (*green*), 100 nm (*purple*) and 50 nm (*cyan*). (b) BAS histograms generated from the burst data in (a). Fraction of total events is the concentration of each bin divided by the total concentration, for each sample. Dashed lines show theoretical diameter distributions (35% CV, *dash*; 50% CV, *dot*) derived from Monte Carlo simulated intensity data in which fluorescence brightness was set proportional to particle surface area. The resulting simulated intensity distributions were analyzed with BAS analysis code. (c) FCS profiles of 200 nm, 100 nm, and 50 nm liposomes. The data shown is representative of two experimental replicates.

As a complementary analysis to BAS, FCS was used to examine each liposome population. Here, FCS is not used to calculate the exact size of populations. Instead, FCS is used as a comparative tool to make sure that the diffusion rate and hydrodynamic radius differ proportionally between populations. The decrease in mean diffusion time with population size is consistent with the BAS measurements (Figure 3-1 C).

Membrane Fission Activity of the Epsin ENTH Domain

In order to examine the ability of cBAS to detect the products of ENTH domain mediated fission, 200 nm and 400 nm liposomes were incubated at 37°C for 40min, with and without the ENTH domain. After incubation all samples were examined by BAS (Figure 3-2 A-D). The presence of the ENTH domain greatly reduced burst size of both 200 nm and 400 nm liposomes. This reduction is size was not due to a loss of liposomes as the material loss was seen as no greater than 10-20% (Figure 3-3).

Burst analysis of the 200 nm liposomes revealed that the larger liposomes had transitioned into a broad range of smaller objects. As expected, the low concentration of bright objects transitioned into a highly concentrated population of dim objects (Figure 3-2 E). In fact, there is a nearly 100-fold increase in the concentration of the smallest fission products relative to the starting 200 nm

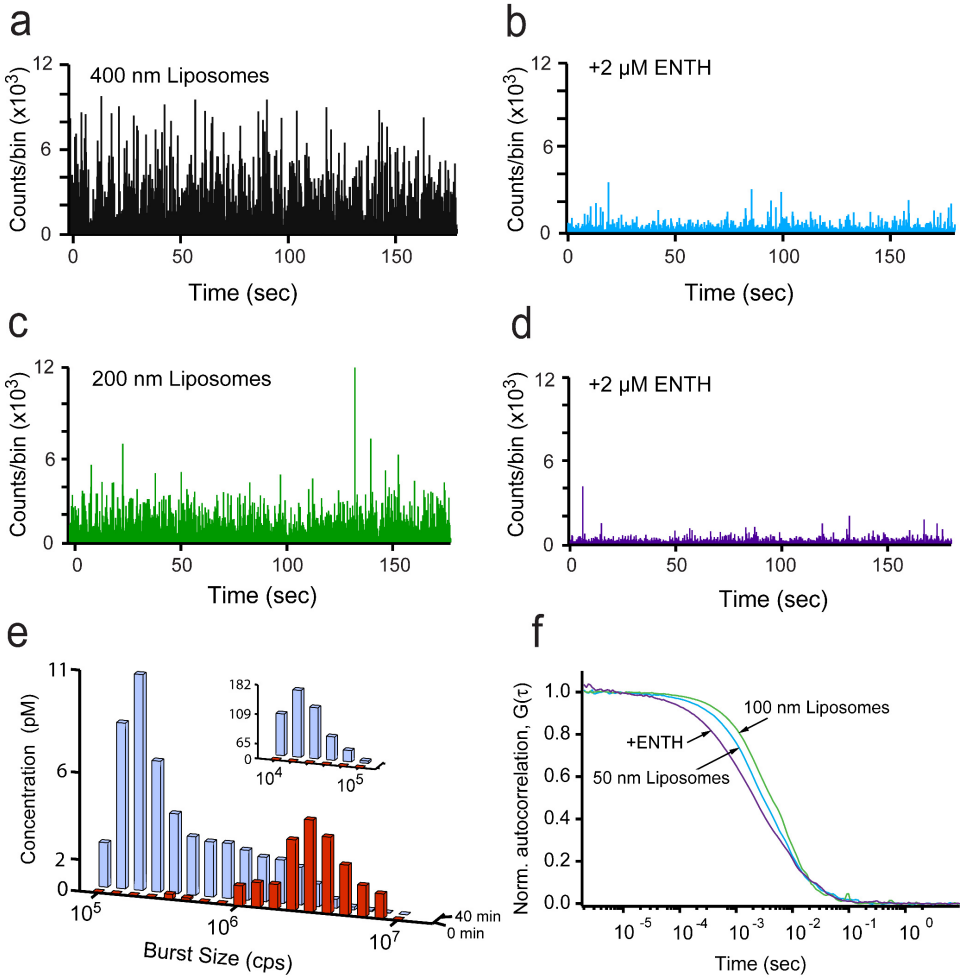

Figure 3-2 BAS Analysis of Liposomes Vesiculated by the ENTH Domain of Epsin. Fluorescent burst data for 400 nm-diameter, TopFluor-labeled, (5%) PtdInsP(4,5)P_2 Folch liposomes incubated at 37°C for 40 min before (a) and after addition of 2 μM ENTH (b). Fluorescent burst data for 200 nm-diameter liposomes incubated at 37°C for 40 min before (c) and after addition of 2 μM ENTH (d). (e) BAS histograms generated from starting 200 nm liposomes before (*red*) and after addition of ENTH (*blue*; insets indicate resolution of small particles in a 10-fold dilution of the same reaction). (f) FCS profiles of liposomes extruded to 100 nm (*green*), 50 nm (*cyan*) and the end products (*purple*) of the fission reaction of 200 nm liposomes from (d). The data shown is representative of three experimental replicates.

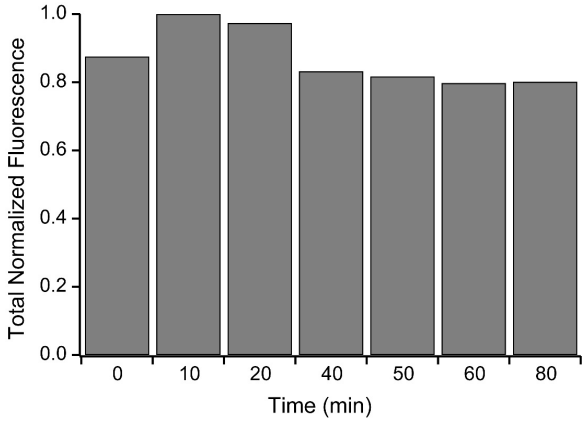

Figure 3-3 Liposome Fission by ENTH is Not Accompanied by Loss of Fluorescent Material. The total fluorescent signal for each time point during ENTH-mediated fission at 37°C (Figure 3-5) is shown. In each case, the integrated signal was normalized to the maximal total signal observed during the experiment. The data shown is representative of three experimental replicates.

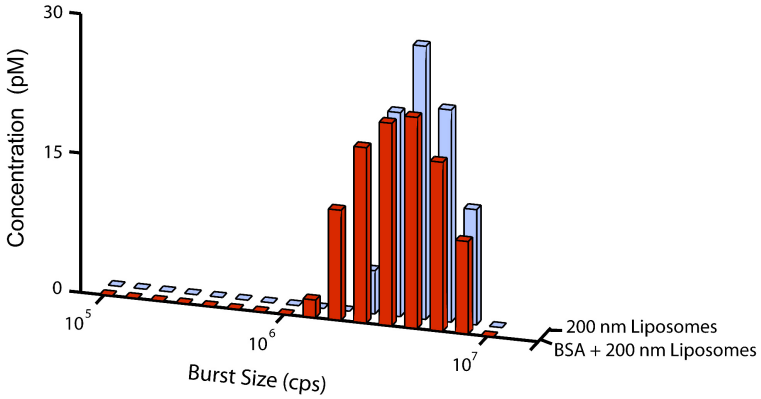

Figure 3-4 Liposome Size Distribution is Not Altered by a Non-Fission Active Protein. A BAS histogram of 200 nm-diameter, TopFluor-labeled, (5%) PtdInsP(4,5)P_2 Folch liposomes (*light blue*) remains relatively unchanged, following a 60 min incubation at 37°C in the presence of 10 μM BSA (*red*). The data shown is representative of duplicate experiments.

liposomes. The large concentrations of dim objects have a smaller mean intensity than the 50 nm liposomes. This observation is validated by FCS, which showed that most of the population diffuses faster than the 50 nm liposomes (Figure 3-2 F). The smallest population is ~100 fold less intense than the 200 nm liposomes. Based upon the proportional intensity scaling with surface area to volume, the smallest population of liposomes is ~20 nm in size. Interestingly, the major product of ENTH mediated vesiculation was 20 nm sized liposomes, which was determined with electron microscopy. In addition, the observed fission activity cannot be replicated by replacing the ENTH domain with a non-specific protein like BSA (bovine serum albumin) (Figure 3-4).

The ENTH Domain Acts on the Timescale of Minutes

In order to map out vesiculation by the ENTH domain, 200 nm liposomes were incubated at 23°C and 37°C both with and without the ENTH domain. At various time points, samples were taken and examined via cBAS. The resulting data was placed in bar plots (Figure 3-5 A,C) and heat maps (Figure 3-5 B,D). The bar plots show the data in concentration while the heat maps show data in fraction total intensity. Within the first 20 min at 23°C (Figure 3-5 A,B) about half of the starting 200 nm liposomes have transitioned into intermediate and small objects. The intermediate population appears to be produced first and then decreases by a small amount with time.

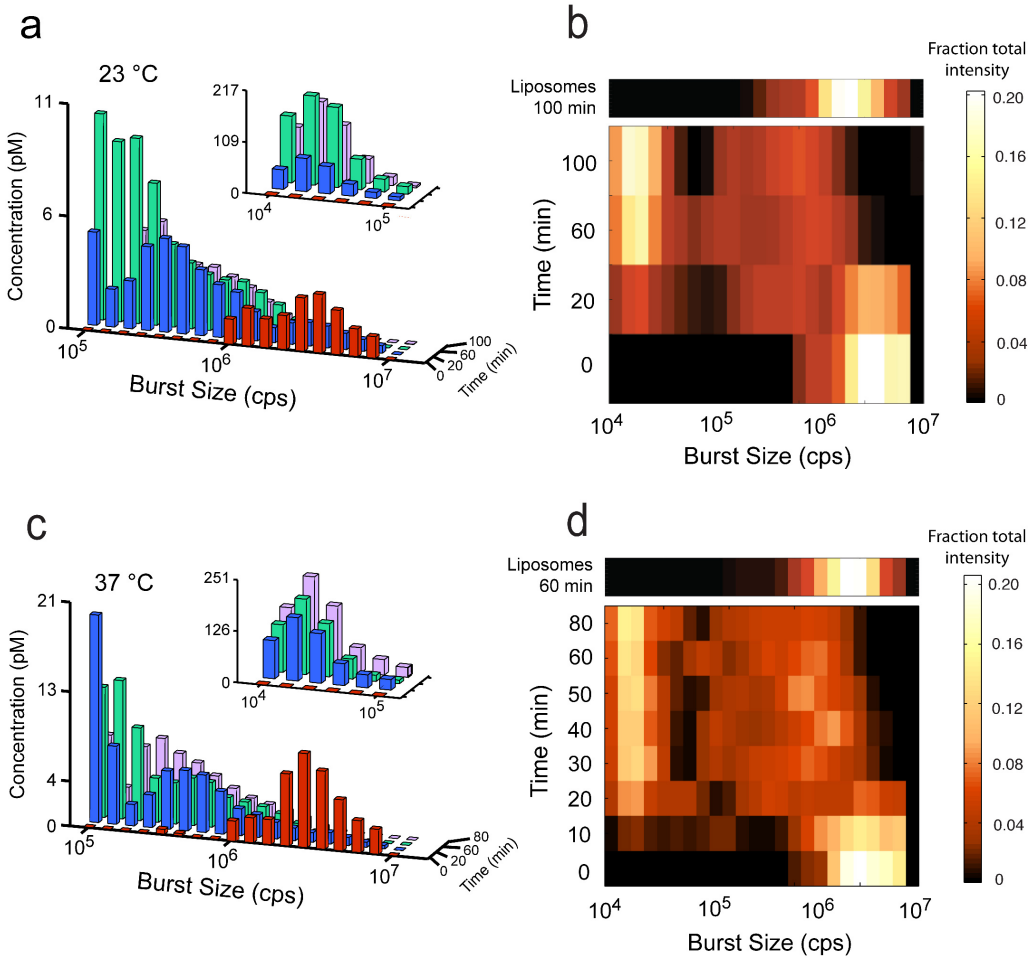

Figure 3-5 Kinetics of Liposome Fission Are Temperature Dependent. (a) Histograms of BAS analyzed 200 nm-diameter, TopFluor-labeled, (5%) PtdInsP(4,5)P2 Folch liposomes (*red*) and products of ENTH incubation at 23°C for 20 (*blue*), 60 (*green*), and 100 min (*purple*) after addition of 2 μM ENTH. At each time point, an aliquot was removed and placed on ice, and measurements were started within 1–2 min. Inset indicates resolution of small particles in a 10-fold dilution of each reaction. (b) Heat map representation of the fractional intensity for each reaction shown in (a). (c) BAS histograms generated from starting liposomes (*red*) and products of ENTH incubation at 37°C for 20 (*blue*), 60 (*green*), and 80 min (*purple*) after addition of 2 μM ENTH. (d) Heat-map representation of the fractional intensity for each reaction shown in (c). Additional time points are shown, for increased resolution. The effect of incubating liposomes in the absence of the ENTH domain for 60 min at 37°C or 100 min at 23°C is shown as an additional row, above the respective heat maps. The data shown for the experiments conducted at 23°C is representative of four experimental replicates. The data shown for experiments conducted at 37°C is representative of three experimental replicates.

The population of smallest objects continues to increase in concentration until about 60 min. It is not known if vesiculation of the intermediates has stalled or if the intermediate and small liposomes reach a point of equilibrium. The same transitions can be seen for the liposomes incubated with ENTH at 37°C, however, vesiculation appears to take place faster (Figure 3-5 C,D).

The smallest products reach their maximum concentration at ~ 30 min for ENTH at 37°C and ~ 60 min for ENTH at 23°C. This indicates that at 37°C, the ENTH domain performs vesiculation at about ~2-fold faster. Liposomes that were incubated at their respective temperature, but not with the ENTH domain, are shown above the heat maps. As can be seen, liposomes do undergo a small shift in population during incubation, but it cannot account for the large shift in the population seen when ENTH is present.

Fission Activity of the ENTH Domain is Dose-Dependent

Next, we determined if ENTH mediated vesiculation was dose dependent. In all cases, liposomes were incubated with ENTH for 20 min at 37°C. In this case, the focus was on the disappearance of large objects, so regular BAS was used (Figure 3-6 A,B). At this early time point, fission activity could be detected with the ENTH domain concentration as low as 500 nm. Incrementally increasing the concentration up to 10 μM resulted in an incremental increase in

fission activity.

Fission Activity of Full-Length Epsin

While the results of this work validate the observation that the ENTH domain is capable of vesiculation, the results also help establish BAS and cBAS as sensitive methods for studying vesiculation. To date, the full-length epsin protein has not been shown to be capable of vesiculation. However, it is possible that the fission activity of epsin is subtle. Thus, epsin was tested for vesiculation activity with cBAS in the hopes of uncovering epsin vesiculation activity or demonstrating that vesiculation by the ENTH domain is an artifact of truncation. In order to test this, 200 nm liposomes were incubated for 40 min with full-length epsin at 37°C. In these experiments, the concentration of epsin ranged from 1μMto 10μM (Figure 3-7 A,B). Using this approach, epsin was seen to perform fission in a dose dependent fashion. Interestingly, full-length epsin was slower than the ENTH domain, but the distribution of end products converges to the same point after a 90 min incubation (Figure 3-7 C).

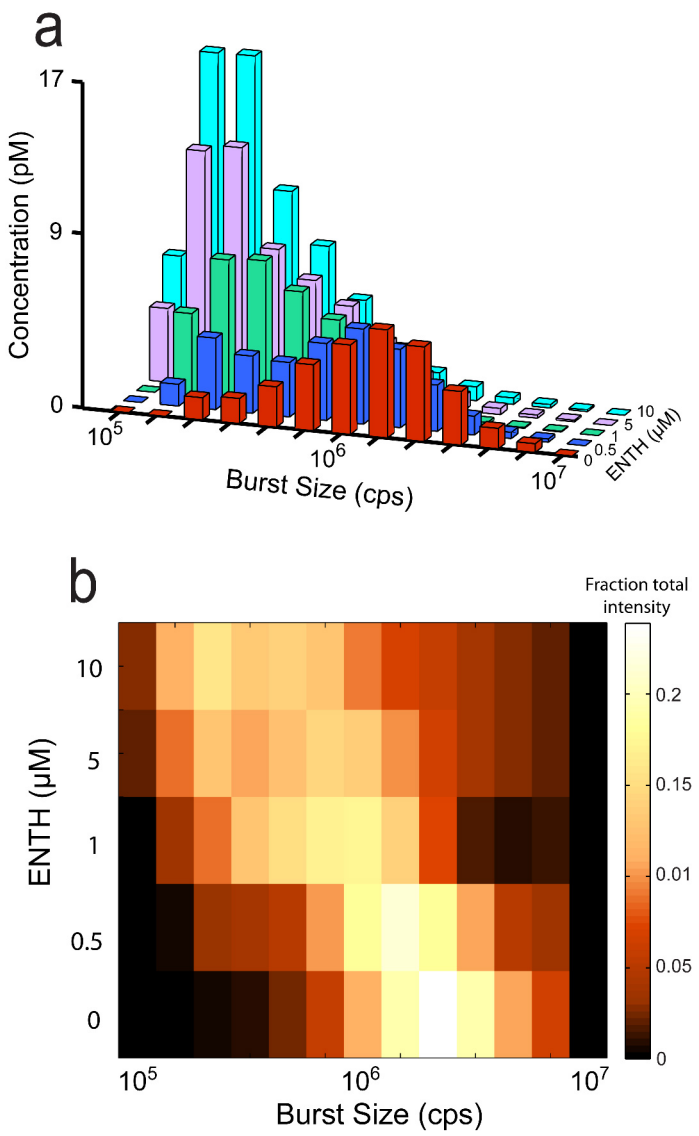

Figure 3-6 Dose Dependence of ENTH-Mediated Vesiculation. (a) BAS histograms of 200 nm-diameter, TopFluor-labeled, (5%) PtdInsP(4,5)P_2 Folch liposomes before (*red*) and after incubation at 37°C for 20 min with 500 nM (*blue*), 1 μM (*green*), 5μM (*purple*), and 10 μM (*cyan*) ENTH. (b) Heat-map representation of the fractional intensity for each reaction shown in (a). The data shown is representative of three experimental replicates.

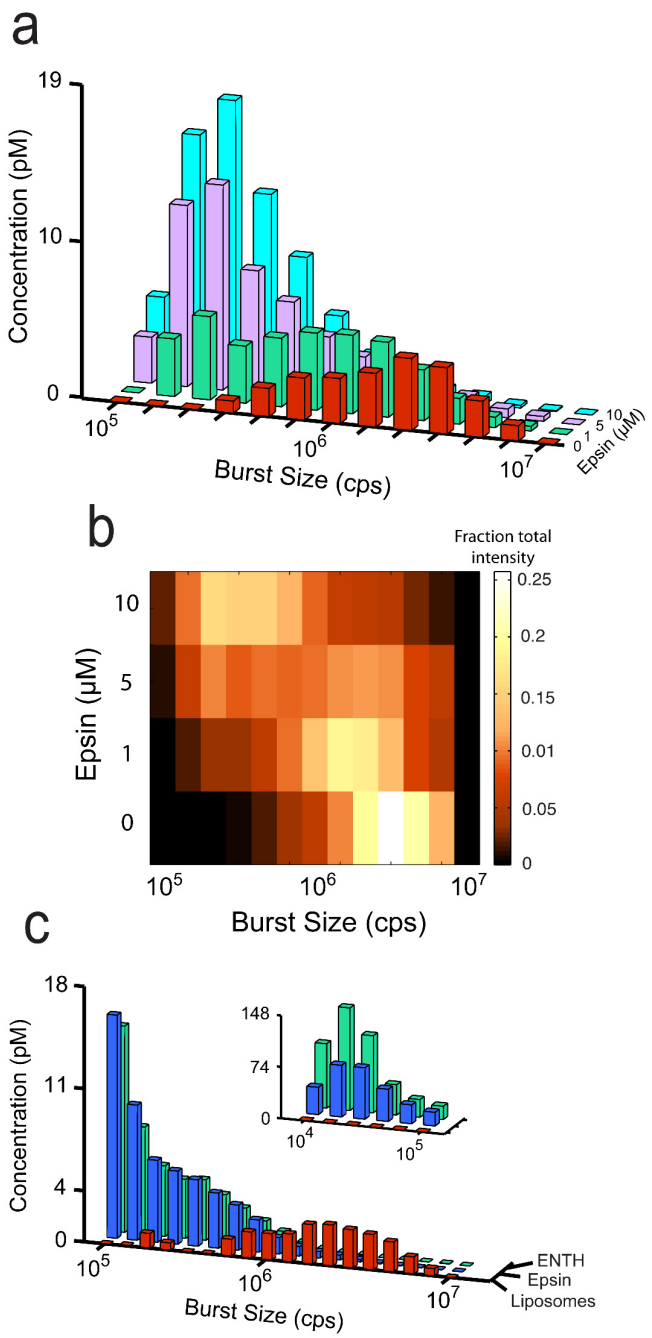

Figure 3-7 Full-Length Epsin Has Vesicle Fission Activity
(a) BAS histograms of 200 nm-diameter, TopFluor-labeled, (5%) PtdInsP(4,5)P_2 Folch liposomes before (*red*) and after incubation at 37°C for 40 min with 1 μM (*green*), 5 μM (*purple*), and 10 μM (*blue*) full-length epsin. (b) Heat-map representation of the fractional intensity for each reaction shown in (a). (c) Comparison of ENTH and epsin activity. BAS histograms of starting liposomes (*red*), and liposomes incubated at 37°C for 90 min with 2 μM ENTH (*blue*) or full-length epsin (*green*). The data shown is representative of three experimental replicates.

Discussion

Using BAS, we observed time-resolved liposome membrane fission in free solution, induced by the potent epsin ENTH domain. These results agree with those of a previous study, which showed, using living cells and an *in vitro* sedimentation assay, that epsin, in particular the ENTH domain, is necessary and sufficient for endocytic vesicle membrane fission (Boucrot et al, 2012). Recently, concerns were raised regarding the physiological significance of the fission activity observed in that study, specifically citing the small size of the starting liposomes (200 nm diameter), the high protein concentration (10 μM), and the likelihood that many of the products, rather than vesicular in nature, were micellar (Neumann et al, 2013). The high sensitivity of BAS allowed us to address these concerns: (i) fission activity was observed at sub-micromolar protein concentration, (ii) fission activity does not depend on the curvature of starting liposomes, as those of 400 nm diameter worked as well as smaller ones and (iii) the products are consistent with 20 nm vesicles and not micelles, as observed previously (Boucrot et al, 2012).

In addition, the high sensitivity of BAS allowed us to uncover attenuated membrane fission activity in experiments with the full-length epsin protein. Attenuation may suggest an inhibited conformation for full-length epsin, as has been suggested for syndapin, another protein involved in formation of vesicles at the recycling endosome (Rao et al, 2010). Intermolecular interactions have also

been observed to cause auto-inhibition, in the case of endophilin A1, a curvature-inducing endocytic protein that also contains an N-terminal amphipathic helix (Chen et al, 2014).

Although epsin is required for clathrin-mediated endocytosis from early to late stages of endocytic vesicle formation (Taylor et al, 2011), it has been classified as an adaptor protein. Like the well-characterized adaptins, epsin was shown to act at an early step, recruiting other adaptins and cargo (Legendre-Guillemin et al, 2004), in addition to binding to the clathrin coat. However, unlike the classic adaptins, little epsin is found in clathrin-coated vesicles (Chen et al, 1998; Mills et al, 2003), raising questions regarding its role solely as an adaptor protein. Furthermore, epsin can rescue a block in the release of endocytic vesicles in dynamin-depleted cells (Boucrot et al, 2012), arguing for a late role in vesicle fission. These results, in addition to the liposome fission activity of the epsin ENTH domain, led those authors to conclude that epsin is also required for fission of clathrin-coated endocytic vesicles. Furthermore, an analogy was made to the early and late requirement for the amphipathic-helix containing proteins, Arf1p and Sar1p, in the formation of COPI coated vesicles at the Golgi apparatus and COPII coated vesicles at the endoplasmic reticulum, respectively (Beck et al, 2011; Lee et al, 2005).

BAS has the ability to resolve membrane fission reactions over a concentration range that is more physiologically significant and on a sub-second timescale. Yet, the fastest fission reactions we observed, at high protein concentration and 37°C, proceeded on the min, to tens of mins timescale. This suggests that other factors are required to increase the fission activity to physiologically significant rates, on the order of seconds, to tens of seconds (Taylor et al, 2011). Notably, the results of recent studies indicated a reciprocal requirement for the amphipathic-helix containing amphiphysin and partner protein, dynamin, in order to stimulate membrane fission (Neumann et al, 2013; Meinecke et al, 2013). Our results using BAS reopen the question of how membrane fission is induced, not only in endocytosis, but also, how transport carriers and vesicles are released at other locations in the cell, where dynamin does not appear to play a role. Our findings also raise others questions: how is epsin regulated, and what stimulates epsin-induced membrane fission? Moreover, our findings indicate that BAS offers a highly sensitive approach to follow single particle dynamics of a membrane fission reactions in free-solution, for identification of membrane fission agents and characterization of the mechanism of membrane fission regulation.

CHAPTER IV

THE IMPACT OF AGGREGATE STRUCTURE ON DISAGGREGATION BY DNAK-CLPB REVEALED BY SINGLE PARTICLE FLUORESCENCE BURST ANALYSIS

Summary

Partially structured protein folding intermediates, populated during biosynthesis or upon exposure to environmental stress, can form cytotoxic non-native protein aggregates. Cells mitigate the toxicity of aggregates and recover protein lost to aggregation through the activity of specialized proteins known as molecular chaperones. However, molecular chaperones often fail to disassemble protein aggregates for reasons that are not well understood. Here, we apply ensemble techniques along side a new single particle fluorescence burst technique, known as Burst Analysis Spectroscopy (BAS), in order to better understand how non-native protein aggregates are dismantled by molecular chaperones. In this work, RuBisCO, from *R. rubrum*, is used as a model, aggregate-forming protein to study disaggregation by the DnaK-ClpB, Hsp70-Hsp100, bi-chaperone system of *E. coli*. This work first demonstrates that denatured RuBisCO can follow at least two general aggregation pathways, distinguishable by their growth rates, structures, and chaperone requirements for disaggregation. In all cases, RuBisCO aggregates become increasingly refractory to disassembly as aggregation continues, independent of size. We

also find that RuBisCO aggregates mature, after aggregation has ceased, and become increasingly refractory to disassembly without losing the ability to bind DnaK. Finally, we show that DnaK can alter the structure of aggregates in a way that substantially enhances disaggregation by ClpB. These results suggest that the internal structure of an aggregate, and not its size, has a profound impact on the ability of the cellular quality control systems to process protein aggregates.

Introduction

Hydrophobic amino acids help drive the folding and oligomerization of protein but are generally buried inside the native conformation and oligomer state of a protein (Spolar et al, 1989). However, non-native proteins tend to expose hydrophobic amino acids, which can drive non-native proteins to aggregate (Dill et al, 1997; Capaldi et al, 2002). Proteins can fold into a multitude of non-native conformations that can grow into aggregates with a wide range of shapes and structures (Tanaka et al). Most aggregates are classified as amorphous, meaning they do not populate unique or specific structures (Simone et al, 2011; Morris et al, 2009, Chiti et al, 2002). However, many, and perhaps most, proteins can also populate a beta sheet rich fold, under the right set of conditions, that assemble into highly structured amyloid fibrils—long fibers with organized beta sheets running their length (Fandrich et al, 2007; Jackson et al, 2000; Groot et al, 2009). The presence of amyloid fibrils and amorphous aggregates can negatively impact the health and fitness of cells. However, the

regular structure of amyloid fibrils has made them easier to identify and study than amorphous aggregates (Sulatskaya et al; 2011). Consequently, more is known about the role of amyloid fibrils in disease and cell fitness, despite amorphous aggregates being a more common occurrence.

Both amyloid fibrils and amorphous aggregates can persist within cells, despite the presence of disaggregation chaperones such as Hsp70, Hsp100, and Hsp110. Why this occurs is not well understood, though it suggests that aggregates become refractory to disaggregation due to some change in their physical properties. The effects of aggregate shape on disaggregation can be considered in a general way by simply noting the impact of shape on the ratio of surface area to volume. Spheroid aggregates have a smaller ratio of surface area to volume than fibrils. This means that fibrils may have more exposed chaperone-binding sites than spheroid aggregates for the same total volume. An aggregate's surface area to volume ratio also decreases as an aggregate increases in size, which could, at least in principle, be a more serious problem for dismantling spheroid aggregates than fibrils. The size and shape of an aggregate could also limit the effectiveness of chaperone activity in other ways. For instance, if chaperones need to destabilize the overall oligomer structure of an aggregate, then disruption of a small aggregate might be efficient. The same mechanism, however, might fail with a large aggregate. At the same time, the oligomer structure of an aggregate is fundamentally dictated by the conformation

of its constituent subunits. The structure of an aggregate will impact the number of exposed chaperone binding sites, the number of contact points between other subunits, and the strength of interactions between contact points. Accordingly, aggregates with more or stronger interactions between subunits are likely to be more difficult to take apart.

In the end, it is likely that several aggregate properties (shape, size, structure, and monomer conformation) contribute to how well a given aggregate can be disassembled by molecular chaperones. Because of the analytical challenges presented by working with protein aggregates, most work to date has assumed that aggregate size and structure are the most important determinants in whether a given aggregate can be dismantled. However, whether size or structure has a greater impact on chaperone-mediated disaggregation, is a matter of debate. Unfortunately, disaggregation is commonly studied with bulk measurement assays that are unable to track individual populations, refolding assays that do not directly track disaggregation, and separation based assays that can perturb the size and structure of aggregates during separation. The use of such assays to study the often dynamic and heterogeneous nature of non-native protein aggregates is undoubtedly one of the reasons it remains unclear whether size or structure has a greater effect on disaggregation.

In this study, sensitive fluorescence techniques, such as BAS and FRET,

will be used to probe how specific qualities, or changes in aggregate qualities, affect disaggregation in a direct and non-perturbative manner. However, probing an aggregate's size, structure, and conformation by fluorescence requires a model, aggregating protein that can be labeled with exogenous fluorescent probes at more than one site. RuBisCO, from *R. rubrum*, is a highly aggregation-prone protein that has been engineered with multiple exogenous surface cysteines that can be conjugated to fluorescent probes (Lin et al 2004). Singly or doubly labeling RuBisCO minimally affects its folding, activity and aggregation, which make it an ideal substrate for doing sensitive fluorescence assays (Rye, 2001).

RuBisCO is a substrate of the *E. coli* disaggregases, DnaK and ClpB (Thomas et al, 2000), and has been studied as a folding substrate of GroEL/ES, the foldase system from *E. coli* (Lin et al, 2004; Lin et al 2008). Here, how the qualities of non-native RuBisCO aggregates affect the disaggregation activity of DnaK and ClpB will be assessed. The goal of this work is to better understand the process of disaggregation and find potentially universal reasons that non-native aggregates become refractory to disaggregation.

Methods

Protein Expression and Purification

Wild-type RuBisCO and all RuBisCO cysteine mutants were expressed

and purified as previously described (Rye et al, 1997; Rye et al, 1997; Lin et al, 2008; Lin et al, 2004; Lin et al, 2006). The gene for DnaK was amplified from *E. coli* genomic DNA and sub-cloned into the pPROEX HTb (Shorter et al, 2008) for expression in the *E. coli* BL21 strain. The genes for ClpB, DnaJ, and GrpE, sub-cloned into a pET 151/D-TOPO vector for expression in the *E. coli* BL21 DE3, were generous gifts from Dr. Steve Burston (University of Bristol, UK). DnaK, ClpB, GrpE, and DnaJ were expressed similarly to a previously described expression protocol for the yeast Hsc70 protein Ssa1p (Shorter et al, 2008), except that DnaK, DnaJ, and GrpE expression was induced at an OD_{600} of 0.6 while ClpB was induced at an OD_{600} of 0.7. Cells were lysed by cell disruption with a Model M-110Y Microfluidizer (Microfluidics), in Ni-NTA Safe Cell Disruption Buffer (50 mM phosphate, 300 mM NaCl, 20 mM imidazole, 1 mM PMSF, 5 mM beta-mercaptoethanol, 20% sucrose, pH 8.0) and then lysates were clarified by ultracentrifugation in a Ti-45 Beckman rotor at 35k RPM for 45 min.

Clarified lysates for DnaK, ClpB, and GrpE were loaded onto a Quiagen Ni-NTA column equilibrated with Ni-NTA Buffer A (50 mM phosphate, 300 mM NaCl, 20 mM imidazole, 5 mM beta-mercaptoethanol, pH 8.0) and were then washed with ~15 column volumes of Ni-NTA Buffer A. After washing, protein was eluted in 20% Ni-NTA Buffer B (50 mM phosphate, 300 mM NaCl, 500 mM imidazole, 5 mM beta-mercaptoethanol, pH 8.0). However, clarified lysate for

DnaJ was loaded onto a Quiagen Ni-NTA column equilibrated with Ni-NTA Buffer A containing 2 M de-ionized urea and was then washed with ~10 column volumes of Ni-NTA Buffer A containing 2 M de-ionized urea. After washing, protein was eluted in 20% Ni-NTA Buffer B that contained 2 M de-ionized urea. Eluted protein was dialyzed in Ni-NTA buffer A with as many exchanges necessary to drop the concentration of urea below 0.1 mM.

Eluted proteins were mixed with the TEV protease at a ratio of 1 to 35 (TEV to protein) and then dialyzed in 8k MWCO dialysis bags (Sigma) against Ni-NTA buffer for 24 hrs. at 4°C. After cleavage, the ClpB, DnaK, and GrpE proteins were re-run over an Ni-NTA column equilibrated in Ni-NTA Buffer A. Cleaved protein flowed through the Ni-NTA column and was collected before being buffer exchanged into Ion Exchange Buffer A (50 mM Tris-HCl, 0.5 mM EDTA, 2 mM DTT, pH 7.4) before being loaded onto a Source 30Q (GE) ion exchange column that had been equilibrated in Ion Exchange Buffer A. However, after cleavage, DnaJ was mixed with de-ionized urea to a final concentration of 2 M before being run over an Ni-NTA column equilibrated in Ni-NTA Buffer A that contained 2 M de-ionized urea. Cleaved DnaJ flowed through the Ni-NTA column and was collected. DnaJ was exchanged into Ion Exchange Buffer A in order to remove urea then loaded onto a Source 30Q ion exchange column that had been equilibrated in Ion Exchange Buffer A.

After a 2 column volume wash in Ion Exchange Buffer A, a gradient to 25% Ion Exchange Buffer B (50 mM Tris-HCl, 2 M NaCl, 0.5 mM EDTA, 2 mM DTT, pH 7.4) was developed over 25 column volumes. DnaK, DnaJ, ClpB, and GrpE are the major peaks in their respective runs and elute between 7% and 20% Ion Exchange Buffer B. DnaK, ClpB, DnaJ, and GrpE were buffer exchanged via 10k MWCO Vivaspins into Storage Buffer (50 mM Tris-HCl, 150 mM KCl, 0.5 mM EDTA, 2 mM DTT, 15% glycerol, pH 7.4) and concentrated to between 15 and 20 mg/ml protein in a Vivaspin concentrator. DnaK, DnaJ, and ClpB were concentrated with 30K MWCO Vivaspins and GrpE was concentrated with a 10K MWCO Vivaspin. Protein was then mixed with glycerol to 15% by volume before being snap frozen in liquid nitrogen and stored at -80°C.

DnaK 517 Phe(4-Azido)-OH Creation and Purification

The DnaK-pProex-HTb expression vector was mutated via Quick Change PCR (Kunkel, 1985) to introduce an amber codon (e.g. UAG) at position 517. Amber mutant DnaK was transformed into *E. coli* BL21 cells simultaneously with the AzPheRS/mutRNA$_{CUA}$-pYC-J17 expression vector. AzPheRS is a mutant of *M. jannaschii* tyrosyl-tRNA synthetase capable of conjugating p-azido-L-phenylalanine to mutRNA$_{CUA}$, a mutant tyrosine amber suppressor (Chin et al, 2002; Wang et al, 2001). Growth and expression was carried out following the same protocol as used for His-tag DnaK, except, prior to induction, 5 mM p-azido-L-phenylalanine was added to cell cultures. During induction, p-azido-L-

phenylalanine is conjugated to mutRNA$_{CUA}$, which recognizes the amber codon at position 517 in DnaK. The mutRNA$_{CUA}$ tRNA inserts p-azido-L-phenylalanine into the translating DnaK at position 517 and allows translation to complete. Purification of DnaK 517-azidoPhe was carried out normally, except the concentration of reductant was maintained at lower concentrations (0.5-1 mM Beta-Mercaptoethanol) in order to prevent reductant-induced loss of the reactive azido group. DnaK 517-azidoPhe was also kept in darkness and the inline absorbance detectors on the FPLC were disabled during purification in order to prevent light from degrading the reactive azido group.

During expression, about 20% of the translating DnaK 517 Amber failed to incorporate p-azido-L-phenylalanine and was truncated (Figure 4-1 A). DnaK 517-azidoPhe and truncated DnaK 517 are not well separated by the standard purification protocol used for DnaK. However, in order to maximize the conjugation efficiency of the azido-Phe site, labeling was initiated immediately following purification (see below) before the truncated DnaK was removed via gel-filtration with a Superose 6 column. In the absence of ATP, DnaK DBCO 488 appears to bind tightly to the truncated DnaK 517. However, addition of ATP to the running buffer of the polishing gel filtration column induces the release of the truncated DnaK 517 from the DnaK DBCO 488, which appears as a shoulder on the trailing edge of the DnaK DBCO 488 peak (Figure 4-1 B). The running buffer for the gel-filtration column was 50 mM HEPES, pH 7.6, 150 mM

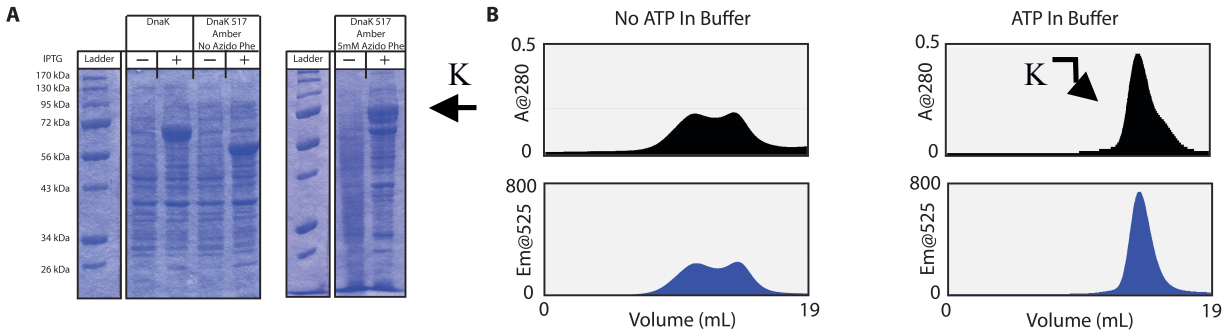

Figure 4-1 DnaK-517 Truncation Can Be Separated from DnaK-DBCO 488 by Gel-Filtration. (A) Expression of DnaK 517 Amber produces a truncated product unless p-azido-L-phenylalanine is present. However, some DnaK 517 truncation is produced in the presence of p-azido-L-phenylalanine. (B) DnaK DBCO 488 binds the truncated DnaK product, resulting two peaks by gel filtration. However, when ATP is present in the running buffer, DnaK DBCO 488 releases the truncated product. The DnaK 517 truncation can be seen as a shoulder on the trailing edge of the DnaK DBCO 488 peak.

KOAc, 10 mM $Mg(OAC)_2$, 5mM ATP, and 2 mM DTT.

Protein Labeling

Exogenous fluorescent dyes were chemically conjugated to RuBisCO using classical cysteine-directed chemistries (Rye, 2001; Lin et al, 2004; Lin et al, 2008; Rye et al, 1999). Labeling reactions were carried out in 50 mM Tris (pH 7.4), 100 mM KCl, 0.5 mM EDTA, and 1 mM TCEP. However, the number of dye additions used, amount of dye added in each addition, length of time between additions, and temperature of the reaction, varied based upon the type of labeling reaction, fluorophores used, and whether or not the reaction was carried out to completion. In most cases where a single cysteine residue was targeted, the reaction was carried to completion by the addition of a large excess of reactive dye, followed by quenching of the excess, unreacted dye with reduced glutathione (Rye, 2001; Lin et al, 2004; Lin et al, 2008; Rye et al, 1999). In cases where RuBisCO was labeled with two different probes on two different cysteine residues, the reaction was quenched with glutathione after the most rapidly labeling site was fully conjugated, but before the second, slower site was fully conjugated (Lin et al, 2004). The singly labeled population was purified away from other labeled species with an anion exchange column, typically a MonoQ 10/10 (GE; Lin et al, 2004). Once the singly labeled RuBisCO was obtained, the second fluorophore was then conjugated to the unreacted, slower reacting site in the purified sample. After each labeling reaction, the labeling

ratio was verified by native ion exchange and denaturing ion exchange (Lin et al, 2004, Rye et al, 1999).

DnaK 517 Phe(4-Azido)-OH (DnaK 517-azidoPhe) was labeled with dibenzocyclooctyne (DBCO) via a metal-free click chemistry (Jewett et all, 2010). The reaction that links the azido group of DnaK 517-azidoPhe to DBCO is promoted by the strained alkyne in DBCO. The reaction is thus referred to as SPAAC, or strain promoted alkyne azide cycloaddition (Jewett et all, 2010). Here, DnaK517-azidoPhe was labeled with DBCO 488, which is a DBCO reactive group conjugated to a variant of the Alexa 448 fluorophore. DnaK 517-azidoPhe was labeled at 100 μM in buffer containing 50 mM Tris (pH 7.4), 100 mM KCl, 0.5 mM EDTA, and 0.5 mM beta-mercaptoethanol. DBCO 488 was prepared by mixing 2.5 mg of DBCO 488 with 0.15 mL DMSO. Labeling was initiated by mixing DBCO 488 to 100 μM with DnaK 517-azidoPhe, which was then gently mixed for 2 hrs in complete darkness at room temperature. After 2 hrs, DBCO 488 was again added to a concentration of 100 μM, making the total concentration of DBCO 488 200 μM, and the reaction was continued for another 2 hrs. The labeled DnaK 517 DBCO 488 was separated from free dye by buffer exchange in a 30k MWCO vivaspin and by purification over a PD10 desalting column.

Aggregate Preparation

Native RuBisCO was denatured in acid urea buffer (25 mM glycine-phosphate, pH 2.0, 8 M urea) at 10 μM for 30 min at 23°C. Denatured RuBisCO was then diluted, using rapid manual inversion, 50-fold (200 nM) into aggregation buffer (50 mM HEPES, pH 7.6, 150 mM KOAc, 10 mM $Mg(OAC)_2$, and 2 mM DTT) at either 4°C or 23°C.

Aggregation started immediately upon mixing into buffer at 23°C, yielding what are referred to here as 'fast growing' aggregates. However, dilution into buffer at 4°C allowed the denatured RuBisCO monomer to rapidly collapse into a non-native state that cannot fold into the native state, but does not readily aggregate (Lin et al, 2004). After incubation at 4°C for 2 min, the non-native RuBisCO was warmed to 23°C by placing a small volume into a pre-warmed tube to initiate aggregation of 'slow growing' aggregates. All aggregation reactions were maintained at 23°C for the duration of aggregation reactions with a high precision temperature block (MJ Research Inc. PTC-100). Aggregation was terminated with a 20-fold dilution to 10 nM monomer in aggregation buffer prior to data collection.

For all BAS experiments, RuBisCO was labeled at cysteine 58 with either Alexa Fluor 647 maleimide or TMRIA (tetramethylrhodamine-5-iodoacetamide) (Puchalla et al, 2008, Lin et al, 2004).

For all ensemble FRET experiments, the acceptor dye used was fluorescein (5-iodoacetamidofluorescein) and the donor dye was IAEDANS (5-(2-acetamidoethyl) aminonapthalene-1-sulfonate). Unless otherwise stated, in both intra- and inter-molecular FRET measurements, the donor was placed on cysteine 454 and the acceptor was placed on cysteine 58 (Lin et al, 2004). For intra-molecular FRET, both dyes were present on a single RuBisCO monomer, while for inter-molecular FRET the dyes located on separate RuBisCO monomers that were aggregated together at an equimolar ratio. For sensitized FRET assays, labeled RuBisCO monomers were mixed with unlabeled RuBisCO prior to aggregation. In sensitized experiments using intra-molecular FRET, the double-labeled RuBisCO was 10% of the total RuBisCO population. In sensitized inter-molecular FRET experiments, donor and acceptor were each 10% of the total RuBsiCO population. In all steady-state ensemble FRET experiments, the FRET efficiency, E, was calculated with

$$\langle E \rangle = (F_D - F_{DA})/F_D.$$

In this equation, F_D is the emission from the donor in the absence of acceptor and F_{DA} is the emission from the donor in the presence of the acceptor (Lakowicz, 1999). The donor excitation wavelength used was 336 nm. The emission from the donor was integrated from 430-450 nm. The integration range is kept short so as to minimize back leakage of the acceptor emission into donor emission window. Emission measurements were taken on a PTI photon-counting spectrofluorometer equipped with a temperature-jacketed holder.

Chaperone Set-Up

The concentrations of DnaK, DnaJ, GrpE, and ClpB, used in all but two experiments, was 0.5 μM, 1 μM, 1 μM, 0.3 μM respectively. The first exception was the DnaK-DBCO-488 binding experiment. In these experiments the concentrations of DnaK, DnaJ, and GrpE were all 0.1 μM. The second exception was the DnaK-induced structure change experiments. In which, concentrations of DnaK, DnaJ, and GrpE was 0.1 μM, 0.2 μM, and 0.2 μM. Wherever DnaK was employed, DnaJ and GrpE were also present. In all cases, ATP was added to 2 mM and a regeneration system composed of creatine kinase and creatine phosphate, at 5 units and 3 μM respectively, was used to keep the ADP concentration low and regenerate ATP.

Electron Microscopy

Aggregate samples were prepared for EM and imaged by Mengqiu Jiang of the Junjie Zhang lab. In general, the protein sample was placed upon a copper coated grid coated first in formvar and subsequently by carbon. After incubated for 1-3 min, the excess liquid was wicked away with the torn edge of ashless filter paper. Protein on the grid was stained with a 2% uranyl acetate solution for 1-3 min before the excess liquid was wicked away with ashless filter paper. The grid was allowed to air dry for ~24 hr prior to examination

Results

RuBisCO Aggregate Growth is Highly Sensitive to Initial Conditions

Temperature was used to control the aggregation of RuBisCO in order to generate chemically identical, but structurally distinct, aggregates. Two previously documented observations with RuBisCO made this approach possible. First, denatured RuBisCO aggregates rapidly upon dilution into buffer at 23°C, but can be kept from aggregating by dilution into buffer at 4°C (Lin et al, 2004). Second, RuBisCO requires the GroEL/GroES chaperones for proper folding (Goloubinoff et al, 1989). Therefore RuBisCO monomers maintained at 4°C can be given a longer time to collapse and at least partially fold, compared to RuBisCO diluted into buffer at 23°C, where the rate of aggregation is far faster than all but the earliest folding transitions (Figure 4-2 A). Nonetheless, upon rapid warming, the folding intermediates populated at 4°C readily aggregate, albeit much more slowly. For this reason, aggregates produced by mixing directly into buffer at 23°C are referred to as fast growing while aggregates produced by warming to 23°C are referred to as slow growing.

Figure 4-2 RuBisCO Can Aggregate by Two Distinct Pathways. (A) Schematic showing how denatured RuBisCO, from *R. rubrum,* is prepared to make fast and slow growing aggregates. (B) The average rate for the initial formation of fast (blue squares) and slow growing (green diamond) aggregates are observed by ensemble inter-molecular FRET between two differently labeled RuBisCO samples. (C and D) Raw (top) and processed (bottom) burst data for early (blue) and late (green) growth time points is shown for fast (C) and slow (D) growing aggregates. Trends in aggregate growth can be visualized in the heat maps shown in (E,F) for slow and fast growing aggregates, respectively.

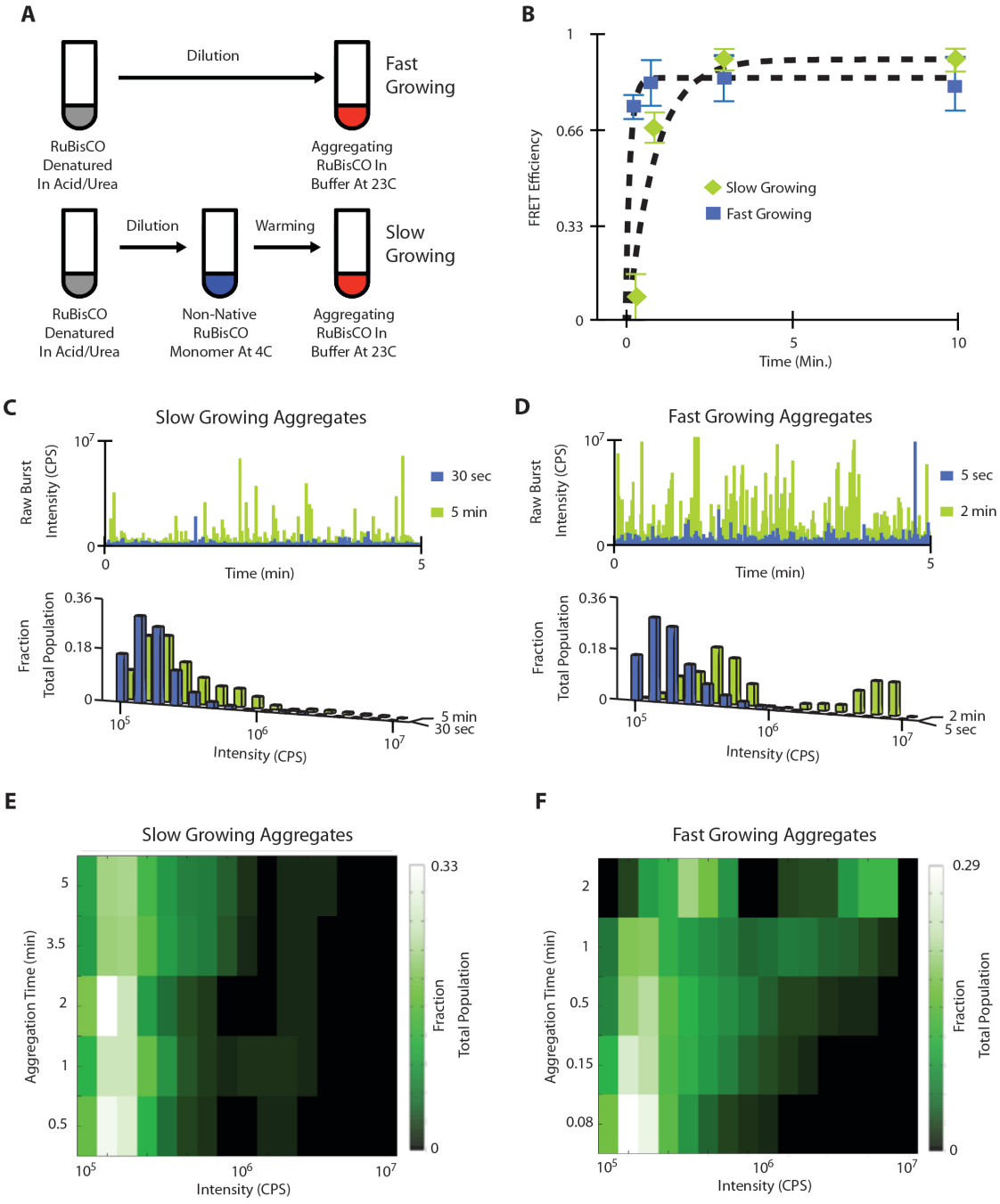
A
Dilution
Fast Growing
RuBisCO Denatured In Acid/Urea
Aggregating RuBisCO In Buffer At 23C
Dilution
Warming
Slow Growing
RuBisCO Denatured In Acid/Urea
Non-Native RuBisCO Monomer At 4C
Aggregating RuBisCO In Buffer At 23C
B
FRET Efficiency
Time (Min.)
Slow Growing
Fast Growing
C
Slow Growing Aggregates
Raw Burst Intensity (CPS)
Time (min)
30 sec
5 min
Fraction Total Population
Intensity (CPS)
5 min
30 sec
D
Fast Growing Aggregates
Raw Burst Intensity (CPS)
Time (min)
5 sec
2 min
Fraction Total Population
Intensity (CPS)
2 min
5 sec
E
Slow Growing Aggregates
Aggregation Time (min)
Intensity (CPS)
Fraction Total Population
F
Fast Growing Aggregates
Aggregation Time (min)
Intensity (CPS)
Fraction Total Population

The rate of RuBisCO aggregation was first examined using inter-molecular FRET between two different RuBisCO populations, one carrying a donor and the other carrying an acceptor fluorophore (Figure 4-2 B). This ensemble assay appears to be most sensitive to the initial steps of aggregation between monomers or small aggregates (data not shown). Thus, the average inter-molecular FRET signal not only provides a lower bound on the initial aggregation rates, but provides an estimate of the point where the non-native monomer has been depleted. Ensemble FRET measurements are, however, insensitive to the formation of larger aggregated states that appear in the later stages growth. To measure changes in aggregate sub-populations with greater sensitivity, we therefore employed BAS. Raw BAS data demonstrated that fast growing RuBisCO aggregates had larger fluorescence bursts at earlier times than slow growing RuBisCO aggregates (Figure 4-2 C,D). Because burst intensity is proportional to size, fast growing aggregates grow bigger much faster than slow growing aggregates. Detailed examination by BAS demonstrated that most of the slow growing aggregates maintained a small size, even at 5 min of growth where the population distribution appeared to stabilize (Figure 4-2 C). On the other hand, after only 2 min of growth, almost half of the aggregates were large in size for the fast growing aggregates (Figure 4-2 D). In order to better visualize the change in aggregate distributions over time, each time point was plotted as a row on a heat map (Figure 4-2 E,F).

In order to determine whether the fast and slow growing aggregates are structurally and conformationally distinct, these aggregates were grown to their end points and were then probed by a combination of inter and intra-molecular FRET, Thioflavin T (THT) binding, bis-ANS binding, and negative stain electron microscopy. Thioflavin T is an indicator dye that increases in fluorescence when bound to the organized beta sheet structures found in amyloid fibril aggregates. Interestingly, fast growing aggregates display substantially greater THT fluorescence than the slow growing aggregates, suggesting that the presence of at least some organized beta-sheet and reminiscent of behavior of amyloid forming proteins (Figure 4-3 A). Fast growing aggregates also show greater bis-ANS binding than the slow growing aggregates. Because bis-ANS is known to preferentially bind to exposed hydrophobic surfaces in proteins, this observation suggests that fast growing aggregates expose more hydrophobic surface than slow growing aggregates (Figure 4-3 B).

The average relative proximity of RuBisCO monomers in both fast and slow growing aggregates was next examined by using inter-molecular FRET between different population of labeled RuBisCO. In order to increase the sensitivity of this assay to subtle changes in aggregate structure, donor-labeled and acceptor-labeled RuBisCO populations were mixed with unlabeled RuBisCO prior to the initiation of aggregation, in order to increase the average distance between donor and acceptor fluorophores in aggregates. Using this sensitized

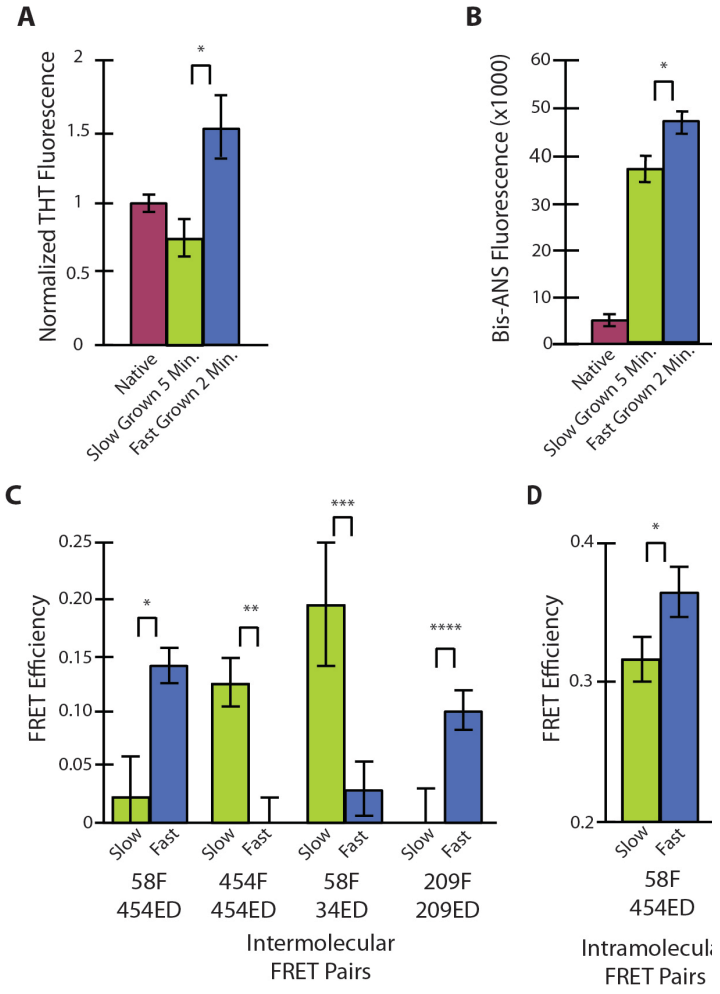

Figure 4-3 Fast and Slow Growing RuBisCO Aggregates Are Structurally Different. Average differences between fast (green) and slow (blue) growing aggregates was ascertained at aggregation endpoints, 2 min and 5 min respectively, and compared to native RuBisCO (plum) when applicable. (A) Average beta sheet content was compared by examining Thioflavin T binding (Sulatskaya et al; 2011). (B) bis-ANS binding was employed to compare the amount of exposed hydrophobic surface (Rosen et al, 1969). (C) The average difference in the arrangement of RuBisCO monomers in fast and slow aggregates was compared using inter-molecular FRET with different combinations of labeled monomers in which the donor and acceptors dye positions were altered. (D) Average, relative positioning of the ends of the RuBisCO monomer were compared via intra-molecular FRET. Stutent's T-Test for A*, B*, C*, C**, C***, C**** and D* are 5.30, 5.19, 5.51, 6.98, 4.91, 4.5, and 3.37 respectively.

inter-molecular FRET assay, we found that the average proximity of different labeling sites on the RuBisCO monomer varied considerably between the fast and slow growing aggregates, suggesting that the structural organization of the aggregates is substantially different (Figure 4-3 C). While these data strongly suggest that the fast and slow growing aggregates are structurally distinct, they provide no information on the local conformation of the RuBisCO monomer in each type of aggregate. In order to address this issue, intra-molecular FRET was employed, where the donor and acceptor probes were coupled to the same RuBisCO monomer using a site-specific labeling strategy (Lin et al, 2006). The average internal proximity of different parts of individual RuBisCO monomers could then be assessed, because the labeled monomers were mixed into a much larger concentration of unlabeled monomers. This strategy minimized FRET between labeled monomers within an aggregate by separating labeled monomers with a much larger number of unlabeled RuBisCO monomers. Strikingly, the conformation of the RuBisCO monomer within the fast and slow growing is distinctly different (Figure 4-3 D).

The difference in THT binding between fast and slow growing aggregates suggested, in analogy with amyloid-like proteins, that the fast growing aggregates might possess a fibril-like shape and would have different hydrodynamic properties. In order to test this idea, both fast and slow growing aggregates were centrifuged at varying speeds and then analyzed by BAS. Fast

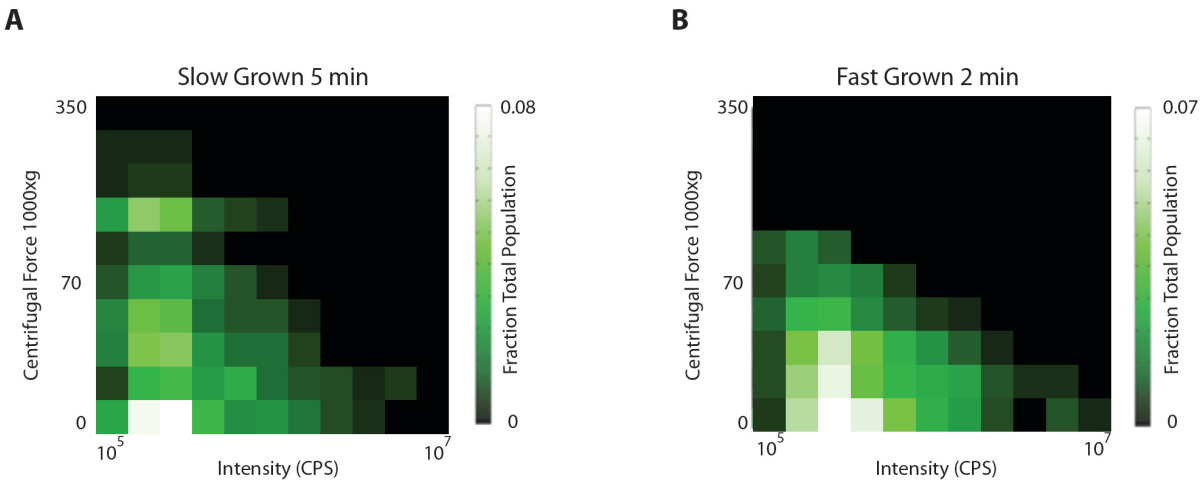

Figure 4-4 Fast and Slow Grown Aggregates Sediment at Different Centrifugal Forces. The loss of different aggregate populations to sedimentation was monitored via BAS following sample centrifugation at different rotational velocities. Aggregates were examined near the end of the growth windows used in this work: slow grown for 5 min (A) and fast grown for 2 min (B).

growing aggregates display a steeper sedimentation response to increasing centrifugation speed than slow growing aggregates, supporting the idea that the two aggregate types are hydrodynamically distinct (Figure 4-4 A,B). In order to examine the structural properties of the fast and slow growing aggregates in greater detail, we next employed negative stain electron microscopy (EM). In strong support of the THT data, fast growing aggregates posses fibroid shapes, while slow growing aggregates posses more spheroid and amorphously globular shapes (Figure 4-5 A-D). Importantly, the structures observed by EM are not contamination or preparation artifacts, as similar structures are not found in buffer only controls (Figure 4-6 A,B).

Fast and Slow Grown RuBisCO Aggregates Display Very Different Susceptibilities to DnaK and ClpB

In order to determine how aggregate size and/or structure impact disaggregation, the growth of fast and slow growing aggregates was first halted by dilution at both early and a late aggregation time points. These aggregate samples were then immediately mixed with a cocktail containing the full DnaK-ClpB bi-chaperone system plus ATP. First, the average rate of aggregate disassembly to dispersed monomers was examined using inter-molecular FRET. The same disaggregation experiments were then repeated with BAS in order to examine the detailed, population-resolved kinetics of disaggregation. Measurement of disaggregation by FRET revealed that both the fast and slow

growing aggregates are capable of complete disassembly when exposed to the DnaK-ClpB system at early times of aggregation growth (Figure 4-7 A). At later time points, both the fast and slow growing aggregates display a much reduced susceptibility to disassembly, with the overall rate of disaggregation slowing dramatically and the appearance of a highly resistant aggregates that appear to be completely resistant to disassembly (Figure 4-7 B). By BAS, the disaggregation process shows dramatic disassembly of both fast and slow growing aggregates at early times, with slow growing aggregates being especially aggressively and quickly dismantled. Strikingly, the efficiency of disassembly does not, in either case, appear to display a substantial size bias. For both fast and slow growing aggregates, objects spanning a 10-100 fold range of sizes, appear to disassemble at similar overall rates. At the longer aggregation time points, BAS reveals the clear presence of refractory aggregate populations that are either partially disassembled or barely dismantled at all. Interestingly, with both fast and slow aggregates, objects of similar size are readily disassembled at early aggregation time points, but become refractory to disaggregation at later time points (Figure 4-7 C-F).

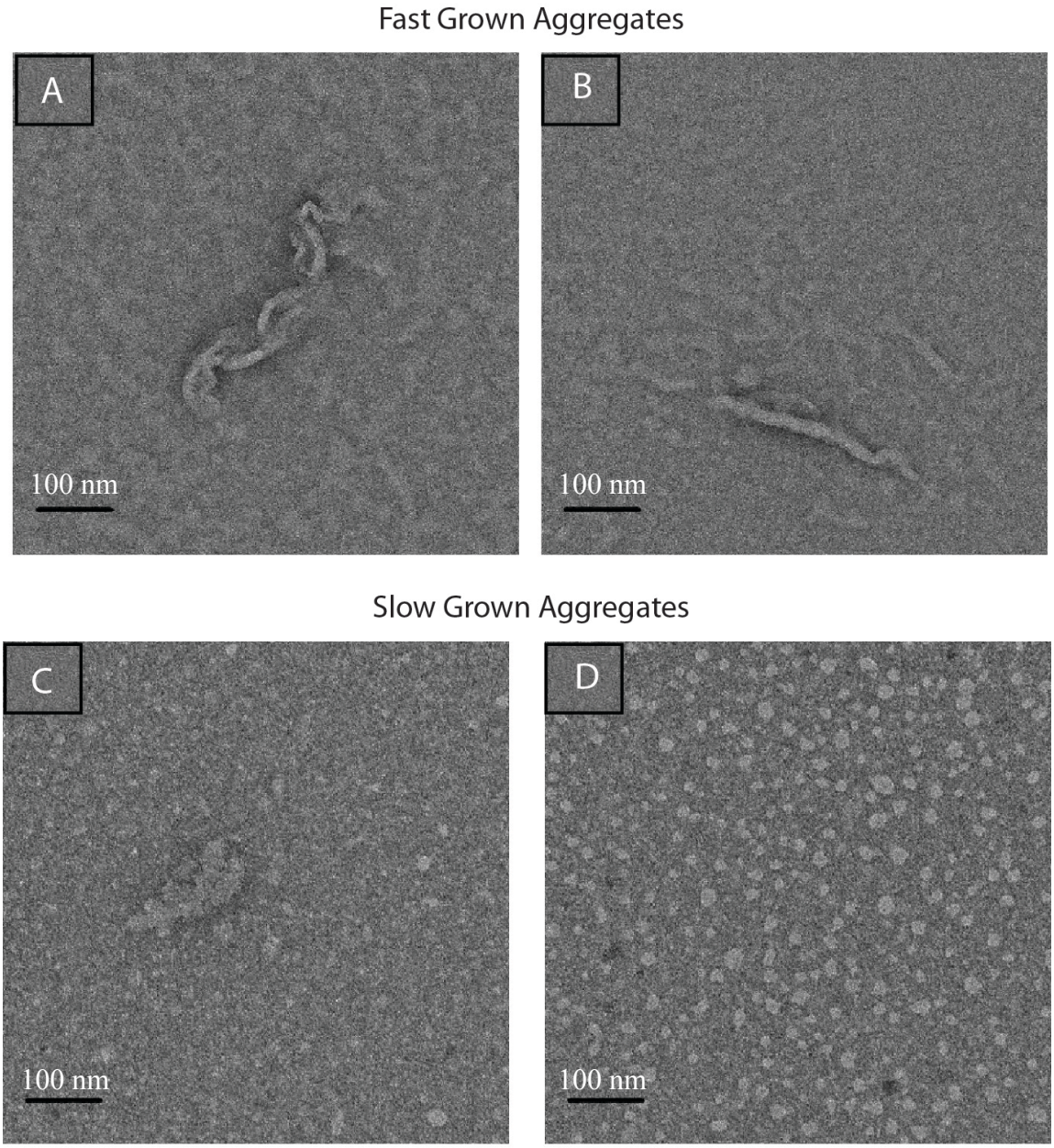

Figure 4-5 Fast Growing Aggregates Are Fibroid in Shape While Slow Growing Aggregates Are Amorphous in Shape. TEM images of RuBisCO aggregates fast grown for 2 Min are shown in (A,B). In (C,D), TEM images of RuBisCO aggregates slow grown for 5min are shown.

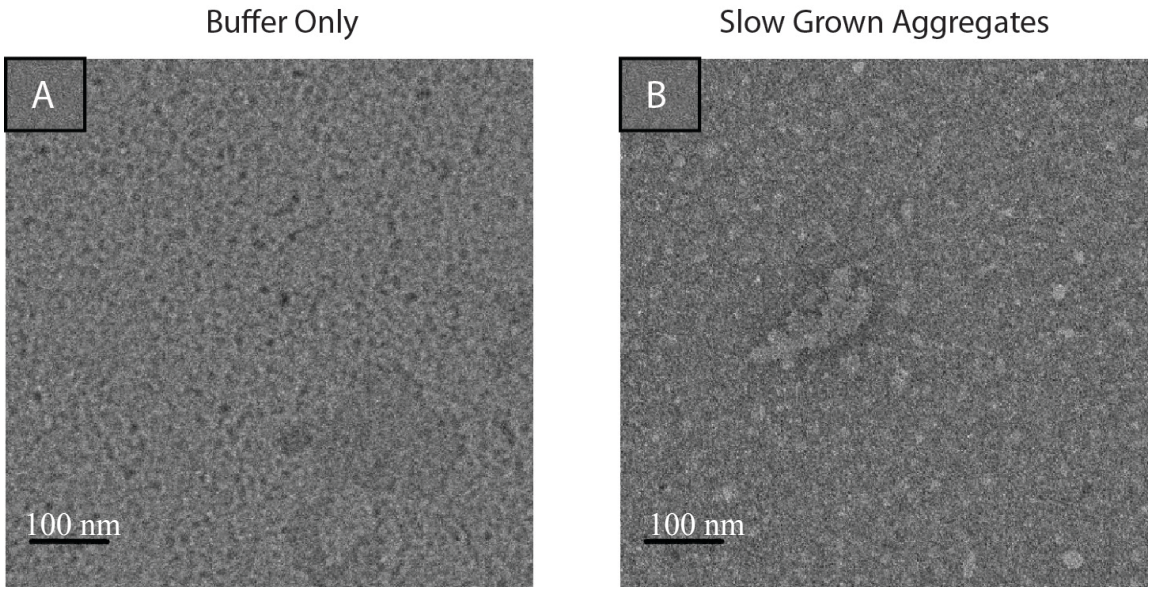

Figure 4-6 Structures in TEM Images Are Not a Product of Buffer Combination. Shown in (A) is a TEM image of the aggregation buffer used for these studies, which was processed in the same manner, and in parallel, with a sample of slow grown aggregates (B).

The threading motor of ClpB is thought to make this molecular machine a highly robust disaggregase, one that is could be insensitive to variations in aggregate structure and conformation. At the same time, disaggregation by ClpB is substantially dependent on the presence of DnaK (Haslberger et al, 2007; Haslberger et al, 2010). While there is some evidence that DnaK could play a direct role in disaggregation, perhaps by impacting the structure of aggregates, most current models assume that DnaK is primarily a targeting and regulatory factor for ClpB (Haslberger et al, 2007). In order to examine this question, we tested the disaggregase capacity of the DnaK system alone toward RuBisCO aggregates. In this case, we only examined the earliest aggregation time points for both fast and slow growing aggregates. Surprisingly, in the complete absence of ClpB, the DnaK system is a very effective disaggregase toward the fast growing aggregates, readily dismantling both small and large aggregates across a 100-fold range of sizes (Figure 4-8 A,C). At the same time, however, the DnaK system alone shows only minimal activity at best toward the slow growing aggregates, failing to dismantle the vast majority of objects in this sample (Figure 4-8 A,B). Interestingly, the rate of fast growing aggregate disassembly by the DnaK system alone, as measured by FRET and BAS, is similar to what is observed when ClpB is also present. This observation suggests that ClpB may be contributing little to the disassembly of the fast growing aggregates and that, at least for this type of aggregate, the DnaK system is the primary disaggregase.

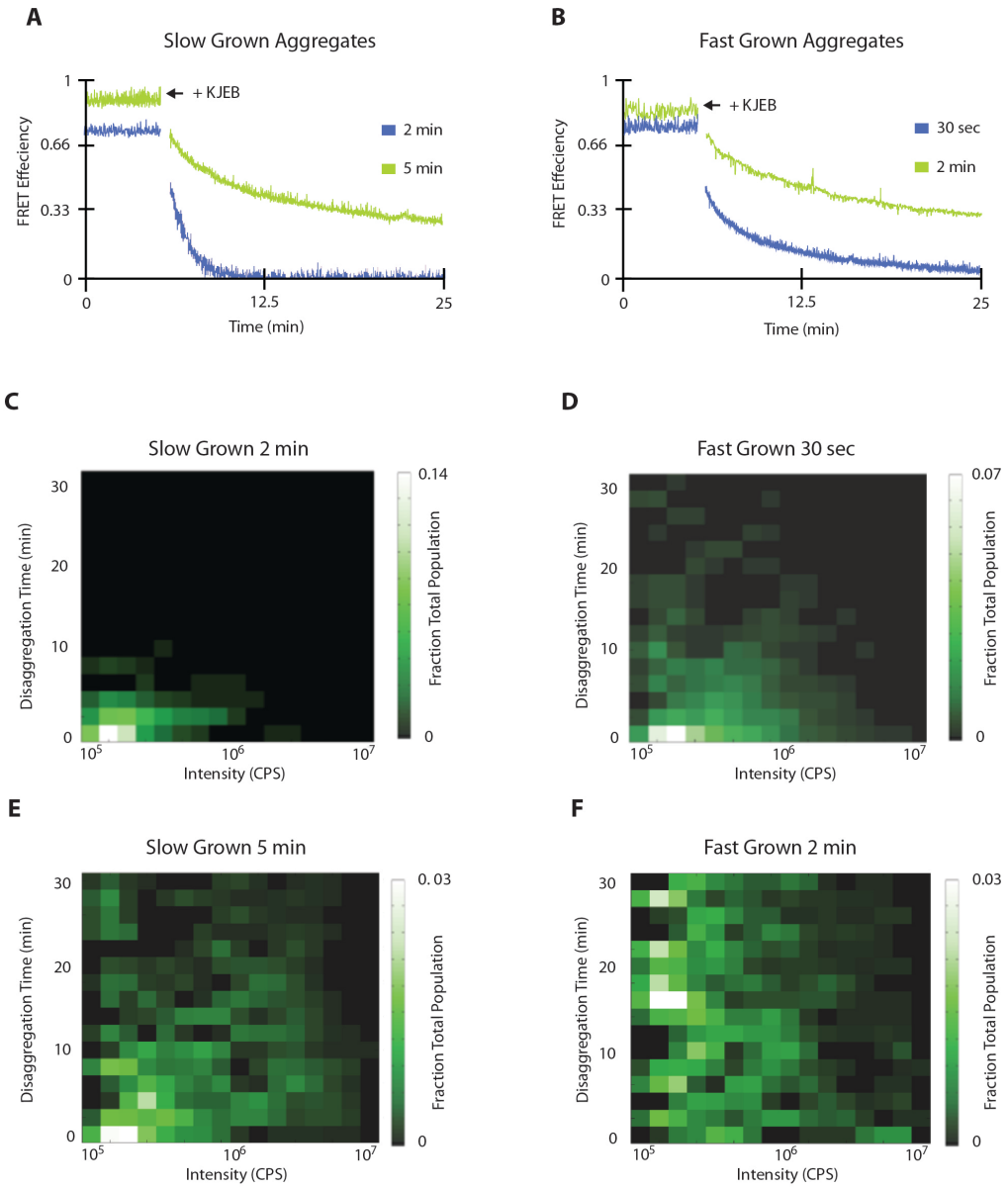

Figure 4-7 Slow Growing Aggregates Become More Refractory to Disaggregation by DnaK and ClpB Than Fast Growing Aggregates As Aggregation Continues. In (A,B), the average rate of disaggregation by DnaK, DnaJ, GrpE, and ClpB (KJEB) is examined by inter-molecular FRET for early (Bblue) and late (green) aggregation time points. KJEB mediated disaggregation of both slow (C and E) and fast (D and F) aggregates was also examined by BAS and plotted as two-dimensional heat maps where each row is a BAS population histogram a given time point during disassembly.

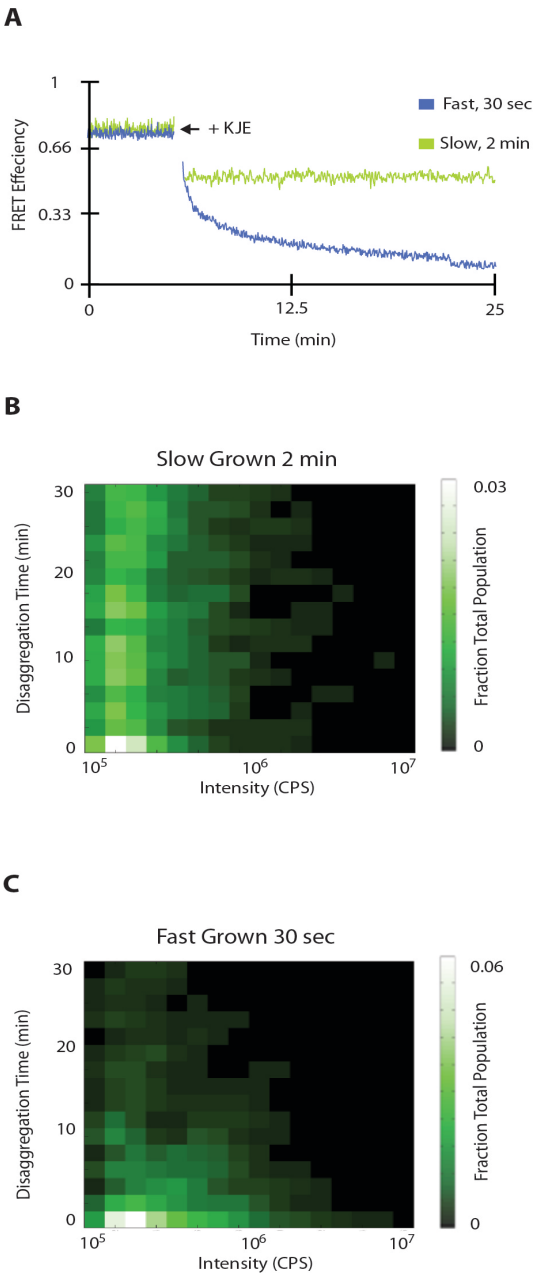

Figure 4-8 Slow Grown Aggregates Are Refractory to Disassembly by DnaK, DnaJ, and GrpE, While Fast Grown Aggregates Are Not. (A) The average rate of disaggregation by the DnaK system alone (DnaK, DnaJ, and GrpE; + KJE) is measured by inter-molecular FRET for fast growing aggregates at 30 sec (blue) and slow growing aggregates at 2 min (green). Disaggregation by KJE alone was examined by BAS for both slow growing (B) and fast growing (C) aggregates.

Even in the Absence of Growth, the Structure of RuBisCO Aggregates Changes Over Time

The size distribution of slow growing aggregates changes little from 2 min to 5 min (Figure 4-2 E), yet this small change in size equates to a large decrease in disaggregation potential (Figure 4-7 C,E). It is possible that continued aggregation from 2 min to 5 min results in the formation of slightly larger aggregates that, for some reason, are more resistant to disaggregation by virtue this terminal growth. However, it is also possible that resistance to disassembly has nothing to do with growth, but rather is the result of a structural transition within the aggregate assembly itself, some type of large-scale conformational shift that renders the aggregates resistant to being taken apart. In order to address this question, slow growing aggregates were grown for 3.5 min prior to dilution below their critical aggregation concentration. This sample was then either immediately examined by BAS or incubated for an additional 30 min at 23°C (Figure 4-9 A). The additional incubation in the absence of further aggregation, resulted in no detectable change in the concentration or size distribution of the aggregate assemblies (Figure 4-9 B). However, the ability of the aggregates to bind bis-ANS decreases (Figure 4-9 C) following the 30 min ageing incubation. At the same time, the average proximity of labeled RuBisCO regions within the aggregate structure appears to increase, based on inter-molecular FRET measurements (Figure 4-9 D). These observations suggest that, with time, the slow growing aggregates expose less hydrophobic surface

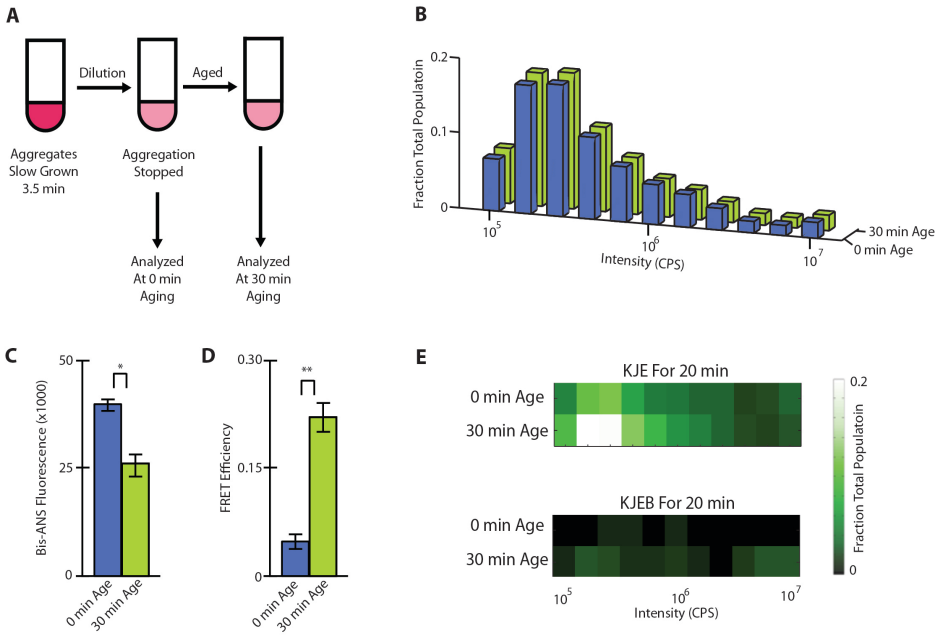

Figure 4-9 Independent of Continued Growth, Slow Grown Aggregates Can Change in Structure and Become Refractory to Disassembly by Molecular Chaperones. (A) Schematic of aggregate aging experiment. slow growing RuBisCO aggregates were grown for 3.5 min, then diluted to 10 nM to halt aggregate growth. Aggregate samples were either analyzed by BAS immediately or incubated for 30 min at 23°C. (B) The size distribution of aggregates analyzed immediately upon dilution (blue) and those aged for 30 min (green) are identical. (C) Changes in aggregate structure during aging were examined by bis-ANS and inter-molecular FRET. Stutent's T-test for * and ** are 10.09 and 13.33 respectively. (E) Aging results in a dramatic decrease in aggregate disassembly by molecular chaperones. The impact of aging on disassembly by the DnaK system only (KJE, upper) and the full DnaK-ClpB bi-chaperone system (KJEB) are shown as BAS heat maps.

and potentially become more compact. Importantly, both the full DnaK-ClpB bi-chaperone system, as well as the DnaK system alone, displayed a much reduced ability to disassemble the aged aggregates in comparison to aggregates of identical size that had not been aged (Figure 4-9 E).

Two general models could explain how aggregate ageing impacts disaggregation. In the first model, the observed decrease in exposed hydrophobic surface and increased compactness could result in a reduction in the number or quality of exposed chaperone binding sites. In this case, older aggregates bind less of the key chaperones at their surface, rendering them much more difficult to disassemble. In the second model, the increase in compactness and reduced hydrophobic surface could signal an increase in the number or strength of internal interactions between aggregate subunits, making it more difficult for chaperones to supply disrupt them. In order to distinguish between these possibilities, we first examined whether the surface properties of aged aggregates is different, in comparison to un-aged aggregates, by testing their ability to grow by adding new monomers.. For this experiment, we employed a two-color BAS experiment in which pre-formed RuBisCO aggregates, labeled with Alexa488, were mixed with non-native RuBisCO monomers, labeled with Alexa647. The number of coincident events between pre-formed aggregates and new monomers is substantially higher when aggregates are not aged. Thus, ageing reduces the ability of slow growing

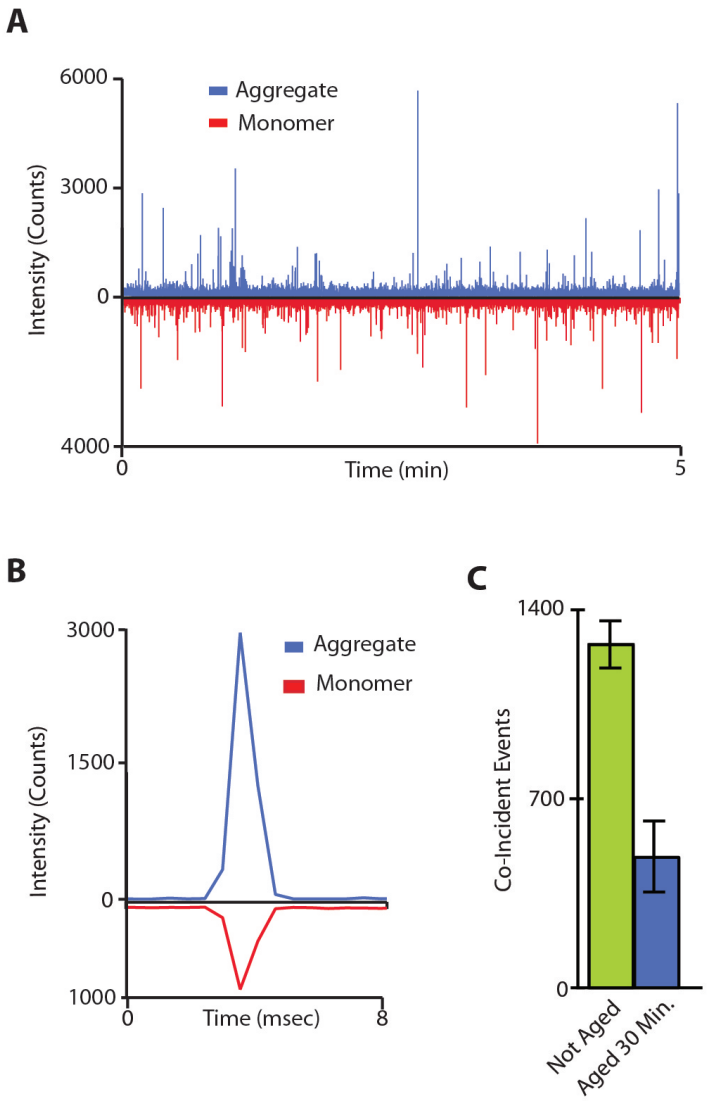

Figure 4-10 Aged Aggregates Lose the Ability to Aggregate. (A) An example of a two-color BAS aggregation experiment. One population of RuBisCO was labeled with a fluorescent probe (blue), aggregated, then mixed with non-native RuBisCO monomers labeled with a different fluorescent probe (red). Coincident bursts in two different detection channels permit the extent of monomer addition, as a function of size and time, to be assessed. (B) An example of a single burst event that shows strong correlated signal in both detection channels. (C) Aging results in a dramatic reduction in the number of correlated burst events detected in two-color aggregation experiments. The number of co-labeled aggregates detected before (green) and after (blue) aggregate aging is shown.

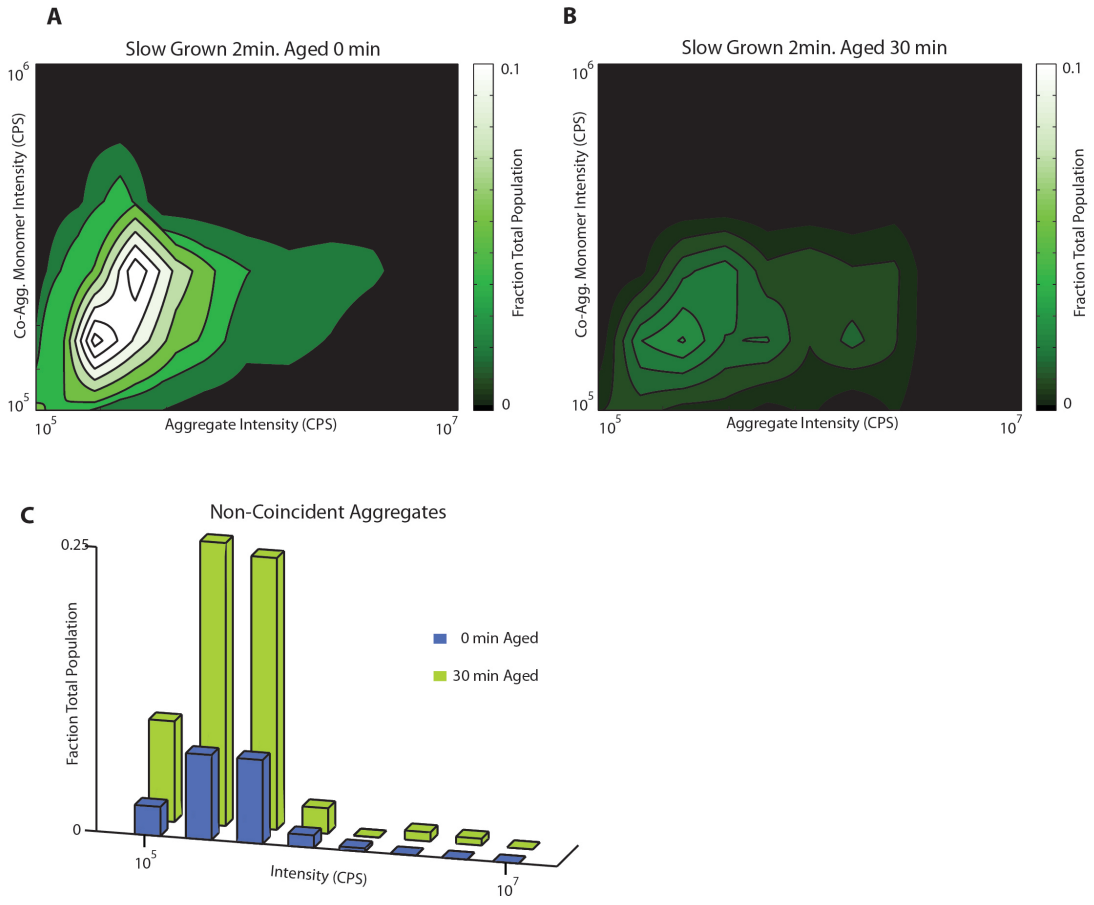

Figure 4-11 A Subset of Aged Aggregates Lose the Ability to Bind Monomer. MC-BAS analysis of two-color co-aggregation experiments displayed as contour heat maps. The distributions of co-labeled aggregates that were either not initially aged (A), or that were aged for 30 min (B) are shown. (C) The sub-population of aggregates that show no coincident signal in the second detection channel (i.e. starting aggregates that bound no additional monomers) were identified and analyzed by standard BAS. The size distribution and levels of the aggregates that displayed no co-labeling, and which were either not aged (blue) or aged for 30 min (yellow), are shown.

aggregates to add new monomers to their surface, suggesting that ageing significantly alters the surface properties of the aggregates (Figure 4-10 A-C). While MC-BAS shows that the size distribution of co-labeled aggregates changes little between aged and non-aged aggregates, the aged aggregates show a dramatic reduction in the ability to add monomers across all aggregate sizes (Figure 4-11 A-C).

The Extent of DnaK Binding to RuBisCO Aggregates Does Not Predict Disassembly Efficiency

In order to determine whether aggregate ageing impacts chaperone binding, a fluorescent variant of DnaK was created using non-natural amino acid incorporation and click chemistry (Jewett et all, 2010). In this process, p-azido-L-phenylalanine was incorporated during DnaK translation and then conjugated to an Alexa488 fluorophore variant, DBCO-488, using click chemistry. Slow growing, Alexa647-labeled aggregates were grown for 3.5 min, then mixed with the full DnaK system containing DnaK-DBCO-488, at a concentration where disaggregation is not observed. The sample was then examined by MC-BAS. The same experiment was also repeated for aggregates that were aged for 30 min. Surprisingly, no difference in DnaK binding was observed between aged and un-aged aggregates (Figure 4-12). In total, these observations suggest that, while the surface properties of aged aggregates change in a way that inhibits the addition of new monomers, this structural alteration appears to have

no impact on the exposure of the short, hydrophobic segments to which DnaK binds. Additionally, these observations further demonstrate that the inability of the DnaK-ClpB bi-chaperone system to disassemble aged aggregates cannot be due to a reduction in the ability of the essential, initiating chaperone to bind.

In Figure 4-7, we observed that both fast and slow growing aggregates become refractory to disassembly by the DnaK-ClpB bi-chaperone system as aggregation proceeds, independent of the size of the aggregate. Our observations with aged, slow growing aggregates suggests that internal structural changes in aggregates, which likely occur while aggregation proceeds but that are independent of growth, might explain this observation. In order to determine whether the conformational changes that occur during an aggregation reaction are similar to those observed with ageing alone, we examined the ability of both fast and slow aggregates to bind DnaK- DBCO-488 over the course of an aggregation reaction. In this case, the RuBisCO used was labeled with Alexa647 and MC-BAS was again employed.

In contrast to aged aggregates, slow growing aggregates lose the ability to bind DnaK as they approach the end of their aggregation trajectory (Figure 4-13 A,C,E). Strikingly, however, the fast growing aggregates do not (Figure 4-13 B,D,F). This observation suggests that the resistance of fast growing aggregates to disassembly is not due to a reduction in the binding capacity of

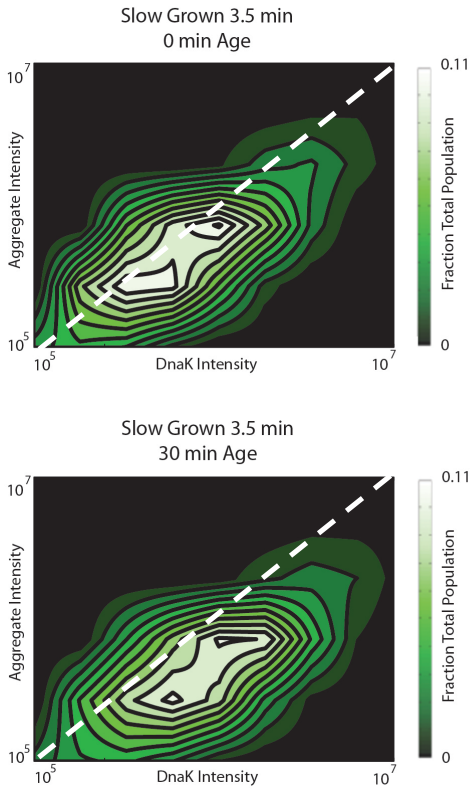

Figure 4-12 Aggregate Aging Does Not Result in Loss of DnaK Binding. The extent and distribution of fluorescent DnaK (DnaK517-DBCO488) binding to labeled RuBisCO aggregates was examined with a two-color MC-BAS experiment. DnaK binding to aggregates that were not subjected to aging (upper) and to aggregates aged for 30 min (bottom) is shown.

the critical initiator chaperone, DnaK. Rather, internal structural stabilization of the aggregates likely exceeds the level of destabilization that the DnaK system can apply. By contrast, it appears that the growth process leading to slow growing aggregates results in both internal and exterior conformational changes that limit the ability of DnaK to bind, and simultaneously increase the internal stability of the aggregate structure.

DnaK Induces Structural Changes in RuBisCO Aggregates That Makes Them More Susceptible to Disassembly by ClpB

Our observations with ClpB-independent disassembly of fast growing aggregates by the DnaK system supports previous observations that DnaK can operate as an disaggregase on its own. This observation, in combination with our demonstration of efficient DnaK aggregate binding to aggregates that resist disassembly, suggest that DnaK's role in disaggregation by ClpB is more involved than simply targeting and regulating the threading motor of ClpB. Specifically, these observations suggest that DnaK may play a critical role in destabilizing or preparing aggregates for disassembly by ClpB. Importantly, when this mechanism fails, even the aggressive ClpB threading motor is helpless to mediate aggregate disassembly. We therefore sought to determine whether the DnaK system has any detectable impact on the internal structure of RuBisCO aggregates Toward this end, slow growing aggregates were prepared at a 3.5 min growth point and mixed with DnaK at a concentration where no

Figure 4-13 Slow Growing Aggregates Bind Less DnaK As Aggregation Progresses. The extent and distribution of DnaK (DnaK517-DBCO488) binding to RuBisCO aggregates growing by either the fast or slow pathways was examined as a function of time using MC-BAS. The level of DnaK binding to fast growing aggregates after 30 sec (A) or 2 min (B) of aggregation is illustrated as a contour heat map. The level of DnaK binding to slow growing aggregates after 2 min (C) and 5 min (D) is also shown. The co-labeled distribution of fast growing aggregates stays clustered along the same diagonal region, indicating that relative level of DnaK binding does not change as the aggregates grow. By contrast, the shift in position of the co-labeled distribution for the slow growing aggregates indicates that these aggregates bind less DnaK as aggregation proceeds. (E and F) Aggregates that display no DnaK binding (i.e. aggregate burst events with no detectable coincident signal in the second detection channel) were identified and processed by traditional BAS. The resulting aggregate size distributions were re-binned into 'small,' 'medium,' and 'large' size ranges. The levels and size range of DnaK-free aggregates does not appear to change when aggregates grow by the fast pathway. However, when aggregates grow by the slow pathway, distinct shifts in the unbound sub-population appear, with notable increases in the number of medium and large sized aggregates that are free of DnaK.

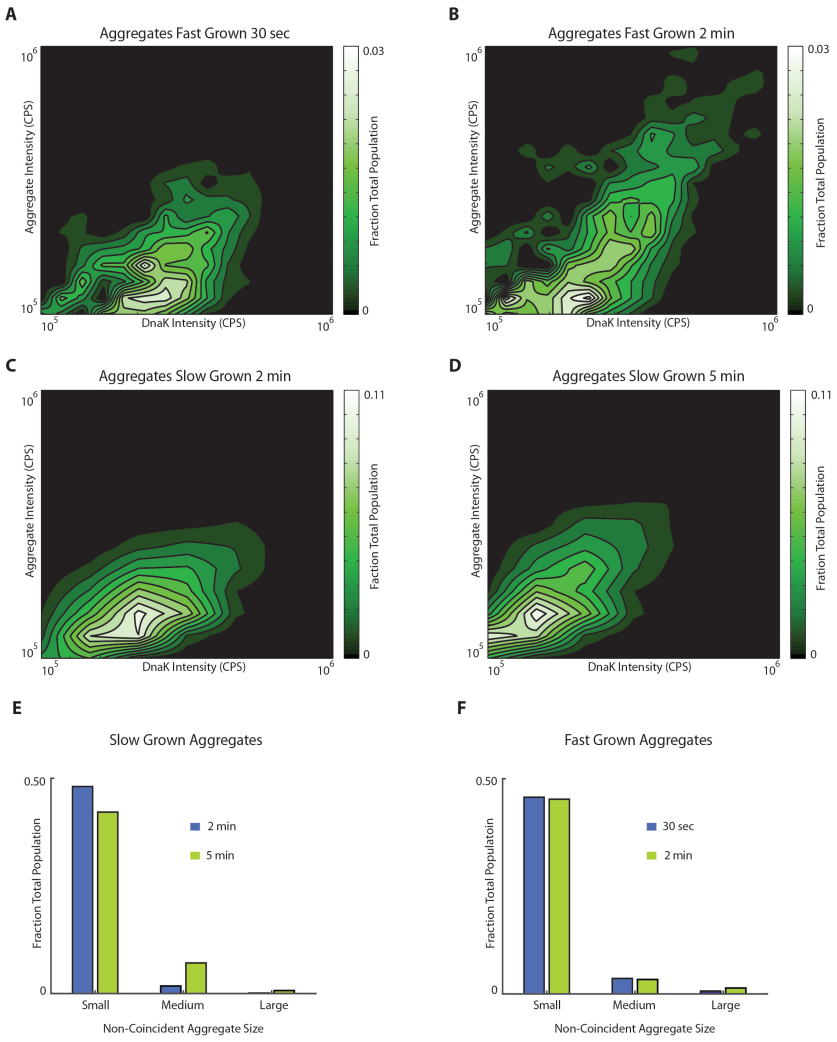
A
Aggregates Fast Grown 30 sec
B
Aggregates Fast Grown 2 min
C
Aggregates Slow Grown 2 min
D
Aggregates Slow Grown 5 min
Aggregate Intensity (CPS)
DnaK Intensity (CPS)
Fraction Total Population
0.03
0.11
0
E
Slow Grown Aggregates
F
Fast Grown Aggregates
0.50
2 min
5 min
30 sec
Small
Medium
Large
Non-Coincident Aggregate Size

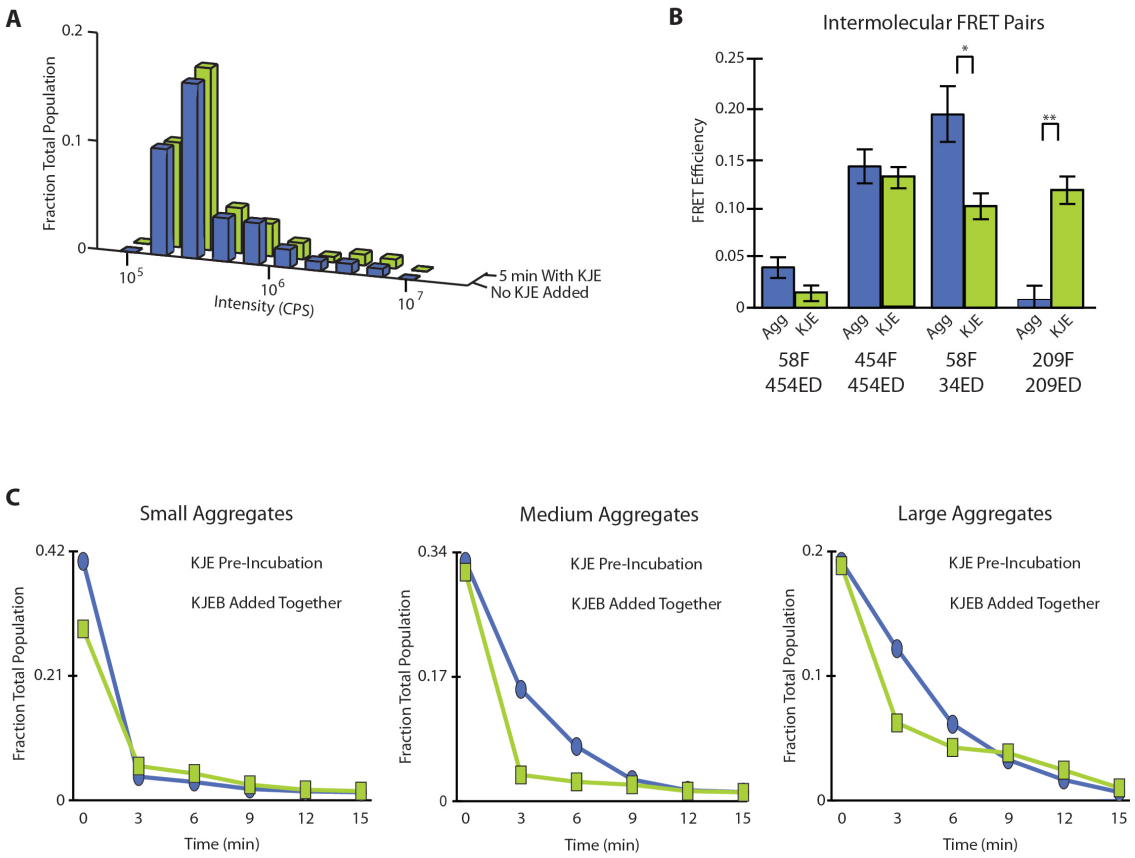

Figure 4-14 DnaK Alters the Structure of Slow Growing RuBisCO Aggregates, Which Enhances the Disassembly of Larger Aggregates By ClpB. (A) slow growing aggregates at 3.5 min of growth were incubated either with (green) or without (blue) the DnaK system alone (KJE), but at a 5-fold lower chaperone concentration (DnaK, DnaJ, and GrpE were 0.1 μM, 0.2 μM, and 0.2 μM respectively) The aggregate size distribution, from a standard BAS measurement, is shown after 5 min incubation at each condition. (B) The structure of slow growing aggregates was examined by inter-molecular FRET in the presence and absence of the DnaK system, under the same conditions as in (A). For three out of four different inter-molecular FRET pairs, the presence of the DnaK system induces a measureable change in average probe position, though no aggregate disassembly is detectable (A). (C) The impact of the DnaK system and ClpB order-of-addition on the disassembly of slow growing aggregates. Disaggregation was a followed as a function of time by BAS and the observed size distributions were re-binned into 'small,' 'medium,' and 'large' ranges. In one experiment, aggregates were pre-incubated with the DnaK system alone for 5 min (same conditions as in panel A), prior to the addition of ClpB. In a complementary experiment, the same KJEB components, at the same concentrations, were added to the aggregates simultaneously. Stutent's T-test for * and ** are 4.96 and 9.90 respectively.

disaggregation can be observed by BAS (Figure 4-14 A). Under these same conditions, however, the sensitized inter-molecular FRET assay demonstrates that DnaK binding significantly alters the average proximity of donor and acceptor labeled subunits within the aggregate (Figure 4-14 B). More importantly, this structural alteration appears to have a direct and substantial impact on the ability of ClpB to mediate efficient aggregate disassembly. When slow growing aggregates were mixed with DnaK for 5 min prior to the addition of ClpB, both medium and large aggregates were disassembled upon addition of ClpB much more quickly than when the DnaK system and ClpB were added to aggregates simultaneously (Figure 4-14 C). Thus, pre-treatment of the aggregates with DnaK presumably permits this chaperone system to begin the process of structural destabilization that ClpB is then required to complete. It is possible that smaller aggregates are similarly affected, however, these smaller objects come apart so quickly in this assay that a reliable comparison was not possible.

DnaK Can Partially Unfold RuBisCO Protein Folding Intermediates

When denatured RuBisCO is injected into buffer at 4°C, it remains monomeric and non-native, but cannot fold to its native state (Lin et al, 2001). Intra-molecular FRET between different donor and acceptor positions on the RuBisCO structure have been used to map out the relative proximity of these regsion in the non-native RuBisCO folding intermediate at 4°C (Lin et al, 2001;

Lin et al, 2004). Strikingly, upon the addition of the DnaK system to a solution containing the low-temperature RuBisCO folding intermediate, we observe a significant increase in the average distance separating these FRET pairs, indicating that DnaK binding, not unlike what was previously observed with GroEL (Lin et al, 2001; Lin et al, 2004), can partially unfold the kinetically trapped RuBisCO folding intermediate. Importantly, this enforced expansion is retained when the RuBisCO-DnaK sample is warmed to 23 °C as well. This observation is consistent with the idea that DnaK binding can alter the structure of the RuBisCO monomer contained within the slow growing aggregates, potentially inducing a range of secondary effects on the inter-subunit contacts that hold the aggregate together. It must be noted, however, that the conformation of the RuBisCO monomers in an aggregate is substantially different than the conformation of the kinetically trapped RuBisCO folding intermediate populated at 4°C. For example, intra-molecular FRET between positions 58 and is two-fold higher in the 4°C intermediate than in slow growing aggregates (Figure 4-15).

Unfortunately, the conformation of the RuBisCO monomer between the aggregated and disassembled state for slow growing aggregates cannot be directly compared, because the DnaK system alone cannot dismantle these aggregates. However, fast growing aggregates can be completely disassembled by DnaK. Interestingly, upon completion of disaggregation by

DnaK, the observed FRET efficiency between position 58 and 454, for what is presumed to be a DnaK bound RuBisCO monomer, is essentially unchanged relative to the FRET value for these positions in the aggregate (Figure 4-15 C) (Figure 4-3 D). While this appears to support the tugging model, the conformation of RuBisCO could be very different elsewhere on the monomer. Thus, in order to properly make that argument, the intra-molecular FRET between the other sites will have to be mapped out for the pre and post disaggregation states of fast growing aggregates.

A second interesting observation can be made from this data. The FRET signal between positions 58 and 454 is different for DnaK-bound folding intermediate that was never aggregated and the DnaK-bound monomer that was extracted from a fast growing aggregate (Figure 4-15 C). This suggests that, even though DnaK alters the conformation of RuBisCO in the course of removing from an aggregate, it cannot fully reverse the folding events that lead to the monomer conformation that is incorporated into the aggregate.

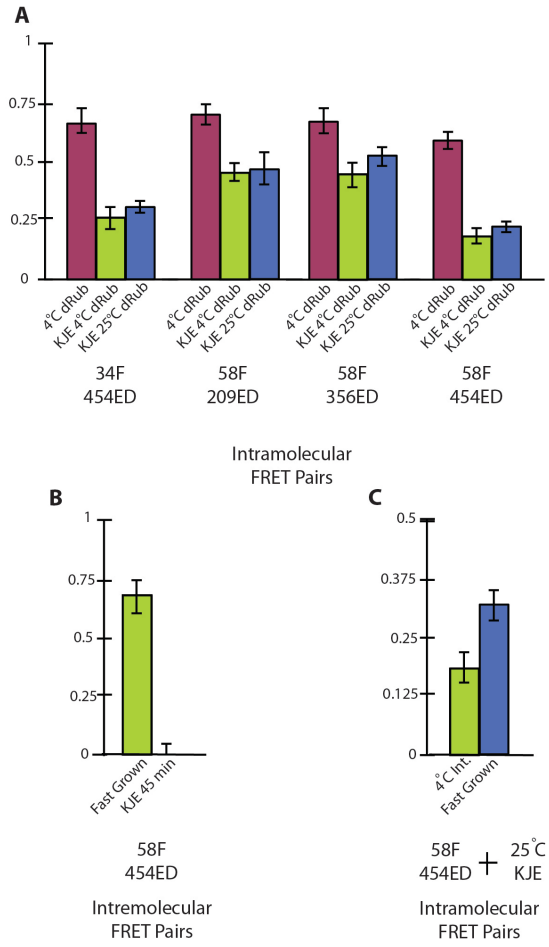

Figure 4-15 DnaK Has a Limited Ability to Induce Partial Unfolding of a Non-Native RuBisCO Monomer. (A) Intra-molecular FRET was used to examine the conformation of non-native RuBisCO, both with and without DnaK, DnaJ, and GrpE present. For these experiments, a monomeric, misfolded RuBisCO monomer was first populated at 4 °C (Lin et al, 2001). Samples of the kinetically trapped RuBisCO monomer were then mixed with the active DnaK system at 4 °C and FRET data acquired. Following an incubation of 5 min at 4 °C, the sample in the presence of the DnaK system was warmed to 25 °C and FRET data re-acquired. (B) Inter-molecular FRET between different RuBisCO monomers was used to determine when disassembly of fast growing aggregates was complete. (C) The conformation of RuBisCO monomers removed from fast growing aggregates and bound by DnaK, was compared to the conformation of the kinetically trapped RuBisCO monomer, also bound by DnaK, but never aggregated, using intra-molecular FRET.

Discussion

Since the time of their discovery, Hsp100s have been viewed as the primary disaggregation chaperones (Haslberger et al, 2010; Maurizi et al, 2004). This is not entirely surprising as most disaggregation studies show that the presence of Hsp100s greatly enhances the disaggregation potential of the Hsp70 system (Zietkiewicz et al, 2004). However, it was unknown whether the enhancement in disaggregation was the sole product of Hsp100s threading activity, or if Hsp70s played a sizable role in preparing aggregates for the activity of Hsp100. In this work, DnaK, Hsp70, is shown to be mostly incapable of disaggregating slow growing RuBisCO aggregates unless ClpB is present (Figure 4-16 A). However, the DnaK system alone can alter the structure of slow growing aggregates and enhance the disaggregation activity of ClpB (Figure 4-16 C). The enhancement in disaggregation provided by DnaK pre-incubation is most likely due to a DnaK-induced destabilization of global aggregate structure prior to the recruitment and engagement of ClpB. It is possible that DnaK always destabilizes the structure of aggregates prior to ClpB binding and this may be important for ClpB activity. In contrast to slow grown aggregates, DnaK alone is capable of disassembling fast growing aggregates (Figure 4-16 A), and the addition of ClpB only mildly enhances disaggregation. In both cases, the ability of DnaK to destabilize the structure of aggregates is a crucial step of disaggregation. Likewise, changes in an aggregates structure

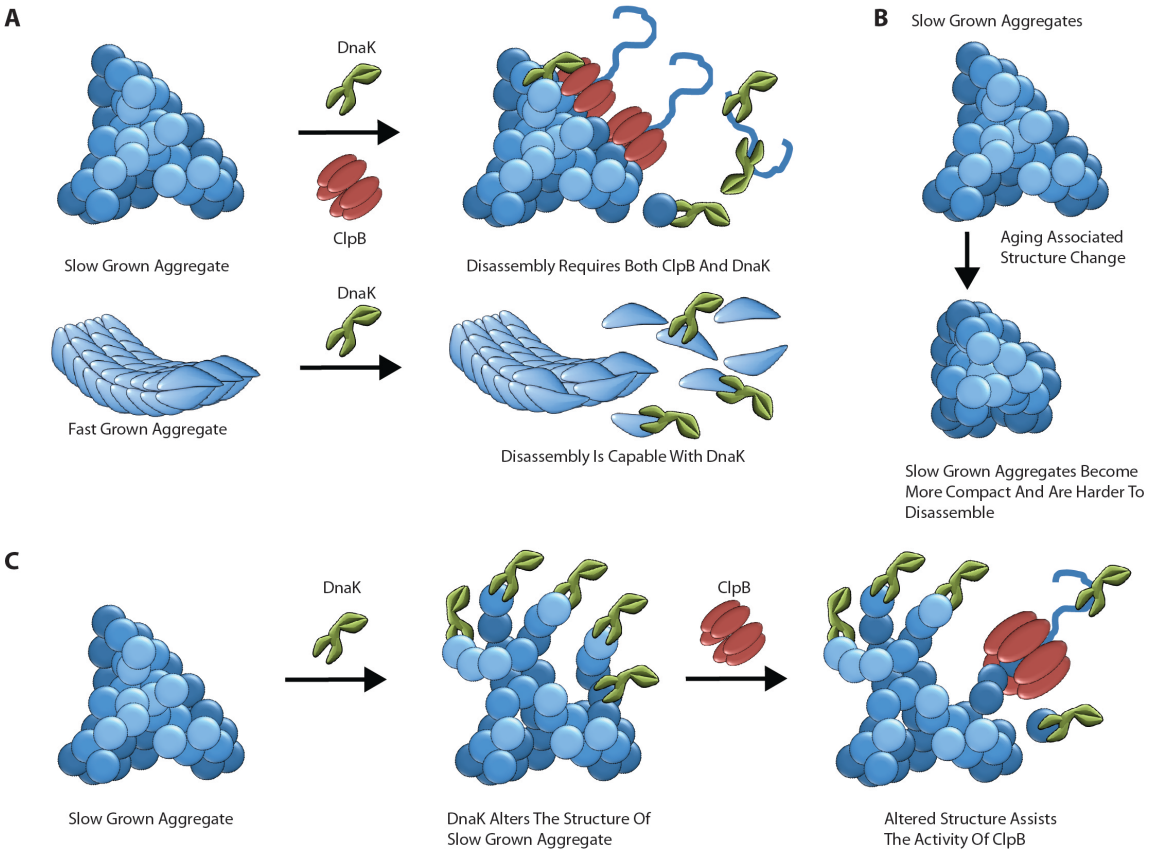

Figure 4-16 Summary of Observations. The schematic shows an overview of the findings in this report. (A) slow growing aggregates require the full DnaK-ClpB bi-chaperone system in order to be fully disassembled. However, the DnaK system alone can disassemble fast growing aggregates. In all cases, the observed disassembly behavior is independent of aggregate size over at least a 100-fold range. Thus, internal aggregate structure, and not size, ultimately dictates how effectively different chaperone systems can disassemble a given aggregate. (B) The structure of amorphous aggregates can continue to change with time, even in the absence of additional growth. Both inter- and intra-molecular FRET measurements are consistent with this structural change being associated with an increase in average compaction. While these structural transitions are not associated with a loss of DnaK binding, they severely compromise chaperone-mediated disaggregation. (C) The DnaK system alone can alter the structure of aggregates in a way that makes their disassembly by ClpB more efficient.

that hinder this activity of DnaK could make an aggregate refractory to disaggregation.

In this work, aging slow grown aggregates makes them refractory to disaggregation, with and with out ClpB. This is likely connected to the change in aggregate structure that occurs during aging (Figure 4-16 B). This likely strengthens the interactions between aggregate subunits and thus makes it more difficult to alter the structure of the aggregate and remove a subunit. In addition, the size of aggregates does not appear to be a major contributing factor to whether an aggregate is refractory to disaggregation. Thus, fast and slow growing aggregates may undergo structural changes during growth that account for the decrease in their ability to be disaggregated. However, unlike fast growing aggregates, slow growing aggregates lose the ability to bind DnaK with growth, which could also affect disaggregation.

These results not only demonstrate the importance of aggregate structure in disaggregation, but also provide a few circumstances through which aggregates could become refractory to disaggregation. For example, uncontrolled aggregate growth could not only make aggregates that are larger and take longer to disaggregate, but also make aggregates with stronger interactions between subunits that are harder to disaggregate. In addition, aggregates that are not disassembled fast enough may mature and strengthen

their interactions between subunits, thus making them more difficult to disassemble.

In total, this work shows that the internal structure of RuBisCO aggregates plays a deep role in disaggregation, more so than aggregate size. While larger aggregates may take longer to disassemble, it appears that the structure of an aggregate can make it completely refractory to disaggregation.

CHAPTER V

SUMMARY AND FUTURE DIRECTIONS

Summary

The development of this project coincided with a turning point in the study of molecular chaperones and their role in protein disaggregation. For almost two decades prior, the chaperone community had been working to unravel the secrets of the wonderfully intricate Hsp100 chaperone family. During this time, many prominent research groups heralded the Hsp100s as the true disaggregase chaperones of the cell. This sentiment was reinforced by the well-conserved structure of the Hsp100s, their almost ubiquitous presence throughout life, and their active, rather than passive, role in disaggregation. However, an Hsp100 homologue could not be found in humans or any other higher metazoan. Eventually, it became accepted that this was because the gene for Hsp100 had been lost in a genomic deletion event early in the evolution of higher metazoans.

Through the work of Bukau, Shorter, Morimoto, and others, it was discovered that higher metazoans compensate for the loss of Hsp100 with a specialized set of co-chaperones that increase the disaggregation capacity of Hsp70. However, the Hsp70 system is still thought to perform disaggregation via entropic pulling and the addition of synergizing Hsp40s and Hsp110s only

serves to increase the local entropic pulling force of the Hsp70s. Thus, the mechanism of disaggregation in higher metazoans fundamentally differs from the disaggregation mechanism employed by organisms that possess a combined Hsp70-Hsp100 bi-chaperone system. However, many eukaryotes, including lower metazoans, posses a full Hsp70-Hsp100 bi-chaperone system as well as synergizing Hsp40s and Hsp110s. Thus, the metazoan that survived the genomic loss of Hsp100, and ultimately gave rise to higher metazoans, was already equipped with a complementary disaggregation system able to compensate for the loss of Hsp100. While this allowed our metazoan ancestors to tolerate the loss of Hsp100, it likely had to evolve to compensate for the loss of Hsp100 by applying selective pressure to chaperone activity and the folding behavior of the proteome. However, it is unlikely that every protein that needs an Hsp100 for disaggregation has either been mutated to not need Hsp100 or removed from the genome. Thus, a better understanding of the relationship between aggregate structure and disaggregation by specific chaperones should shed light on what our chaperone system may or may not be able to disassemble and why.

The original goal of this work was to better understand the impact of aggregate qualities, like size and structure, on the disaggregation capacity of molecular chaperones, specifically the Hsp100 and Hsp70 chaperones from *E. coli*. However, after the first few experiments, it became clear that aggregate

size does not predict whether an aggregate can be disassembled. This strongly suggested that the internal structure of aggregates is a more important quality for determining whether aggregates can be dismantled. The data outlined here strongly supports this concept. In total, this work also suggests that the impact of aggregate structure and subunit conformation on disaggregation could reasonbly be rationalized in terms of intermolecular and intramolecular interactions. This simple way of rationalizing the data also provides a means to interpret the potential impact of similar aggregates in a cellular setting.

Somewhat surprisingly, fast growing RuBisCO aggregates can be disassembled by the DnaK system alone. At the same time, the addition of ClpB provided little or no addition help in taking fast growing aggregates apart. This suggests that ClpB is either not able to engage fast growing aggregates, is unable to thread them through its central pore, or the threading activity of the ClpB motor simply provides no additional benefit beyond what the DnaK system achieves. If ClpB is unable to thread the fast growing aggregates, this would indicate that the intra-molecular interactions may be too strong for ClpB to disrupt. This hypothesis is supported by the observation that DnaK is not able to fully unfold the RuBisCO that it removes from fast grown aggregates to the same extent that it can unfold RuBisCO that was never aggregated. Conversely, the inter-molecular interactions in fast growing aggregates appear to be relatively weak, because DnaK can disassemble them without the assistance of ClpB. It

is also possible that this observation can be attributed to the fibroid shape of the fast growing aggregates. Fibroid objects should have a higher ratio of surface area to volume than spheroid objects of the same approximate volume. In turn, this would mean that a fibrous aggregate might have more exposed chaperone binding sites than a spheroid one. Also, fibrous aggregates assemble by connecting subunits in a substantially end-to-end manner, whereas subunits of spheroid aggregates can be completely buried within an aggregate and are thus more likely to make intermolecular interactions than fibrous aggregates. This may be why DnaK can disassemble fast growing aggregates, which are more fibroid in shape, than slow grown aggregates, which are more spheroid in shape.

These observations with fast growing aggregates may help explain certain facets of amyloid related diseases, such as Alzheimer's. *In vitro*, the human Hsp70 system is able to disassemble amyloid-beta fibrils. This led to the conclusion that the Hsp70 system is essentially overworked within neurons and cannot keep up with the continuous growth of fibrils. However, it is possible that the amyloid-beta fibrils are resistant to AAA+ threading motors in the same way that the fast growing aggregates are. While humans do not have an Hsp100 chaperone, they do have AAA+ proteases that may not be able to degrade the subunits of amyloid-beta fibrils. In this case, the Hsp70 system may be disassembling the amyloid-beta fibrils, but, because of their strong intramolecular interactions, the AAA+ proteases cannot unfold and degrade the

amyloid-beta protein. With time, the amyloid-beta subunits could re-aggregate into fibrils.

In aggregate aging experiments, slow growing aggregates were diluted below their critical aggregation concentration and aged for 30 min. During the aging process, the structure of the aggregates changes in a way that prevents disaggregation by DnaK both with and without ClpB. This change is associated with an increase in intermolecular FRET and a loss of bis-ANS binding. Thus, it is likely that the aggregates are either becoming more compact, denser or the aggregate subunits are rearranging with time. In any case, this change in aggregate structure is likely to strengthen the intermolecular interactions between aggregate subunits. This, in turn, appears to completely abolish disaggregation by the DnaK system alone and makes the aggregates more difficult for ClpB to disassemble. However, the loss of susceptibility to DnaK and ClpB activity is much greater when slow growing aggregates are allowed to continue growing for even a few minutes. Minor changes in the size distribution of aggregates that were slow grown from 2 min to 5 min appear to have an enormous impact on disaggregation potential.

In human cells, the presence of aggregates that are similar to slow growing RuBisCO aggregates could be catastrophic. While higher metazoans have a more advanced Hsp70 disaggregation network, aggregates with strong

intermolecular interactions, which can develop even stronger intermolecular interactions with age, may still be too difficult to disassemble. While this could explain how amorphous pre-fibrillar aggregates are able to escape the Hsp70 system, it does not explain why the human AAA+ proteases are not able to degrade pre-fibrillar aggregates. However, the truth may be that the AAA+ proteases are hindered in aggregate degradation because they do not synergize with the Hsp70 system the way that the Hsp100 chaperones do. Consider the experiments presented earlier in this work where DnaK was pre-incubated with slow growing aggregates before ClpB was added. When DnaK was pre-incubated with slow grown aggregates, aggregate disassembly was not observed. Despite the lack of disaggregation, DnaK was able to perturb either the intermolecular or intramolecular interactions in slow growing aggregates, which altered their structure. This increased the efficiency of ClpB mediated disaggregation, which indicates that DnaK not only recruits and activates ClpB, but also synergizes with the activity of ClpB to increase the productivity of disaggregation. However, the key to this synergy is likely that DnaK has evolved to recruit ClpB and activate its activity at just the right time. It is this timed, synergistic activity that higher metazoans lack. Although they have both the Hsp70 system and AAA+ proteases, they lack the synergy between these two systems that could be crucial for clearing these aggregates. Interestingly, when the yeast Hsp100, which can synergize with the human Hsp70, is introduced into neurons containing alpha-synuclein fibrils, both the amyloid fibrils and the pre-

fibrillar aggregates are cleared (Shorter, 2010; Vashist et al, 2010; Bianco et al, 2008). When Hsp100 from yeast was introduced into neurons that contained fibril or pre-fibril amyloid-beta protein, Hsp104 was able to clear the pre-fibrillar forms of amyloid-beta and prevent fiber formation. However, Hsp100 was unable to disassemble pre-formed amyloid-beta fibrils (Bianco et al, 2008).

Ultimately, both the Hsp70 and the Hsp100s may have their disaggregation activity limited by the structure of their substrates. However, the entire system hinges upon the capability of the Hsp70 system to not only recruit and activate assisting chaperones but to also perform disaggregation on its own, or prepare aggregates for disaggregation by other chaperones. Interestingly, evolution has seen fit to not only maintain the Hsp70s as key chaperones in a wide variety of cellular functions, but to also conserve the basic function and structure of the Hsp70s. Instead, evolution has selected for the diversification of co-chaperones and partner chaperones that can interact with the well-conserved Hsp70. One reason for this persistent selection may be the passive activity of the Hsp70s. Whether or not a protein will fold or unfold upon interaction with an Hsp70 is ultimately dictated by the strength of the intramolecular interactions within the substrate protein. This allows the Hsp70 to “detect” whether a mutant protein will be able to fold independently and helps evolution select for folding stability that results in a “healthier” proteome.

Future Directions

An obvious next step for this work would be to perform similar experiments with eukaryotic chaperones. However, having set-up a wonderful system from *E. coli*, it would be wasteful to not attempt to understand the interplay of other protein quality control systems from *E. coli* with the disaggregase system. RuBisCO has already been well studied as a folding substrate for GroEL/ES, and it could prove fruitful to test the ability of GroEL/ES to fold different conformations of RuBisCO. An example would be to examine the ability of GroEL/ES to fold RuBisCO monomers that have been removed from fast growing aggregates, which cannot be completely unfolded by DnaK. The strong intra-molecular interactions of this conformation may make it difficult or impossible to fold, which could make an extraordinary story.

Another avenue of study is the AAA+ proteases from *E. coli*. Their activity is crucial for homeostasis, but the impact of aggregate structure and monomer conformation has not been well studied. Examining each of these systems may result in the discovery of a protein conformation that is resistant to DnaK, AAA+ threading motors, and GroEL. Such a fold may provide a better understanding of disease states in humans and other organisms.

REFERENCES

Adams, M., Blundell, T., Dodson, E., Dodson, G., Vijayan, M., Baker, E., Harding, M., Hodgkin, D., Rimmer, B., Sheat, S.; Structure of Rhombohedral 2 Zinc Insulin Crystals; Nature 224 (1969)

Alvarez-Erviti, L., Seow, Y., Schapira, A., Gardiner, C., Sargent, I., Wood, M., Cooper, J. M.; Lysosomal dysfunction increases exosome-mediated alpha-synuclein release and transmission. Neurobiology of Disease; 42 (3): 360–367 (2011)

Alzheimer, A.; Uber eine eigenartige Erkrankung der Hirnrinde. Allgemeine Zeitschrift fur Psychiatrie und Psychisch-Gerichtliche Medizin; 64 (1907)

Andrade, J., Hlady, V.; Protein Adsorption and Materials Biocompatibility: A tutorial Review and Suggested Hypothesis. Advances in polymer science; 79 (1986)

Anfinsen, C., Haber, E., Sela, M., White, F.; The kinetics of formation of native ribonuclease during oxidation of the reduced polypeptide chain; PNAS 47: 1309-1314 (1961)

Ang, D., Liberek, K., Skowyra, D., Zylicz M., Georgopoulos, C.; Biological role and regulation of the universally conserved heat shock proteins; J. Biol. Chem. 266: 24233–24236 (1991)

Anguiano, M., Nowak, R. J., Lansbury, P. T. J.; Protofibrillar islet amyloid polypeptide permeabilizes synthetic vesicles by a pore-like mechanism that may be relevant to type II diabetes. Biochemistry; 41: 11338–11343 (2002)

Astbury, W. T.; Some problems in the x-ray analysis of the structure of animal hairs and other protein fibres; transactions of the Faraday Society 29: 140 (1933)

Baker-Nigh, A.,Vahedi, S., Davis, E. G., Weintraub, S., Bigio, E. H., Klein, W. L., Geula, C.; Neuronal amyloid-β accumulation within cholinergic basal forebrain in ageing and Alzheimer's disease; Brain: Journal of Neurology 138: 1722-1737 (2015)

Bakthisaran, R., Tangirala, R., Rao, C.; Small heat shock proteins: Role in cellular functions and pathology. Biochimica et Biophysica Acta (BBA) - Proteins and Proteomics; 1854 (4): 291–319 (2015)

Bashkirov, P., Akimov, S., Evseev, A., Schmid, S., Zimmerberg, J., Frolov, V.; A partnership between dynamin and lipids defines dynamics and intermediates of membrane fission; Cell 135 (7): 1276-1286 (2008)

Becker, J., Craig, E. A.; Heat-shock proteins as molecular chaperones. Eur J Biochem; 219 (1-2): 11-23 (1994)

Beck, R., Prinz, S., Diestelkotter-Bachert, P., Rohling, S., Adolf, F., Hoehner, K., et al; Coatomer and dimeric ADP ribosylation factor 1 promote distinct steps in membrane scission; Cell Biol, 194: 765-777 (2011)

Bennhold, H.; Eine spezifische amyloidfarbung mit Kongorot; Munchener Medizinische Wochenschrifte 69 (1922)

Berhanu, W., Hansmann, U.; Structure And Dynamics Of Amyloid-β Segmental Polymorphisms; doi:10.1371/journal.pone.0041479. (2012)

Bieschke, J. Ultrasensitive detection of pathological prion protein aggregates by dual-color scanning for intensely fluorescent targets; Proc Natl Acad Sci USA 97: 5468-5473 (2000)

Bocking, T., Aguet, F., Harrison, S.C., Kirchhausen, T; Single-molecule analysis of a molecular disassemblase reveals that mechanism of Hsc70-driven clathrin uncoating; Nat Struct Mol Biol 18 (3): 295-301 (2011)

Boucrot, E., Pick, A., Camdere, G., Liska, N., Evergren, E., McMahon, H. T. Membrane fission is promoted by insertion of amphipathic helices and is restricted by crescent BAR domains; Cell 149: 124-136 (2012)

Bowen, B., Enderlein, J., Woodbury, N.; Single-molecule fluorescence spectroscopy of TOTO on Poly-AT and Poly-GC DN; Photochemistry and Photobiology 78 (6): 576-581 (2003)

Brehmer, D., Gassler, C., Rist, W., Mayer, M. P., Bukau, B.; Influence of GrpE on DnaK-substrate interactions; The Journal of Biological Chemistry 279 (27): 27957-27964 (2004)

Brinker, A., Scheufler, C., Von Der Mulbe, F., Fleckenstein, B., Herrmann, C., Jung, G., Moarefi, I., Hartl, F.; Ligand discrimination by TPR domains: Relevance and selectivity of EEVD-recognition in Hsp70 x Hop x Hsp90 complexes; J Biol Chem (22): 19265-75 (2002)

Bucciantini, M., Giannoni, E., Chiti, F., Baroni, F., Formigli, L., Zurdo, J., Taddei, N., Ramponi, G., Dobson, C., Stefani, M.; Inherent Toxicity of aggregates implies a common mechanism for protein misfolding diseases; Nature 416 (2002)

Bukau, B., Horwich, A. L.; The Hsp70 and Hsp60 chaperone machines; Cell 92: 351–366 (1998)

Camilleri, A., Zarb, C., Caruana, M., Ostermeier, U., Ghio, S., Högen, T., Schmidt, F., Giese, A., Vassallo, N.; Mitochondrial membrane permeabilisation by amyloid aggregates and protection by polyphenols; BBA – Biomembranes 1828 (11): 2532–2543 (2013)

Campelo, F., Malhotra, V.; Membrane Fission: the biogenesis of transport carriers. Annu Rev Biochem; 81: 407-427 (2012)

Capaldi, A. P., Kleanthous, C., Radford, S. E.; Im7 folding mechanisms: misfolding on a path to the native state; Nature Structural Biology 9 (3) (2002)

Carr, C., Rizo J.; At the junction of SNARE and SM protein function; Curr Opin Cell Biol. 22: 488-495 (2010)

Cataldo, A. M., Peterhoff, C. M., Troncoso, J. C., Gomez-Isla, T., Hyman, B. T., Nixon, R. A.; Endocytic pathway abnormalities precede amyloid beta deposition in sporadic Alzheimer's disease and Down syndrome: differential effects of APOE genotype and presenilin mutations; Am J Pathol 157 (1): 277-86 (2000)

Chen, H., Fre, S., Slepnev, V. I., Capua, M. R., Takei, K., Butler. M. H.; Epsin is an EH-domain-binding protein implicated in clathrin-mediated endocytosis; Nature 394: 793-797 (1998)

Chen, Y. W., Fersht, A. R., Henrick, K.; Contribution of buried hydrogen bonds to protein stability. The crystal structures of two barnase mutants; J. Mol. Biol. 234 (4) (1993)

Chen, Y., Muller, J., So, P., Gratton, E. The photon counting histogram in fluorescence fluctuation spectroscopy; Biophys J 77: 553-567 (1999)

Chen, Y., Wei, L., Muller, J. Probing protein oligomerization in living cells with fluorescence fluctuation spectroscopy; Proc Natl Acad Sci USA 100: 15492-15497 (2003)

Chen, Z., Chang, K., Capraro, B., Zhu, C., Hsu, C.J., Baumgart, T. ; Intradimer/Intermolecular interactions suggest auto inhibition mechanism in endophilin A1; J Am Chem Soc 136: 4557-4564 (2014)

Chernomordik, L. V., Kozlov, M.; Mechanics of membrane fusion; Nat Struct Mol Bio 15: 675-683 (2008)

Chin, W., Santoro, S., Martin, A., King, D., Wang, L., Schultz, P.; Addition of p-Azido-L-phenylalanine to the genetic code of Escherichia coli; J. Am. Chem. Soc. 124 (31): 9026-9027 (2002)

Chiti, F., Taddei, N., Baroni, F., Cappanni, C., Stefani, M., Ramponi, G., Dobson, C. M.; Kinetic Partitioning of protein folding and aggregation; Nature Structural Biology 9 (2) (2002)

Clark, S., Mathies, R.; High-speed parallel separation of DNA restriction fragments using capillary array electrophoresis; Anal Biochem 215: 163-170 (1993)

Cornish-Bowden, A., Koshland, D.; The Quaternary Structure Of Proteins Composed Of Identical Subunits; The Journal Of Biological Chemistry 246 (10) (1971)

Craig, E. A., Huang, P., Aron, R., Andrew, A.; The diverse roles of J-proteins, the obligate Hsp70 co-chaperone; Rev. Physiol. Biochem. Pharmacol. 156: 1–21 (2006)

Daumke, O., Roux, A., Haucke, V.; Bar domain scaffolds in dynamin-mediated membrane fission; Cell 156: 882-892 (2014)

David. D. C., Ollikainen, N., Trinidad, J. C., Cary, M. P., Burlingame, A. L., et al; Widespread Protein Aggregation as an Inherent Part of Aging in C. elegans. doi:10.1371/journal; pbio.1000450 (2010)

Groot, N. S., Sabate, R., Ventura, S.; Amyloids in bacterial inclusion bodies; Trends in Biochemical Sciences 34 (8) (2009)

De Simone, A., Dhulesia, A., Soldi, G., Vendruscolo, M., Hsud, S. D., Chitic, F., Dobson, C. M.; Experimental free energy surfaces reveal the mechanisms of maintenance of protein solubility; PNAS 108 (52): 21057-21062 (2011)

Dill, K. A., Chan, H. S.; From Levinthal to pathways to funnels; Nature Structural Biology 4 (1) (1997)

Di Stasio, E., De Cristofaro, R.;The effect of shear stress on protein conformation: Physical forces operating on biochemical systems: The case of von Willebrand factor; Biophysical Chemistry 153 (1): 1–8 (2010)

Erives, A.J., Fassler, J. S.; Metabolic and chaperone gene loss marks the origin of animals: evidence for Hsp104 and Hsp78 chaperones sharing mitochondrial enzymes as clients; PloS One 10 (2): e0117192 journal.pone.0117192 (2015)

Erjavec, N., Larsson, L., Grantham, J., Nyström, T.; Accelerated aging and failure to segregate damaged proteins in Sir2 mutants can be suppressed by overproducing the protein aggregation-remodeling factor Hsp104p; Genes Dev. 21: 2410–2421 (2007)

Erjavec, N., Larsson, L., Grantham, J.; Accelerated aging and failure to segregate damaged proteins in sir2 mutants can be suppressed by overproducing the protein aggregation-remodeling factor hsp104p; Genes Dev. 21: 2410-2421 (2007)

Fandrich, M.; On the structural definition of amyloid fibrils and other polypeptide aggregates; Cell and Molecular Life Sciences 64: 2066-2078 (2007)

Farr, G. W., Fenton, W. A., Chaudhuri, T.K., Clare, D. K., Saibil, H. R., Horwich, A. L.; Folding with and without encapsulation by cis- and trans-only GroEL-GroES complexes; The EMB Journal 22 (13): 3220-3230 (2003)

Felsovalyi, F., Patel, T., Mangiagalli, P., Kumar, S., Banta, S.; Effect of thermal stability on protein adsorption to silica using homologous aldo-keto reductases; Protein Sci. (8): 1113–1125, doi: 10.1002/pro.2099. (2012)

Fink, A.; Protein aggregation: folding aggregates, inclusion bodies and amyloid; Folding and Design 3 (1) (1998)

Fischer, E., Fourneau, E.; Ueber einige Derivate des Glykocolls; Berichte der deutschen chemischen Gesellschaft 4 (2) (1901)

Ford, M. G. J., Mills, I. G., Peter, B. J., Vallis, Y., Praefcke, G. J. K., Evans, P. R., McMahon, H. T.; Curvature of clathrin-coated pits is driven by epsin; Nature 419: 361-366 (2002)

Friedreich, N., Kekule, F. A.; Zur Amyloidfrage; Virchows Arch Pathol Anat Physiol XVI:50-65 (1859)

Garcia-Fruito, E., Sabate, R., Groot, N., Villaverde, A., Ventur, S.; Biological role of bacterial inclusion bodies: a model for amyloid aggregation; FEBS J. 278 (14) (2011)

Garrido, C., Paul, C., Seigneuric, R., Kampinga, H. H.; The small heat shock proteins family: the long forgotten chaperones; International Journal of Biochemistry and Cell Biology (2010)

Gendron, T., Petrucelli, L.; The role of tau in neurodegeneration; Mol Neurodegener 4: 13, doi: 10.1186/1750-1326-4-13 (2009)

Georgopoulos, C.; A new bacterial gene (groPC) which affects lambda DNA replication; Mol. Gen. Genet.151: 35–39 (1977)

Georgopoulos, C.; Bacterial mutants in which the gene N function of bacteriophage lambda is blocked have an altered RNA polymerase; Proc. Natl. Acad. Sci. USA 68: 2977–2981(1971)

Georgopoulos, C., Hendrix, R. W., Casjens, S. R., Kaiser, A. D.; Host participation in bacteriophage lambda head assembly; J. Mol. Biol. 76: 45–60 (1973)

Georgopoulos, C., Hendrix, R. W., Kaiser, A. D.,Wood, W. B.; Role of the host cell in bacteriophage morphogenesis: effects of a bacterial mutation on T4 head assembly; Nat. New Biol. 239: 38–41 (1972)

Georgopoulos, C., Herskowitz, I.; Escherichia coli mutants blocked in lambda DNA synthesis, in The Bacteriophage Lambda; Cold Spring Harbor Laboratory Press, Cold Spring Harbor, NY: 553–565 (1971)

Georgopoulos, C., Hohn, B.; Identification of a host protein necessary for bacteriophage morphogenesis (the groE gene product); Proc. Natl. Acad. Sci. USA 75: 131–135 (1978)

Georgopoulos, C.; Toothpicks, Serendipity and the Emergence of the Escherichia coli DnaK (Hsp70) and GroEL (Hsp60) Chaperone Machines; Genetics 174 (4): 1699–1707, doi: 10.1534/genetics.104.68262. (2006)

Glover, J., Lindquist, S.; Hsp104, Hsp70, and Hsp40: a novel chaperone system that rescues previously aggregated protein; Cell (94): 73-82 (1998)

Goloubinoff, P., Christeller, A., Gatenby, A., Lorimer, G.H.; Reconstitution of active dimeric ribulose bisphosphate carboxylase from an unfolded state depends on two chaperonin proteins and Mg-ATP; Nature 342: 884-889 (1989)

Goloubinoff, P., De Los Rios, P.; The mechanism of Hsp70 chaperones: (entropic) pulling the models together; Trends in Biochemical sciences 32 (8): 372-380 (2007)

Hai-Dong, W., Hui Niu, C., Yang, Q., Badea, I.; Study on protein conformation and adsorption behaviors in nanodiamond particle–protein complexes; Nanotechnology Journal 22 (14) (2011)

Harriette, C., Martin, C. J.; On The “Heat Coagulation” Of Proteins; The Journal Of Physiology 40 (5) (1910)

Hartl, F., Bracher, A., Hayer-Hartl, M.; Molecular chaperones in protein folding and proteostasis; Nature 475: 324–332, doi:10.1038/nature10317 (2011)

Haslbeck, M., Franzmann, T., Weinfurtner, D., Buchner, J.; Some like it hot: the structure and function of small heat-shock proteins; Nat Struct Mol Biol 12 (10): 842-6 (2005)

Haslberger, T., Bukau, B., Mogk, A.; Towards a unifying mechanism for ClpB/Hsp104-mediated protein disaggregation and prion propagation; Biochemistry and Cell Biology 83: 63-75 (2010)

Haslberger, T., Weibezahn, J., Zahn, R., Lee, S., Tsai, F.T.F., Bukau, B., Mogk. A.; M Domains couple the ClpB threading motor with the DnaK chaperone activity; MolecularCell 25: 247–260 (2007)

Hendrix, R. W.; Purification and properties of groE, a host protein involved in bacteriophage assembly; J. Mol. Biol. 129: 375–392 (1979)

Hernandez, V. A., Karlsson, G., Edwards, K. Intrinsic heterogeneity in liposome suspensions caused by the dynamic spontaneous formation of hydrophobic active sites in lipid membranes; Langmuir 27 (8): 4873-4883 (2011)

Hohn, T., B. Engel, H., Wurtz, M., Smith, P. R.; Isolation and characterization of the host protein groE involved in bacteriophage lambda assembly; J. Mol. Biol. 129: 359–373 (1979)

Hook, A., Beard, D., Taylor, A., Sharp, D., Beard, J.; Isolation and characterization of the T2 bacteriophage of *E. coli*; J.Biol.Chem. 165: 241-258 (1946)

Hope, M., Wong, K., Cullis, P.; Freeze-fracture of lipids and model membrane systems; J Electron Microsc tech. 13: 277-287 (1989)

Huang, T. H. J., Yang, D., Fraser, P.E., Chakrabartty, A.; Alternate aggregation pathways of the Alzheimer's B-Amyloid Peptide; JBC 275 (46): 36436-36440 (2000)

Hurley, J., Hanson, P.; Membrane budding and scission by the ESCRT Machinery: it's all in the neck; Nat Rev Mol Cell Biol 11: 556-566 (2010)

Imlay, J.; The molecular mechanisms and physiological consequences of oxidative stress: lessons from a model bacterium; Nature Reviews Microbiology 11: 443–454, doi:10.1038/nrmicro3032. (2013)

Jahn, T., Radford, S.; Folding Versus Aggregation: Polypeptide conformations on competing pathways; Arch Biochem Biophys 469 (1) (2008)

Jewett, J. C., Sletten, E. M., Bertozzi, C. R.; Rapid cu-free click chemistry with readily synthesized biarylazacyclooctynones; J. Am. Chem. Soc. 132 (11): 3688-3690 (2010)

Johnston, J., Ward, C., Kopito, R.; Aggresomes: A Cellular Response to Misfolded Proteins; J. Cell Biol 143 (1998)

Jones, S., Thornton, J.; Principles of protein-protein interactions; Proc Natl Acad Sci USA 93 (1) (1996)

Kampinga, H. H., Craig, E. A. The HSP70 chaperone machinery: J proteins as drivers of functional specificity; Molecular Cell Bilogy 11 (2010)

Kauzmann, W.; Structural Factors in Protein Denaturation; Journal Of Cellular Physiology 47 (1) (1956)

Kawahara, M.; Neurotoxicity of beta-amyloid protein: oligomerization, channel formation, and calcium dyshomeostasis; Curr. Pharm. Des. 16: 2779–2789 (2010)

Kikis, E., Gidalevitz, T., Morimoto, R.; Protein homeostasis in models of aging and age-related conformational disease; Adv Exp Med Biol. 694: 138–159 (2012)

King, N., Westbrook, M. J., Young, S. L., Kuo, A., Abedin, M., et al.; The genome of the choanoflagellate Monosiga brevicollis and the origin of metazoans; Nature 451: 783–788 (2008)

Knowles, T., Vendruscolo, M., Dobson, C.; The amyloid state and its association with protein misfolding disease; Nature Reviews Molecular Cell Biology 15 (2014)

Kochan, J., Murialdo, H.; Early intermediates in bacteriophage lambda prohead assembly. II. Identification of biologically active intermediates; Virology, 131: 100-115 (1983)

Kongsberg, W., Liu, T., Matthews, B., Niall, H., Steinman, H.; The Proteins: Volume III, Third Edition; Academic Press New York (1977)

Koniarek, J.P., Thomas, J.L., Vazquez, M.; Detection of microlesions induced by heavy ions using liposomes filled with fluorescent dye; Adv Space Res 34 (6): 1373-7 (2004)

Konopa, G., Taylor, K.; Isolation of coliphage lambda ghosts able to adsorb onto bacterial cells; Biochimica et Biophysica acta 399: 460-467 (1975)

Krantz, K., Puchalla, J., Thapa, R., Kobayashi, C., Bisher, M., Viehweg, J., et al; Clathrin coat disassembly by the yeast Hsc70/Ssa1p and auzilin/Swa2p proteins observed by single-particle Burst Analysis Spectroscopy; J. Biol Chem 288: 26721-26730 (2013)

Krebs, M.; Domike, K., Cannon, D., Donald, A.; Common motifs in protein self-assembly; Faraday Discuss. 139 (2008)

Kummer, E., Oguchi, Y., Seyffer, F., Bukau, B., Mogk, A.; Mechanism of Hsp104/ClpB inhibition by prion curing Guanadinium Hydrochloride; FEBS lett. 18 (6): 810-7 (2013)

Kunkel, T.; Rapid and efficient site-specific mutagenesis without phenotypic selection; Proc Natl Acad Sci U S A 82(2):488-92 (1985).

Lakowicz, J.; Fluorescence anisotropy. In Principles of Fluorescence Spectroscopy; JR. Lakowicz, ed (New York: Kluwer Academic/Plenum publishers): 368-391 (1999)

Langmuir, I., Wrinch, D.; Nature of the Cyclol bond; Nature 143 (3611) (1939)

Lashuel, H., Hartley, D., Petre, B. M., Walz, T., Lansbury, P.; Neurodegenerative disease: Amyloid pores from pathogenic mutations; Nature 418: 291. doi:10.1038/418291a (2002)

Laskey, R. A., Honda, B. M., Mills, J. A. D., Finch, T.; Nucleosomes are assembled by an acidic protein which binds histones and transfers them to DNA; Nature 275: 416 – 420, doi:10.1038/275416a0 (1978)

Lederberg, E. M., Lederberg, J.; Genetic studies of lysogenicity in *E. coli*; Genetics 38 (1): 51-64 (1953)

Lee, H., Patel, S., Lee, S.; Intravesicular localization and exocytosis of alpha-synuclein and its aggregates; J. Neurosci 25: 6016-6024 (2005)

Lee, M., Orci, L., Hamamoto, S., Futai, E., Ravazzola, M., Schekman, R.; Sar1p N-terminal helix initiates membrane curvature and completes the fission of a COPII vesicle; Cell 122: 605-617 (2005)

Legendre-Guillemin, V.; ENTH/ANTH proteins and clathrin-mediated membrane budding; J Cell Sci 117: 9-18 (2004)

Levinthal, C.; How to fold graciously; Mossbaun Spectroscopy in biological systems proceedings 67 (41) (1969)

Lewandowska, A., Matuszewska, M., Liberek, K.; Conformational properties of aggregated polypeptides determine ClpB-dependence in the disaggregation process; Journal of Molecular Biology 371: 800-811 (2007)

Liberek, K., Georgopoulos, C., Zylicz, M. ; Role of the Escherichia coli DnaK and DnaJ heat shock proteins in the initiation of bacteriophage lambda DNA replication; Proc Natl Acad Sci U S A. 85 (18): 6632–6636 (1988)

Lin, H., Bhatia, R., Lal, R.; Amyloid β protein forms ion channels: implications for Alzheimer's disease pathophysiology; FASEB 15 (13): 2433-2444. doi:10.1096/fj.01-0377com (2001)

Lin, Z., Madan, D., Rye, H.; GroEL stimulates protein folding through forced unfolding; Nat Struct Mol Biol. 15 (3): 303–311 (2008)

Lin, Z., Rye, H.; Expansion and Compression of a protein folding intermediate by GroEL; Molecular Cell 16: 23–34 (2004)

Lin, Z., Rye, H.; GroEL-mediated protein folding: Making the impossible, possible; Critical Reviews In Biochemistry and Molecular Biology 41 (2006)

Lindner, A. B., Madden, R., Demarez, A., Stewart, E. J., Taddei, F.; Asymmetric segregation of protein aggregates is associated with cellular aging and rejuvenation; PNAS 105 (8): 3076-3081 (2008)

Liu, B., Larsson, L., Caballero, A., Hao, X., Oling, D., Grantham, J., Nystrom, T.; The polarisome is required for segregation and retrograde transport of protein aggregates; Cell 140: 257-267 (2010)

Lloyd-Price, J., Häkkinen, A., Kandhavelu, M., Marques, I., Chowdhury, S., Lihavainen, E., Yli-Harja, O., Ribeiro, A.; Asymmetric Disposal of Individual Protein Aggregates in Escherichia coli, One Aggregate at a Time; J Bacteriol. 194 (7): 1747–1752, doi: 10.1128/JB.06500-11. (2012)

Lo Bianco, C., Shorter, J., Régulier, E., Lashuel, H., Iwatsubo, T., Lindquist, S., Aebischer, P.; Hsp104 antagonizes α-synuclein aggregation and reduces dopaminergic degeneration in a rat model of Parkinson disease; Journal of Clinical Investigation 118 (9): 3087-3097 (2008)

Loerke, D., Mettlen, M., Yarar, D., Jaqaman, K., Jaqaman, H., Danuser G., et al; Cargo and Dynamin Regulate Clathrin-Coated Pit Maturation; PLoS Biol 7: e57 (2009)

Madan, D., Lin, Z., Rye, H.; Triggering protein folding within the GroEL-GroES complex; Journal of Biological Chemistry 283 (2008)

Maisonneuve, E., Ezraty, B., Dukan, S.; Protein aggregates: an aging factor involved in cell death; Journal of Bacteriology 18: 6070-6075 (2008)

Maisonneuve, E., Fraysse, L., Moinier, D., Dukan, S.; Existence of abnormal protein aggregates in healthy Escherichia coli cells; J. Bacteriol. 190 (3): 887-893 (2008)

Martinez-Vicente, M., Talloczy, Z., Wong, E., Tang, G., Koga, H., Kaushik, S., Vries, R., Arias, E., Harris, S., Sulzer, D., Cuervo, A.; Cargo recognition failure is responsible for insufficient autophagy in Huntington's disease; Nature Neuroscience (13): 567-576 (2010)

Massol, R., Boll, W., Griffin, A., Kirchhausen, T.; A burst of auxilin recruitment determines the onset of clathrin-coated vesicle uncoating; Proc Natl Acad Sci USA 103: 10265-10270 (2006)

Maurizi, M. R., Xia, D.; Protein binding and disruption by ClpB/Hsp100 chaperones; Structure 12 (2): 175-83 (2004)

Mayer, M. P., Bukau, B.; Hsp70 chaperones: Cellular functions and molecular mechanism; Cellular and Molecular Life Sciences 62 (6): 670–684, doi: 10.1007/s00018-004-4464-6. (2005)

McCarty, J. S., Buchberger, A., Reinstein, J., Bukau, B. The role of ATP in the functional cycle of the DnaK chaperone system; Journal of Molecular Biology 249: 126-137 (1995)

McDonough, H., Patterson, C.; CHIP: a link between the chaperone and proteasome systems; Cell Stress Chaperones 8 (4): 303-308 (2003)

Meinecke, M., Boucrot, E., Camdere, G., Hon, W.C., Mittal, R., McMahon, H.T.; Cooperative recruitment of dynamin and BIN/amphiphysin/Rvs (BAR) domain-containing proteins leads to GTP-dependent membrane scission; J Biol Chem 288: 6651-6661 (2013)

Merrifield, C. J., Perrais, D., Zenisek, D.; Coupling between Clathrin-coated-pit invagination, cortactin recruitment, and membrane scission observed in live cells; Cell 121: 593-606 (2005)

Mills, I., Praefcke, G., Vallis, Y., Peter, B.J., Olesen, L., Gallop, J.; EpsinR:an AP1/Clathrin interacting protein involved in vesicle trafficking; J Cell Biol 160: 213-222 (2003)

Mogk, A., Kummer, E., Bukau, B.; Cooperation of Hsp70 and Hsp100 chaperone machines in protein disaggregation; Front Mol Biosci. 19: 2-22, doi: 10.3389/fmolb.2015.00022. (2015)

Morano, K.A.; New tricks for an old dog: the evolving world of Hsp70; Ann. N. Y. Acad. Sci. 1113: 1–14, doi:10.1196/annals.1391.018. PMID 17513460. (2007)

Morley, J., Brignull, H., Weyers, J., Morimoto, R.; The threshold for polyglutamine-expansion protein aggregation and cellular toxicity is dynamic and influenced by aging in Caenorhabditis elegans; Proc Natl Acad Sci USA, 99 (16): 10417–10422. doi: 10.1073/pnas.152161099 PMCID: PMC124929, Cell Biology (2002)

Morris, A. M., Watzky, M. A., Finke, R. G.; Protein aggregation kinetics, mechanisms, and curve-fitting: A review of the literature; Biochimica et Biophysica Acta 1794: 375-397 (2009)

Moskovitz, Y., Srebnik, S.; Conformational changes of globular proteins upon adsorption on a hydrophobic surface; Phys. Chem. Chem. Phys. 16: 11698-11707, doi: 10.1039/C4CP00354C. (2014)

Muller, F., Lustgarten, M. S., Jang Y., Richardson, A., Van Remmen, H.; Trends in oxidative aging theories; Free Radical Biology & Medicine 43 (4): 477–503 (2007)

Muller, J., Chen, Y., Gratton, E. Resolving heterogeneity on the single molecular level with the photon-counting histogram; Biophys J 78: 474-486 (2000)

Natalello, A., Mattoo, R., Priya, S., Sharma, S.K., Goloubinoff, P., Doglia, S.M.; Biophysical characterization of two different stable misfolded monomeric polypeptides that are chaperone-amneable substrates; JMB 425 (7): 1158-1171 (2013)

Neumann, S., Schmid, S. L.; Dual role of BAR domain-containing proteins in regulating vesicle release catalyzed by the GTPase, dynamin-2; J. Biol Chem 288: 25119-25128 (2008)

Nichols, M. R., Moss, M. A., Reed, D. K., Cratic-McDaniel, S., Hoh, J. H., Rosenberry, T. L.; Amyloid-protofibrils differ from amyloid-aggregates induced in dilute hexafluoroisopropanol in stability and morphology; Journal of Biological Chemistry 280 (4): 2471-2480 (2005)

Nillegoda, N. B., Kirstein, J., Szlachcic, A., Berynskyy, M., Stank, A., Stengel, F., Arnsburg, K., Gao, X., Scior, A., Aebersold, R., Guilbride, D. L., Wade, R. C., Morimoto, R. I., Mayer, M. P., Bukau, B.; Crucial Hsp70 co-chaperone complex unlocks metazoan protein disaggregation; Nature 524: 247-251 (2015)

Pace, N., Fu, H., Fryar, K., Landua, J., Trevino, S., Shirley, B., Hendricks, M., Limura, S., Gajiwala, K., Scholtz, M., Grimsley, G.; Contribution Of Hydrophobic Interactions To Protein Stability; J. Mol. Biol. 408 (3) (2011)

Palade, G. E.; A small particulate component of the cytoplasm; J. Biophys Biochem Cytol 1 (1) (1955)

Pant, S., Sharma, M., Patel, K., Caplan, S., Carr, C. M., Grant, B.D.; AMPH-1/Amphiphysin/Bin1 functions with Rme-1/Ehd1 in endocytic recycling; Nat Cell Biol 11 (12): 1399-410 (2009)

Parsell, D. A., Kowal, A. S.,Singer, M. A., Lindquist, S.; Protein disaggregation mediated by heat-shock protein Hsp104; Nature 372 (6505): 475-478 (1994)

Pauling, L., Corey, R. B., Branson, H. R.; The structure of proteins; two hydrogen-bonded helical configurations of the polypeptide chain; proceedings of the National Acadamey of Sciences of the United States of America 37 (4) (1951)

Pearce, M., Mintseris, J., Ferreyra, J., Gygi, S., Darwin, K., Ubiquitin-like protein involved in the proteasome pathway of Mycobacterium tuberculosis; Science 322: 1104-1107 (2008)

Philo, J. Is any measurement method optimal for all aggregate sizes and types?; AAPS J 8: E564-E571 (2006)

Prakash, S., Tian, L., Ratliff, K., Lehotzky, R., Matouschek, A.; An unstructured initiation site is required for efficient proteasome-mediated degradation; Nat Struct Mol Biol 11 (9): 830-7 (2004)

Prangkio, P., Yusko, E.C., Sept, D., Yang, J., Mayer, M.; Multivariate analyses of amyloid-beta oligomer populations indicate a connection between pore formation and cytotoxicity; PLoS One, 7: e47261 (2012)

Pucadyil, T., Schmid, S.; Real-time visualization of dynamin-catalyzed membrane fission and vesicle release; Cell 135: 1263-1275 (2008)

Puchalla, J., Krantz, K., Austin, R., Ry, H. Burst analysis spectroscopy: A versatile single-particle approach for studying distributions of protein aggregates and fluorescent assemblies; PNAS 105: 14400-14405 (2008)

Rampelt, H., Kirstein-Miles, J., Nillegoda, N.B., Chi, K., Scholz, S.R., Morimoto, R.I., Bukau, B.; Metazoan Hsp70 Machines Use Hsp110 to power protein disaggregation; EMBO Jounal 31 (21): 4221-4235 (2012)

Rao, Y., Ma, Q., Vahedi-Faridi, A., Sundborger, A., Pechstein, A., Puchkov, D., et al; Molecular basis for SH3 domain regulation of F-BAR-mediated membrane deformation; Proc Natl Acad Sci USA 107: 8213-8218 (2010)

Ratajczak, E., Zierkiewicz, S., Liberek, K.; Distinct activities of *E. coli* small heat shock proteins IbpA and IbpB promote efficient protein disaggregation; J Mol Biol 386 (1): 178-89 (2009)

Revel, H. R. , Stitt, B. L., Lielausis, I., Wood, W. B.; Role of the host cell in bacteriophage T4 development. I. Characterization of host mutants that block T4 head assembly; J Virol. 33 (1): 366–376. (1980)

Ritossa, F.; A new puffing pattern induced by temperature shock and DNP in Drosophila; Experientia 18: 571–573, doi: 10.1007/BF02172188. (1962)

Ritossa, F.; Discovery of the heat shock response; Cell Stress and Chaperones 1 (2) 97-98 (1996)

Roberts, C.; Non-native Protein Aggregation; Springer (2006)

Rodreguez, F., Arsene-Ploetze, F., Rist, W., Rudiger, S., Schneider-Mergener, J., Mayer, M. P., Bukau, B.; Molecular basis for regulation of the heat shock transcription factor sigma 32 by the DnaK and DnaJ chaperones; Molecular Cell 32: 347-358 (2008)

Roher, A., Debbins, J., Malek-Ahmadi, M., Chen, K., Pipe, J., Maze, S., Belden, C., Maarouf, C., Thiyyagura, P., Mo, H., Hunter, J. M., Kokjohn, T., Walker, D., Kruchowsky, J., Belohlavek, M., Sabbagh, M.N., Beach, T.; Cerebral blood flow in Alzheimer's disease. Vasc Health Risk Manag. 8: 599–611 (2012)

Rosen, C., Weber, G.; Dimer formation from 1-amino-8-naphthalenesulfonate catalyzed by bovine serum albumin. A new fluorescent molecule with exceptional binding properties; Biochemistry, 8(10):3915-20 (1969).

Rothnie, A., Clarke, A. R., Kuzmic, P., Cameron, A. , Smith, C.J. A Sequential mechanism for clathrin cage disassembly by 70kDa heat-shock cognate protein (Hsc70) and auxilin; PNAS 108: 6927-6932 (2011)

Roux, A., Uyhazi, K., Frost, A., De Camilli, P.; GTP-dependent twisting of dynamin implicates construction and tension in membrane fission; Nature 441: 528-531 (2006)

Rudiger, S., Germeroth, L., Schneider-Mergener, J., Bukau, B.; Its substrate specificity characterizes the DnaJ co-chaperone as a scanning factor for the DnaK chaperone; EMBO j. 20 (5): 1042-1050 (2001)

Rudiger, S., Germeroth, L., Schneider-Mergener, J., Bukau, B.; Substrate specificity of the DnaK chaperone determined by screening cellulose-bound peptide libraries; EMBO j. 16 (7): 1501-1507 (1997)

Rye, H., Glazer, A.; Stable dye-DNA intercalation complexes as reagents for high-sensitivity fluorescence detection; Nature 359: 859-861 (1992)

Rye, H. S., Roseman, A. M., Chen, S., Furtak, K., Fenton, W. A., Saibil, H. R., Horwich, A. L.; GroEL-GroES cycling: ATP and nonnative polypeptide direct alternation of folding-active rings; Cell 97: 325–338 (1999)

Rye, H., Burston, S., Fenton, W., Xu, Z., Sigler, P., Horwich, A.; Distinct actions of cis and trans ATP within the drouble ring of the chaperonin GroEL; Nature 388: 792-798 (1997)

Rye, H., Roseman, A., Chen, S., Furtak, K., Fenton, W.; GroEL-GroES cycling: ATP and nonnative polypeptide direct alternation of folding-active rings; Cell 97 (1999)

Rye, H., Yue, S., Quesada, M., Haugland, R., Mathies, R., Glazer, A.; Picogram detection of stable dye-DNA intercalation complexes with two-color laser-excited confocal fluorescence gel scanner; Methods Enzymol 217: 414-431 (1993)

Rye, H., Yue, S., Wemmer, D., Quesada, M., Haugland, R., Mathies, R., Glazer, A.; Stable fluorescent complexes of double-stranded DNA with bis-intercalating asymmetric cyanine dyes: properties and applications; Nucleic Acids Res 20: 2803-2812 (1992)

Rye, H. S.; Application of Fluorescence Resonance Energy Transfer to the GroEL-GroES Chaperonin Reaction; Methods 24 (3): 278-288 (2001)

Rye, H. S., Dabora, J. M., Quesada, M. A., Mathies, R. A., Glazer, A. N.; Fluorometric assay using dimeric dyes for double- and single-stranded DNA and RNA with picogram sensitivity; Analytical Biochemistry 208 (1): 144-150 (1993)

Saito, H., Uchida, H.; Initiation of the DNA replication of bacteriophage lambda in Escherichia coli K12; J. Mol. Biol. 113: 1–25 (1977)

Sanchez, Y., Taulien, J., Borkovich, K. A., Lindquist, S.; Hsp104 is required for tolerance to many forms of stress; EMBO J 11: 2357–2364 (1992)

Sanger, F.; The terminal peptides of insulin; The Biochemical Journal 45 (5) (1949)

Sauer, R. et al. Sculpting the proteome with AAA(+) proteases and disassembly machines; Cell 119: 9-18 (2004)

Schirmer, E. C., Lindquist, S.; Interactions of the chaperone Hsp104 with yeast Sup35 and mammalian PrP; Proc. Natl. Acad. Sci. USA 94: 13932–13937 (1997)

Schlecht, R., Erbse, A. H., Bukau, B., Mayer, M. P.; Mechanics of Hsp70 chaperones enables differential interaction with client proteins; Nature Structural and Molecular Biology 18 (3) (2011)

Scholl, Z. N., Yang, W., Marszalek, P. E.; Chaperones rescue luciferase folding by separating its domains; J Biol Chem 289 (41): 28607-18 (2014)

Schubert, U., Antón, L. C., Gibbs, J., Norbury, C. C., Yewdell, J. W., Bennink, J. R.; Rapid degradation of a large fraction of newly synthesized proteins by proteasomes; Nature 404 (6779):770-4 (2000)

Schuermann, J. P., Jiang, J., Cuellar, J., Llorca, O., Wang, L., Gimenez, L. E., Jin, S., Taylor, A. B., Demeler, B., Morano, K. A., Hart, P. J., Valpuesta, J. M., Lafer, E.M., Sousa, R.; Structure of the Hsp110: Hsc70 Nucleotide Exchange Machine; Molecular Cell 31 (2): 232-243 (2008)

Schweet, R., Heintz, R.; Protein Synthesis; Annual Review Of Biochemistry 35 (1996)

Sciacca, M. F., Kotler, S. A., Brender, J. R., Chen, J., Lee, D. K., Ramamoorthy, A.; Two-step mechanism of membrane disruption by Abeta through membrane fragmentation and pore formation. Biophys. J. 103: 702–710 (2012)

Scott, D. W.; Averaged shifted histogram. Computational Statistics 2 (2): 160-164 (2009)

Sheng, M., Sabatini, B., Südhof, T.; Synapses and Alzheimer's Disease; Cold Spring Harb Perspect. Biol, doi: 10.1101/cshperspect.a005777 (2012)

Shorter, J.; Hsp104: a weapon to combat diverse neurodegenerative disorders; Neurosignals. 16 (1): 63-74 (2008)

Shorter, J., Lindquist, S.; Hsp104 catalyzes formation and elimination of self-replicating Sup35 prion conformers; Science 304 (5678):1793-7 (2004)

Shorter, J., Lindquist, S.; Hsp104, Hsp70 and Hsp40 interplay regulates formation, growth and elimination of Sup35 prions; EMBO J. 27: 2712-2724 (2008)

Shorter, J.; The mammalian disaggregase machinery: Hsp110 synergizes with Hsp70 and Hsp40 to catalyze protein disaggregation and reactivation in a cell-free system; PlosONE journal.pone.0026319 (2011)

Shoup, D., Brooks, A., Kustigian, L., Puchalla, J., Carr, C., Rye, H.; Single particle fluorescence burst analysis of Epsin induced membrane fission; 10.1371/journal.pone.0119563 (2015)

Simpson, F., Hussain, N., Qualmann, B., Kelly, R., Kay, B., McPherson, P., et al; SH3-domain-containing proteins function at distinct steps in clathrin-coated vesicle formation; Nat Cell Biol 1: 119-124 (1999)

Spolar, R., Ha, J., Record, M.; Hydrophobic effect in protein folding and other noncovalent processes involving proteins; Proc. Natl. Acad. Sci. U.S.A. 86 (21): 8382-8385 (1989)

Stancu, I., Vasconcelos, B., Terwel, D., Dewachter, I.; Models of β-amyloid induced Tau-pathology: the long and “folded” road to understand the mechanism; Molecular Neurodegeneration 9: 51, doi: 10.1186/1750-1326-9-51 (2014)

Starck C., Sutherland-Smith, A.; Cytotoxic aggregation and amyloid formation by the myostatin precursor protein; doi: 10.1371/journal.pone.00009170. (2010)

Stefani, M., Dobson, C.; Protein aggregation and aggregate toxicity: new insights into protien folding, misfolding dissease and biological evolution; J Mol Med 81 (2003)

Strandkvist, C., Juul, J., Bendtsen, K.M.; Asymmetric Segregation of Damaged Cellular Components in Spatially Structured Multicellular Organisms; doi: 10.1371/journal.pone.0087917 Plosone (2014)

Sulatskaya, A.I., Kuznetsova, IM., Turoverov, KK.; Interaction of thioflavin T with amyloid fibrils: stoichiometry and affinity of dye binding, absorption spectra of bound dye; J Phys Chem B 6 (115): 11519-24 (2011)

Sunshine, M., Feiss, M., Stuart, J., Yochem, J.; A new host gene (groPC) necessary for lambda DNA replication; Mol. Gen. Genet. 151: 27–34 (1977)

Takano, T., Kakefuda, T.; Involvement of a bacterial factor in morphogenesis of bacteriophage capsid; Nat. New Biol. 239: 34–37 (1972)

Tanaka, M., Komi, Y.; Layers of structure and function in protein aggregation; Nature chemical biology 11 (6): 373-377 (2015)

Tanik, S. A., Schultheiss, C. E., Volpicelli-Daley, L. A., Brunden, K. R., Lee, V. M..; Lewy body-like α-synuclein aggregates resist degradation and impair macroautophagy; J Biol Chem. 288 (21): 15194-210, doi: 10.1074/jbc.M113.457408. (2013)

Taylor, M., Perrais, D., Merrifield, C.; A High precision survey of the molecular dynamics of mammalian clathin-mediated endocytosis; PLoS Biol 9: e1000604 (2011)

Tessarz, P., Mogk, A., Bukau, B.; Substrate threading through the central pore of the Hsp104 chaperone as a common mechanism for protein disaggregation and prion propogation; Molecular Microbiology 68 (1): 87-97 (2008)

Thomas, J. G., Baneyx, F.; ClpB and HtpG facilitate de novo protein folding in stressed *E. coli* cells; Mol Microbiol 36 (6): 1360-70 (2000)

Tilly, K., Georgopoulos, C.; Evidence that the two Escherichia coli groE morphogenetic gene products interact in vivo; J. Bacteriol. 149: 1082–1088 (1982)

Tilly, K., Murialdo, H., Georgopoulos, C.; Identification of a second Escherichia coli groE gene whose product is necessary for bacteriophage morphogenesis; Proc. Natl. Acad. Sci. USA 78: 1629–1633 (1981)

Trathnigg, B., Size-exclusion chromatography of polymers; Encyclopedia of analytical chemistry, John Wiley & Sons Ltd, Chichester (2000)

Umeda, T., Ramser, E., Yamashita, M., Nakajima, K., Mori, H., Silverman, M. A., Tomiyama, T.; Intracellular amyloid β oligomers impair organelle transport and induce dendritic spine loss in primary neurons; Acta Neuropathol Commun. 3: 51, doi: 10.1186/s40478-015-0230-2 (2015)

Ünal, E., Amon, A.; Gamete formation resets the aging clock in yeast; Cold Spring Harb Symp Quant Biol. 76: 73–80, doi: 10.1101/sqb.2011.76.011379. (2011)

Vassar, P., Culling, C.; Fluorescent stains, with special reference to amyloid and connective tissues; Arch Pathol 68 (1959)

Vashist, S., Cushman, M., Shorter, J.; Applying Hsp104 to protein-misfolding disorders; Biochem Cell Biol 88(1) 2010

Vetri, V., Canale, C., Relini, A., Librizzi, F., Militello, V., Gliozzi, A., Leone, M.; Amyloid fibrils formation and amorphous aggregation in concanavalin A; Biophysical Chemistry 125 (1) (2007)

Virchow, R.; Zur Cellulose-Frage; Archiv fur pathologische Anatomie und Physiologie und fur Klinishe Medicin (1854)

Vulevic, B., Correia, J. J.; Thermodynamic and structural analysis of microtubule assembly: the role of GTP hydrolysis; Biophys. J. 72: 1357-1375 (1997)

Wang, H. D., Niu, C. H., Yang, Q., Badea, I.; Study on protein conformation and adsorption behaviors in nanodiamond particle-protein complexes; Nanotechnology 22 (14): 145703, doi: 10.1088/0957-4484/22/14/145703. (2011)

Wang, L., Brock, A., Herberich, B., Schultz, P.; Expanding the genetic code of Escherichia coli; Science 292 (5516): 498-500 (2001)

Wang, L., Sudhof, T., R., Anderson, T.; The appendage domain of alpha-adaptin is a high affinity binding site for dynamin; JBC 270 (17): 10079-10083 (1995)

Weiss, W., Hodgdon, T., Kaler, E., Lenhoff, A., Roberts, C.; Nonnative protein polymers: structure, morphology, and relation to nucleation and growth; Biophysical Journal 93 (12) (2007)

Weller, R.; Pathology of cerebrospinal fluidand interstitial fluid of the CNS: significance for Alzheimer's disease, prion disorders and multiple sclerosis; J. Neuropathol. Exp Neurol. (1998)

Wickner, S.; DNA replication proteins of Escherichia coli and phage lambda; Cold Spring Harbor Symp. Quant. Biol. 43 (1): 303–310 (1979)

Wickner, W., Schekmann, R.; Membrane fusion; Nat Struct Mol Biol 15: 658-664 (2008)

Yochem, J., Uchida, H., Sunshine, M., Saito, H., Georgopoulos, C. P. et al.; Genetic analysis of two genes, dnaJ and dnaK, necessary for Escherichia coli and bacteriophage lambda DNA replication; Mol. Gen. Genet. 164: 9–14 (1978)

Zaarur, N., Meriin, A. B., Bejarano, E., Xu, X., Gabai, V. L., Cuervo, A. M., Sherman, M.Y.; Proteasome failure promotes positioning of lysosomes around the aggresome via local block of microtubule-dependent transport; Mol. Cell Biol. 34 (7): 1336-1348 (2014)

Zeng, L., Golding, I.; Following cell-fate in *E. coli* after infection by phage lambda; J Vis Exp. (56): 3363 (2011)

Zhao, X. L., Wang, W. A., Tan J., X., Huang, J. K., Zhang, X., Zhang, B. Z., Wang, Y. H., Yangcheng, H. Y., Zhu, H. L., Sun, X. J., Huang, F. D; Expression of beta-amyloid induced age-dependent presynaptic and axonal changes in Drosophila; J. Neurosci. 30: 1512–1522 JNEUROSCI 10.1523.3699-09.2010 (2010)

Zhu,Y. J., Lin, H., Lal, R.; Fresh and nonfibrillar amyloid beta protein(1-40) induces rapid cellular degeneration in aged human fibroblasts: evidence for AbetaP-channel-mediated cellular toxicity; FASEB J. 14: 1244-1254 (2000)

Zietkiewicz, S., Krzewska, J., Liberek, K.; Succesive synergistic action of the Hsp70 and Hsp100 chaperones in protein disaggregation; JBC 279: 44376-44383 (2004)

Zietkiewicz, S., Lewandowska, A., Stocki, P., Liberek, K.; Hsp70 chaperone machine remodels protein aggregates at the initial step of Hsp70-Hsp100-dependent disaggregation; Journal of Biological Chemistry 281 (11) (2006)